2017

Histone Variant Macroh2a In The Gut And Beyond: A Study Of Intestinal Fortitude

Ryan James Cedeno
University of Pennsylvania, rcedeno@mail.med.upenn.edu

Histone Variant Macroh2a In The Gut And Beyond: A Study Of Intestinal Fortitude

Abstract

Epigenetic factors guide chromatin remodeling during cell state transitions and confer resistance to genotoxic stressors that could induce deleterious transformations. A particularly peculiar component of the epigenome with emerging roles in fine-tuning cell identity and upholding genomic stability is the structural histone variant macroH2A. Relatively little is currently known about macroH2A's influence on overall cell developmental potency and less still is known about macroH2A's contributions to adult stem cell identity and function in vivo. In this work, we use induced pluripotent stem cell (iPSC) reprogramming and the murine intestinal stem cell (ISC) system to model macroH2A's overall impact on cell epigenetic identity from embryo to adult. We manipulated macroH2A content during iPSC reprogramming and concluded that macroH2A removal from somatic chromatin constitutes a mild, but present epigenetic bottleneck to pluripotency acquisition. Using epitope-tagged-macroH2A-expressing cells, we demonstrated that embryonic stem cells (ESCs) display significantly more dynamic macroH2A incorporation and turnover than fibroblasts, particularly proximal to the promoters of highly transcribed genes, concluding that macroH2A is less stably associated with ESC chromatin. In a separate study, we bred macroH2A double germline knockout (DKO) and strain-matched wildtype (WT) mice into reporter strains for ISC subpopulations, enabling us to functionally test active and reserve ISCs during homeostasis and following γ-irradiation injury. We showed that macroH2A DKO intestine is host to elevated numbers of putative reserve ISCs, suggesting that macroH2A may normally limit the size of the reserve ISC pool. We further determined that although macroH2A is unnecessary for intestinal homeostasis, macroH2A strongly bolsters the intestinal regeneration response following irradiative injury by promoting reserve ISC radioresistance. We thus conclude overall that macroH2A imposes a minor resistance to induced pluripotency, limits the size of the reserve ISC pool in adult mice and finally upholds genomic stability by providing resistance to genotoxic stress in vivo.

Degree Type
Dissertation

Degree Name
Doctor of Philosophy (PhD)

Graduate Group
Cell & Molecular Biology

First Advisor
Christopher J. Lengner

Keywords
Epigenetics, Histones, Histone variants, Induced pluripotent stem cells, Intestinal stem cells, Stem cells

Subject Categories
Cell Biology | Developmental Biology | Molecular Biology

HISTONE VARIANT MACROH2A IN THE GUT AND BEYOND:

A STUDY OF INTESTINAL FORTITUDE

Ryan Cedeno

A DISSERTATION

in

Cell and Molecular Biology

Presented to the Faculties of the University of Pennsylvania

in

Partial Fulfillment of the Requirements for the

Degree of Doctor of Philosophy

2017

Supervisor of Dissertation

_____

Christopher J. Lengner, Ph.D., Associate Professor of Cell and Developmental Biology

Graduate Group Chairperson

_____

Daniel S. Kessler, Ph.D., Associate Professor of Cell and Developmental Biology

Dissertation Committee

Kenneth S. Zaret, Ph.D., Joseph Leidy Professor of Cell and Developmental Biology

Edward E. Morrisey, Ph.D., Robinette Foundation Professor of Cardiovascular Medicine

Paul J. Gadue, Ph.D., Associate Professor of Pathology and Laboratory Medicine

Gerd A. Blobel, M.D., Ph.D., Professor of Pediatrics

Acknowledgements

I am incredibly lucky to have amazing people in my life who have helped make this document possible. I could probably write another 150 pages or so thanking everyone who has helped me over the years and still wouldn't do them justice.

To start, I owe many thanks to my fantastic thesis advisor, mentor, fellow beer aficionado and friend Chris Lengner. Chris took a huge risk taking me on as his first graduate student, and I'll never forget that. Chris's enthusiasm for rigorous science is incredibly contagious. It's a shock to no one that Chris was recently granted tenure because he inspires everyone around him to do his or her best work, and everyone wants to work with him. I wouldn't be half the scientist I am today if it weren't for Chris's guidance over the years and the incredibly hard working and hyper-analytical example that he sets. I probably also wouldn't have learned to appreciate the finer things in life – super hoppy / 'juicy' IPAs – or tried to improve my ability to brew them myself if it weren't for Chris's tutelage either!

Of course, I'd also like to thank the members of my thesis committee – Ken Zaret, Ed Morrisey, Paul Gadue and Gerd Blobel. Each and every one of you gave me invaluable input over the years, and helped me improve my science. Your collective faith in me was incredible – not one of you gave up on me when I hit my lowest point, and I can't express how much it meant. Thank you all for being so patient, kind and understanding – and thanks especially for helping me grow as a scientist!

I also want to thank Meagan Schoefer for her help with, well, just about everything in keeping my graduate school experience smooth and seamless. I'd also like

iv

ABSTRACT

HISTONE VARIANT MACROH2A IN THE GUT AND BEYOND:

A STUDY OF INTESTINAL FORTITUDE

Ryan J. Cedeno

Christopher J. Lengner

Epigenetic factors guide chromatin remodeling during cell state transitions and confer resistance to genotoxic stressors that could induce deleterious transformations. A particularly peculiar component of the epigenome with emerging roles in fine-tuning cell identity and upholding genomic stability is the structural histone variant macroH2A. Relatively little is currently known about macroH2A's influence on overall cell developmental potency and less still is known about macroH2A's contributions to adult stem cell identity and function *in vivo*. In this work, we use induced pluripotent stem cell (iPSC) reprogramming and the murine intestinal stem cell (ISC) system to model macroH2A's overall impact on cell epigenetic identity from embryo to adult. We manipulated macroH2A content during iPSC reprogramming and concluded that macroH2A removal from somatic chromatin constitutes a mild, but present epigenetic bottleneck to pluripotency acquisition. Using epitope-tagged-macroH2A-expressing cells, we demonstrated that embryonic stem cells (ESCs) display significantly more dynamic macroH2A incorporation and turnover than fibroblasts, particularly proximal to the promoters of highly transcribed genes, concluding that macroH2A is less stably associated with ESC chromatin. In a separate study, we bred macroH2A double germline knockout (DKO) and strain-matched wildtype (WT) mice into reporter strains for

ISC subpopulations, enabling us to functionally test active and reserve ISCs during homeostasis and following γ-irradiation injury. We showed that macroH2A DKO intestine is host to elevated numbers of putative reserve ISCs, suggesting that macroH2A may normally limit the size of the reserve ISC pool. We further determined that although macroH2A is unnecessary for intestinal homeostasis, macroH2A strongly bolsters the intestinal regeneration response following irradiative injury by promoting reserve ISC radioresistance. We thus conclude overall that macroH2A imposes a minor resistance to induced pluripotency, limits the size of the reserve ISC pool in adult mice and finally upholds genomic stability by providing resistance to genotoxic stress *in vivo*.

TABLE OF CONTENTS

LIST OF TABLES

LIST OF FIGURES

Chapter Three:

Chapter Four:

Chapter One:

Introduction

Histones and their modifications

Histones are proteins that compose the fundamental units around which eukaryotic genomic DNA is wound and assembled into organized, compact structures. The main category of histones consists of the core histones: H2A, H2B, H3, and H4. Two H2A-H2B dimers and one H3-H4 tetramer combine to form a histone octamer, around which 145 to 147 base pairs of DNA encircle to form the nucleosome core particle (NCP). The NCP is further stabilized by a second category of histone – the linker histone H1 – which secures DNA to nucleosome octamers and thus makes possible higher-order chromatin organization (Luger et al., 1997).

In addition to their histone-fold domains, histones also contain highly basic N-terminal histone tails, which protrude from the nucleosome octamer and are available for a wide array of covalent modifications (Bannister and Kouzarides, 2011; Luger et al., 1997). Histone modifications include acetylation, methylation, phosphorylation, and ADP-ribosylation to name a few (Bannister and Kouzarides, 2011). The precise modifications in combination with the specific histone tail amino acid residues that are modified determine the functional outcome(s) of the adjacent chromatin.

Histone acetylation occurs at various lysine residues on histone tails, introducing a negatively-charged functional group which destabilizes histone-DNA interactions, 'opening' chromatin for greater access by transcriptional machinery (Bannister and Kouzarides, 2011). Histone acetylation and deacetylation are governed by the actions of histone acetyltransferase (HAT) and histone deacetylase (HDAC) proteins, respectively (Bannister and Kouzarides, 2011).

Histone methylation is unique in the sense that methyl groups do not contribute any charge, and thus likely do not significantly alter histone-DNA association on their own. Methylation occurs on lysine and arginine residues, and depending on the amino acid, mono-, di-, and even tri-methylation events are possible. Methylation of specific residues makes possible binding by various epigenetic factors, which can in turn alter chromatin structure. For instance, heterochromatin protein 1 (HP1) is known to bind the repressive methylation element, H3K9me3 (Bannister et al., 2001) while the active element H3K4me3 is recognized by other factors including PHD fingers (Bannister and Kouzarides, 2011).

Histone phosphorylation, like methylation, can either result in chromatin condensation or decondensation depending on context. Histone phosphorylation is accomplished by various histone kinases and occurs on serine, threonine, and tyrosine residues (Bannister and Kouzarides, 2011). It's somewhat surprising that attachment of a negatively-charged phosphate group to histone tails does not always result in looser histone-DNA affinity. However, some studies suggest that certain histone phosphorylation events can promote decoupling of HP1 protein from interphase scaffolding and thus enable mitotic spindle anchoring and further remodeling toward ultra-condensed metaphase chromosomes (Fischle et al., 2005; Hirota et al., 2005).

PARylation is another form of histone and general protein modification that is covered in detail in a subsequent section. In sum, covalent modifications of canonical core histones represent one mode of epigenetic control with many combinatorial permutations that ultimately dictate chromatin organization, gene expression and by extension, cell fate and function.

Histone structural variants and their functions

Aside from covalent modification of canonical core histones, another histone-driven mechanism of epigenetic modification is the substitution of entire core histones for structural variants encoded by separate genes. Unlike core histones which are largely transcribed from multiple gene clusters during S phase, histone variants for the most part are transcribed from single or relatively few genes in a replication-independent manner (Buschbeck and Hake, 2017). Of the four core histones, H3 and H2A in particular have the greatest variety of diverse structural variants with unique functional properties that they contribute to nucleosome assemblies and by extension, local chromatin architecture.

One H3 variant, known as CENP-A, has a histone domain that specifically localizes to centromere chromatin (Sullivan et al., 1994). Further, CENP-A is critical for establishing the domain and function of centromere chromatin, to the extent that CENP-A knockout is lethal in yeast and human cells (Black et al., 2007). Centromere function including kinetochore loading, checkpoint signaling during mitosis and chromosome segregation were all shown to be dependent on the histone domain of H3 variant CENP-A (Black et al., 2007). Interestingly, CENP-A is overexpressed in some cancers (Zink and Hake, 2016), suggesting that aberrant histone variant expression and/or deposition may lead to epigenomic disruption that potentially contributes to oncogenesis.

Another H3 variant described in the literature in some detail is the highly-conserved H3.3, which has broadly been characterized as a transcriptional activator (Ahmad and Henikoff, 2002). Interestingly, the amino acid sequence of H3.3 differs from canonical H3 by only four residues, yet this difference is sufficient to enable H3.3

incorporation independent of DNA replication, displacing canonical H3-containing nucleosomes in the process (Ahmad and Henikoff, 2002). Beyond general transcriptional activation, H3.3 also plays a role in maintaining genome integrity during development, as H3.3 knockout led to lethal chromosomal anomalies (Jang et al., 2015). H3.3 is thus an important example of how subtle changes in histone sequence can have profound effects on function.

A well-described structural variant of histone H2A is H2AX. Histone H2AX is phosphorylated at serine 139 upon DNA double-strand break formation (Rogakou et al., 1998). This γ-H2AX signal is initiated extremely rapidly upon exposure to γ-irradiation – reaching maximum signal intensity within 10 minutes, or phosphorylation of approximately 1% of total H2AX per 1 Gy of γ-irradiation (Rogakou et al., 1998). γ-H2AX subsequently serves as a beacon for components of the DNA-damage response including 53BP1, which in turn directs further signaling including cell cycle pause, damage repair, and/or apoptosis dependant on damage extent (Fernandez-Capetillo et al., 2002).

Another H2A variant of interest is H2A.Bbd (Barr-body deficient), originally described by its specific exclusion from the inactive X-chromosome, despite robust localization throughout the active X and autosomes (Chadwick and Willard, 2001a). Interestingly, H2A.Bbd has a relatively unique histone domain with only 48% sequence homology to canonical H2A (Chadwick and Willard, 2001a). Functionally, H2A.Bbd has been implicated in transcriptional activation, yet interestingly H2A.Bbd overexpression induces nucleosome destabilization and subsequent DNA damage hyper-susceptibility (Goshima et al., 2014). Thus, one could infer that H2A.Bbd is an example of a histone

variant whose spatiotemporal deposition patterns must be kept at the proper balance to ensure genomic stability.

H2AZ is another example of a structural variant of canonical core histone H2A. H2AZ is broadly associated with open and relatively nucleosome-sparse chromatin, and facilitates both self-renewal and differentiation in ESCs (Creyghton et al., 2008; Hu et al., 2013). Somewhat paradoxically, H2AZ facilitates both gene activation and silencing, which it accomplishes by enabling greater chromatin access to both active and repressive protein complexes (Hu et al., 2013). Additionally, H2AZ-H3.3 composite nucleosome core particles (NCPs) are particularly labile, and are able to simultaneously block heterochromatin spread while enabling transcription factor access at promoters and other regulatory elements (Jin et al., 2009). In this manner, H2AZ-H3.3 NCPs has been described as a 'placeholder' to prevent incorporation of more stable canonical NCPs and while maintaining local chromatin integrity despite low nucleosome density (Jin et al., 2009). H2AZ is thus a prime example of the versatility of function that histone variants can provide as a result spatiotemporal expression, epigenetic context, and the relative stability of histone-DNA interaction.

Histone variant macroH2A: form and function

Of all the histone variants, none are as drastically structurally distinct from its canonical counterpart as the histone variant macroH2A. While macroH2A contains an N-terminal histone domain which shares 64% sequence homology with canonical H2A, macroH2A also contains a large globular domain on its C-terminus known as a macrodomain, connected to its histone domain via a short linker (Pehrson and Fried,

1992). MacroH2A's macrodomain combined with its histone domain renders macroH2A nearly three times the size of canonical core histone H2A, making macroH2A the largest histone variant by far (Pehrson and Fried, 1992).

MacroH2A is very highly conserved throughout the vertebrate lineage, and is present in some sequenced invertebrate species including a sea urchin (*Strongylocentrotus purpuratus*), a tick (*Ixodes scapularis*), and an annelid worm (*Capitella teleta*) (Pehrson et al., 2014; Pehrson and Fuji, 1998). In mammals, macroH2A is encoded by two paralogous genes, *H2afy* and *H2afy2* (Costanzi and Pehrson, 2001; Pehrson and Fried, 1992). Alternate splicing of H2afy produces two distinct protein-coding transcripts, macroH2A1.1 and macroH2A1.2, while H2afy2 produces a single transcript, macroH2A2 (Costanzi and Pehrson, 2001; Pehrson et al., 1997; Rasmussen et al., 1999). Intriguingly, despite macroH2A's extensive evolutionary conservation, relatively little is understood about its function.

MacroH2A displays tissue-specific expression patterns, exhibiting particularly high expression in adult mouse liver and kidney, yet notably reduced expression in adult mouse thymus (Pehrson et al., 1997). Strikingly, macroH2A also exhibits age and developmentally specific expression differences within tissues, with less macroH2A protein in fetal mouse liver and kidney compared to adult counterpart tissue (Pehrson et al., 1997), and greater macroH2A chromatin content in old (24 month) mouse liver and lung compared to young (4 month) mouse chromatin (Kreiling et al., 2011). In agreement with this observed age and developmental macroH2A expression paradigm, macroH2A is depleted in undifferentiated mouse embryonic stem cells, yet macroH2A1.2 levels were shown to increase coincident with induction of embryonic stem cell differentiation *in vitro* (Pehrson et al., 1997).

7

A striking observation of macroH2A's chromatin deposition patterns is its localization to heterochromatic regions including the Xi (Costanzi and Pehrson, 1998; Hernández-Muñoz et al., 2005), senescence-associated heterochromatin foci (Kreiling et al., 2011; Zhang et al., 2005), and centromeres (Foltz et al., 2006). Additionally, macroH2A is noticeably depleted on transcriptionally active regions of the genome (Changolkar and Pehrson, 2006), leading to the hypothesis that macroH2A contributes to transcriptional silencing. Concomitantly, macroH2A was shown to fine-tune the spatiotemporal expression of HoxA cluster genes during retinoic acid-induced differentiation of embryonic stem cells (Buschbeck et al., 2009), suggesting a role for macroH2A in precision control of gene expression. MacroH2A1 was even shown to downregulate rRNA transcription, suggesting that macroH2A deposition can have far-reaching consequences for protein synthesis and thus cell growth and activity as a whole (Cong et al., 2014). The aforementioned studies highlight the general dogma that macroH2A is a transcriptional silencer. However, it is also known that macroH2A protects at least a subset of its target genes from silencing and in some cases even potentiates transcription (Chen et al., 2014; Gamble et al., 2010), emphasizing that context specificity should be taken into account with respect to macroH2A deposition.

Additional macroH2A functions and functional partners

While macroH2A remains relatively understudied compared to some histone variants, a multitude of studies have implicated macroH2A in a diverse array of mechanisms and functions. Interestingly, macroH2A1 knockout (KO) mice are significantly leaner, displayed greater glucose tolerance and higher energy expenditure

8

than their wildtype (WT) counterparts while fed a high fat diet (Sheedfar et al., 2015). Concomitantly, a separate study showed that macroH2A1 KO mice exhibit differences in liver lipid metabolic genes (Changolkar et al., 2007), further highlighting a role for macroH2A in modulating metabolism. This function may carry disease relevance as well, since in yet another study macroH2A1.2 overexpression was associated with an aberrant increase in liver fat accumulation, a hallmark of steatosis (Boulard et al., 2010). Interestingly, overexpression of the other H2AFY splice variant – the PAR-binding macroH2A1.1, was protective against fat accumulation, suggesting that the macroH2A1 splice variants may have opposing functions (Pazienza et al., 2014). This last result further suggests that factors that govern macrohistone splicing and/or loading may play a key role in dictating broad downstream gene expression and phenotypic processes.

MacroH2A has also been shown to participate in mechanisms that influence cell cycle kinetics. MacroH2A1.2's macrodomain was shown to suppress mitotic kinase VRK1's enzymatic activity during interphase and by doing so ensured proper spatiotemporal histone phosphorylation necessary for mitotic progression (Kim et al., 2012). MacroH2A was also shown to silence transcription of the TRPC3 and TRPC6 Ca^{2+} channels, which govern Ca^{2+}-dependent proliferation responses (Kim et al., 2013). MacroH2A1 knockdown in bladder cancer cells increased TRPC3/6 gene-proximal histone acetylation, Ca^{2+} influx, and in turn cell growth and invasion (Kim et al., 2013). It's tempting to speculate that these observed mechanisms may be at least in part responsible for macroH2A's purported tumor suppressive properties, yet many cancers reproducibly exhibit a relative increase in macroH2A1.2 isoform expression compared to its splice variant macroH2A1.1, suggesting that macroH2A1.1 may have stronger tumor

suppressive influences that have yet to be fully characterized. The influence of macroH2A on tumorogenesis is discussed in a later section.

With respect to H2AFY splicing, the RNA helicases Ddx17 and Ddx5 have been shown to influence macroH2A1 isoform choice – Ddx17/5 depletion results in increased macroH2A1.1 exon inclusion (Dardenne et al., 2012). Additionally, the QKI splicing factor has been shown to specifically promote macroH2A1.1 exon inclusion (Novikov et al., 2011). Regarding macroH2A localization, a few histone chaperones have been shown to promote macroH2A deposition or removal. The chaperone APLF was demonstrated to deposit macroH2A1 at pluripotency-related genes, which reduced their transcription during induced pluripotency (Syed et al., 2016). Conversely, the ATRX chaperone was shown to remove macroH2A1 from chromatin and instead favor loading octomers containing the transcription-activating H3.3 variant (Ratnakumar et al., 2012).

Several papers reveal mechanistic insights into macroH2A's methods for influencing local chromatin architecture and thus regulating transcription. One study showed that macroH2A preferentially associates with the repressive ACF nucleosome remodeling complex compared to the activating SWI/SNF complex (Chang et al., 2008). Interestingly, while macroH2A's histone domain was shown to reduce SWI/SNF nucleosome remodeling complex activity, macroH2A's nonhistone domain (consisting of the macrodomain plus the linker region) was shown to block chromatin access to the transcription factor NF-kB (Angelov et al., 2003). Another study showed that macroH2A's basic linker binds and stabilizes extranucleosomal DNA, increasing the stability of chromatin-histone association (Chakravarthy et al., 2012). These results together demonstrate that all three major macroH2A domains have properties that promote DNA compaction.

Contrary to dogma that macroH2A is a transcriptional silencer; a few studies have discovered macroH2A-dependant transcriptional activation mechanisms. MacroH2A1.2 was shown to bind muscle-specific enhancers in such a conformation that enabled binding of a muscle-specific transcription factor Pbx1, macronucleosome repositioning, and subsequent activation of downstream targets (Dell'Orso et al., 2016). Interestingly PARP1 was shown to specifically recruit the PAR-binding macroH2A1.1 isoform, which in turn directed H2B acetylation at lysines 12 and 120, conferring either epigenetic activation or silencing respectively (Chen et al., 2014). These results in sum demonstrate that the macroH2A isoforms have diverse and sometimes opposing function, and further emphasize the importance of context in understanding macroH2A's influence on epigenetic organization.

MacroH2A in stem cells and development

Several studies suggest that macroH2A guides cell fate during development and differentiation. Interestingly, macroH2A is present on the chromatin of oocytes, but upon fertilization this maternal macroH2A is actively depleted in a microtubule-dependant process as the zygote undergoes the first few divisions (Chang et al., 2005), suggesting that macroH2A may not be crucial for chromatin rearrangements in the early, epigenetically plastic embryo. At approximately the 8-cell embryo stage, zygotic macroH2A transcription and chromatin deposition initiates, and further globally increases thereafter in development (Chang et al., 2005), suggesting that macroH2A helps 'lock in' cell fate toward functional specialization in differentiation and development. In agreement with this, morpholino-based translational inhibition of macroH2A2 in the 24 hour

zebrafish embryo leads to severe developmental abnormalities in gross body structure (Buschbeck et al., 2009), suggesting that macroH2A may indeed be necessary for early developmental processes in the vertebrate embryo.

MacroH2A has been suggested to broadly promote cellular differentiation at the expense of stem cell self-renewal (Creppe et al., 2012). Specifically, macroH2A1 knockdown during differentiation of ESCs into embryoid bodies (EBs) significantly reduced the size and phenotypic cavitation of EBs compared to control knockdown (Creppe et al., 2012). Additionally, teratomas formed from macroH2A1-depleted ESCs were larger than control, yet found to contain more undifferentiated malignant carcinoma-like tissue and significantly less differentiated tissue (Creppe et al., 2012). In another assay, primary human keratinocyte (PHK) grafts containing stem cells were cultured in *in vitro* 3D cultures and concomitantly depleted of macroH2A1, and were found to have reduced expression of the differentiated skin cell marker involucrin compared to controls (Creppe et al., 2012). Additionally, PHKs were dissociated, seeded at low cell density, and plated to induce stem cell self-renewal and holoclone colony formation. Knockdown of either macroH2A1.1 or macroH2A1.2 increased colony formation, and macroH2A1.2 overexpression had the opposite effect – reduced colony formation, and by extension reduced stem cell self-renewal (Creppe et al., 2012). These striking results strongly suggest that macroH2A1 potentiates stem cell differentiation and limits stem cell self-renewal, even in adult stem cell populations.

Macrodomain-containing proteins other than macroH2A

Looking beyond macroH2A, several other macrodomain-containing proteins have been identified in all domains of life - bacteria, archaea and eukarya and even in some ssRNA viruses (Karras et al., 2005). Karras and colleagues describe macrodomains as functional binders of poly ADP-ribose (PAR) and other byproducts of NAD^+ metabolism. Karras et. al. extensively biochemically characterized the macrodomain-containing thermophile protein Af1521. In their work, they describe Af1521's ability to bind ADP-ribose and PAR with high affinity and hydrolyze a phosphoester bond in ADP-ribose *in vitro* (Karras et al., 2005). Crystal structure analysis of Af1521 and other macrodomain containing proteins revealed a highly-conserved ligand-binding pocket specific to ADP ribose, yet interestingly outside of this pocket the structure of the examined macrodomains varied considerably (Karras et al., 2005).

Interestingly, Karras and colleagues also demonstrated that the PARP-family member Bal/PARP9 protein has the capacity to bind both ADP-ribose and PAR, suggesting that it is capable of interacting with its own metabolic products (Karras et al., 2005). The authors conclude by suggesting that multiple macrodomain-containing proteins evolved with the specific capacity to bind ADP-ribose, albeit in different contexts dependant on protein location and function (Karras et al., 2005). The authors further postulate that ADP-ribosylation may be a general mechanism for guiding chromatin remodeling by attracting both soluble macrodomain proteins with chromatin-interacting functions as well as chromatin-bound macrodomain proteins such as macroH2A (Karras et al., 2005). It is thus unusual that only the macroH2A1.1 isoform displays an affinity for ADP-ribose, a feature that even its splice variant macroH2A1.2 lacks (Karras et al., 2005). As such, caution must be taken when interpreting studies that investigate

13

macroH2A1 mechanisms but do not employ methodologies that distinguish between macroH2A1.1 and macroH2A1.2, as both PAR-binding-dependant and PAR-binding-independent processes may be at play.

Poly ADP-ribosylation, Parp-1, and interactions with macroH2A

Since the macrodomain of only one macroH2A isoform, macroH2A1.1, has the unique functional capacity to bind poly-ADP ribose (PAR) and PARylated moieties, (Karras et al., 2005; Kustatscher et al., 2005), PARylation is worth exploring in some detail. In brief, PAR synthesis is catalyzed from a nicotinamide adenine dinucleotide (NAD^+) donor via the actions of a family of proteins known as poly ADP ribose polymerases (Parps), the most well-studied being Parp-1 (Kim et al., 2005). In brief, Parps catalyze the transfer of ADP-ribose units from NAD^+ onto protein substrates, generating free nicotinamide in the process (Kim et al., 2005). Poly-ADP ribose glycohydrolase (Parg) proteins accomplish the converse reaction: hydrolysis of ADP ribose units from PARylated proteins, producing free ADP ribose in the process (Kim et al., 2005).

PAR has been described as the "third type of nucleic acid" in addition to DNA and RNA due to its unique polymeric structure, which can consist of as many as 200 consecutive ADP-ribose units *in vitro* with approximately one branching structure per 20-50 units (D'Amours et al., 1999). PAR chains are highly negatively charged and as such PARylation can serve as a highly dynamic mechanism for insertion of a particularly attractive (or repulsive) polymer (Kim et al., 2005). Both chromatin-associated and freely

diffusing proteins are capable of being PARylated, and the specific contexts of these modifications have far-reaching implications for epigenetics, cell fate and function.

One consequence of histone PARylation is regional chromatin decondensation, perhaps in part by PAR increasing local electrostatic repulsion (Poirier et al., 1982). Another mechanism of PAR-induced euchromatinization was discovered when linker histone H1 was shown to have a higher affinity for PAR than DNA itself; thus H1 PARylation highly destabilizes H1-DNA interaction and in turn locally relaxes chromatin (Malanga et al., 1998). Interestingly, it was shown that PAR-binding macroH2A1.1, but not non-PAR-binding macroH2A1.2, is capable of binding localized PAR signal and inducing chromatin re-condensation (Timinszky et al., 2009), perhaps suggesting that macroH2A1.1 sequesters PAR to reform heterochromatin. In another study, macroH2A was shown to inhibit Parp-1 enzymatic activity, suggesting that macroH2A maintains heterochromatin at least in part by limiting Parp-1's ability to PARylate histones and open up chromatin (Nusinow et al., 2007).

PARylation, Parp-1, and macroH2A all have roles in bolstering genotoxic stress responses. Parp-1 was shown to promote survival following exposure of mice and murine cells to γ-irradiation induced DNA damage (de Murcia et al., 1997). Of particular interest, Parp-1 knockout mice exposed to 8 Gy of whole-body irradiation died of acute small intestine injury, suggesting that Parp-1 contributes to the intestinal stem cell driven regeneration response (de Murcia et al., 1997). Interestingly, both Parp1 and macroH2A have been shown to guide DNA damage repair (DDR). Parp1 is recruited to DNA break sites where it PARylates itself and local chromatin, ultimately enabling access for DDR machinery including the DDR protein scaffold, Xrcc1 (Mortusewicz et al., 2007). In another example, PARP-1 and macroH2A together were shown to bolster homology-

driven repair by ultimately recruiting BRCA1 to break sites (Khurana et al., 2014). Finally, excess accumulation of PAR as a consequence of DNA damage can induce cell death by a unique mechanism known as parthanatos, which in the briefest of terms is characterized by Parp-1 overactivation, recruitment of the macrophage mitigation inhibitory factor nuclease into the nucleus, and ultimately widespread genomic DNA lysis (David et al., 2009; Gupte et al., 2017). Overall, one might speculate that since macroH2A is known to limit Parp-1 activity (Nusinow et al., 2007), by extension macroH2A may also limit excessive Parp-1 activation and in turn protect against at least one mechanism of cell death. Thus, it's apparent that Parp-1, PARylation, and macroH2A together are key players on a cooperative axis of the DDR, and can impose checks and balances upon one another to guide cells toward DNA damage repair and survival, or alternatively cell death in the advent of overwhelming genotoxic insult.

MacroH2A's contribution to genomic stability and the DNA damage response

MacroH2A has been shown in several contexts to uphold genome integrity against genotoxic stressors. In one study, macroH2A1 was shown to buffer against gene expression changes and reduce transcriptional "noise" in Namalwa cells following induction of genotoxic stress by Sendai virus infection (Lavigne et al., 2015). Specifically, macroH2A1 was shown to maintain robustness of gene expression against environmental perturbations, and this property was shown to depend at least in part on macroH2A's interaction with the transcription factor NRF-1 (Lavigne et al., 2015). Interestingly, this study provides another example of macroH2A's ability to 'fine-tune' gene expression by showing that macroH2A nucleosomes stably block activator-binding

sites of repressed genes and silencer-binding sites of active genes, effectively minimizing promiscuous gene activation or silencing (Lavigne et al., 2015). In another example of this phenomenon, macroH2A1.1 and PARP-1 were shown to cooperatively occupy the promoter of the hsp70 gene in HeLa cells, effectively silencing transcription (Ouararhni et al., 2006). Upon heat shock initiation, macroH2A1.1 and PARP-1 were shown dissociate from the hsp70 promoter and enable transcription of components of the heat shock response (Ouararhni et al., 2006), providing yet another example of macroH2A enabling a robust and dynamic response to changing conditions, and upholding genomic integrity.

In several other studies, macroH2A has been shown to safeguard gene expression by promoting, directing, and bolstering the DNA damage response (DDR). In one example, 293T cells were rendered significantly more radiosensitive following macroH2A1 knockdown (Xu et al., 2012). In this system, 53BP1 foci formation following γ-IR was reduced in macroH2A1-depleted 293T cells, and phosphorylation of 53BP1-target Chk2 at threonine 68 was correspondingly reduced as well (Xu et al., 2012). In another study, the PAR-binding isoform macroH2A1.1 was recruited to DNA double-strand break (DSB) sites within seconds of targeted laser microirradiation of HeLa cells in a PARP1-dependant manner (Timinszky et al., 2009). Interestingly, the non-PAR binding splice variant, macroH2A1.2, was not recruited to DSB sites over the same time span. PAR-ylation of DSB-proximal elements by PARP1 is known to be an early signaling hallmark of the DDR (de Murcia et al., 1997), thus it's interesting to note that macroH2A1.1 deposition proximal to DSB sites is an early event in the DDR response as well.

Interestingly, while PAR-binding macroH2A1.1 is recruited to DSB sites within seconds of DSB induction and non PAR-binding macroH2A1.2 is initially depleted, 15 minutes later macroH2A1.2 is re-deposited and further enriched at DSB sites (Khurana et al., 2014). This initial macroH2A1.2 removal (and by extension macroH2A1.1 recruitment by PARP-1) is associated with a relative de-condensation of DSB-proximal chromatin, and the later macroH2A1.2 deposition phenomenon coincides with a relative local chromatin re-condensation (Khurana et al., 2014). This local heterochromatin is formed in part by macroH2A1.2's recruitment of the histone methyltransferase PRDM2, which locally increases the H3K9me2 heterochromatin mark (Khurana et al., 2014). PRDM2 then recruits BRCA1 to the DSB site, which in turn promotes key components of homology-directed repair (HDR) at the DSB site, without altering recruitment of 53BP1, a known mediator of the less-proofreading process of non-homologous end joining (NHEJ) (Khurana et al., 2014). Overall, macroH2A1.1 and macroH2A1.2 appear to work in concert to direct the DDR response and promote the choice of HDR over NHEJ (Khurana et al., 2014; Timinszky et al., 2009).

MacroH2A and cancer

Many studies identify macroH2A expression patterns in several cancers that suggest that macroH2A may have tumor suppressor properties (Cantariño et al., 2013), consistent with macroH2A's known role in upholding genomic integrity. For instance, macroH2A1.1 and macroH2A2 expression was shown to anti-correlate with tumor proliferation in lung cancer (Sporn et al., 2009). Further, macroH2A1.1 was shown to be up-regulated in lung tumor cells undergoing senescence, providing more granular insight

into macroH2A's tumor suppressive quality since senescence protects cells from malignant transformation (Sporn et al., 2009). MacroH2A loss or knockdown was also shown to correlate with increased melanoma proliferation and malignancy (Kapoor et al., 2010). This increased malignancy as a result of macroH2A knockdown coincided with transcriptional up-regulation of the CDK8 oncogene (Kapoor et al., 2010).

Importantly for the purposes of our study, macroH2A's purported tumor suppressor role has been shown to extend to colorectal cancer. In one study, the splice variants macroH2A1.1 and macroH2A1.2 were revealed to have distinct, and often opposing expression patterns across different colorectal cancer cell states (Sporn and Jung, 2012). Specifically, loss of macroH2A1.1 and gain of macroH2A1.2 expression was observed in primary human colorectal cancers compared to healthy tissue (Sporn and Jung, 2012). Additionally, observed macroH2A1.1 loss was correlated with greater metastatic phenotype *in vitro* and worse prognostic outcome in human patients, further highlighting the PARP-binding macroH2A1.1 as the true tumor suppressor isoform of macroH2A (Sporn and Jung, 2012).

Intriguingly, another study showed an opposing role for macroH2A in cancer; specifically that macroH2A1 can also potentiate silencing, heterochromatin formation, and hypermethyllation of the promoter of the tumor suppressor gene p16 in colorectal cancer (Barzily-Rokni et al., 2011). While Barzili-Rokni and colleagues also found that macroH2A1 knockdown in combination with DNA demethylation reversed p16 silencing and decreased cell proliferation, the pan-macroH2A1 knockdown cannot distinguish between the effects of knockdown of the individual splice variants of macroH2A1 (Barzily-Rokni et al., 2011). It's tempting to speculate that the non PAR-binding macroH2A1.2 was the isoform primarily responsible for p16 silencing as described in this

study, since the PAR-binding macroH2A1.1 splice variant has been described as a tumor suppressor in other systems, with minimal such behavior convincingly attributed to macroH2A1.2.

Induced pluripotent stem cell reprogramming

The *in vitro* dedifferentiation of somatic cells back to a pluripotent state via induced pluripotent stem cell (iPSC) reprogramming technology holds tremendous promise for the generation of cells for regenerative medicine. In 2006, Takahashi and Yamanaka first demonstrated in a Nobel-prize winning body of work that differentiated cells can be reprogrammed back into pluripotency via expression of just four transcription factors – Oct4, Sox2, Klf4 and c-Myc (Takahashi and Yamanaka, 2006). During this drastic transition, a somatic nucleus must undergo considerable chromatin remodeling to undo epigenetic marks of differentiation and reacquire a pluripotent epigenetic identity. Due to the stochastic nature of iPSC reprogramming, It's understood that such chromatin-remodeling events can be rate limiting (Hanna et al., 2009). Since iPSC generation is a time and labor-intensive process, greater understanding of the epigenetic transitions between cell states is paramount to reducing the costs and increasing the efficiency of iPSC reprogramming.

Several groups have manipulated components of the epigenome and achieved improvements in iPSC reprogramming efficiency. One group showed that supplementation of valproic acid, an HDAC inhibitor, dramatically increased reprogramming efficiency (Huangfu et al., 2008). Another study found that treatment of cells with the maintenance methyltransferase Dnmt1 inhibitor 5-aza-cytidine also

resulted in significant increase in iPSC reprogramming efficiency (Mikkelsen et al., 2008). Yet another group showed that overexpression of constituents of the BAF ATP-dependent chromatin remodeling complex improved reprogramming efficiency by allowing greater Oct4 binding at pluripotency promoters (Singhal et al., 2010). These studies in sum suggested that certain forms of euchromatinization might enable greater Yamanaka factor access and thus accelerate reprogramming. This notion is consistent with the idea that ESC chromatin is globally transcriptionally hyperactive compared to somatic chromatin (Efroni et al., 2008).

Interestingly however, another study suggested that at least some forms of heterochromatin are necessary to induce and maintain pluripotency. H3K27 methyltransferase EZH2 inhibition was shown to antagonize iPSC generation due to a reduction of repressive H3K27me3 accumulation at fibroblast-specific loci during reprogramming (Onder et al., 2012). This result suggests that histone methylation may be an important mechanism for silencing lineage-specific genes in pluripotent cells, and highlights the importance of context and location of specific epigenetic marks in defining the epigenetic landscapes of pluripotent and differentiated cells. Therefore, it's easy to imagine the need for acquisition of 'repressive' marks such as macroH2A at some sites during iPSC reprogramming, and conversely the loss of macroH2A at other loci to remove silencing at some genes and induce silencing at others.

MacroH2A's role in induced pluripotent stem cell reprogramming

Since macroH2A chromatin content increases during development, and macroH2A has been shown to promote stem cell differentiation and limit stem cell self-

renewal, it follows that macroH2A removal at key genes, particularly those of the pluripotency network may be epigenetic bottlenecks during iPSC reprogramming.

With respect to epigenetic differences between pluripotent and somatic cells, one study in particular detailed key differences between the epigenome of mESCs and MEFs as pertaining to phenomena of macrohistone deposition, localization and dynamic incorporation and turnover (Yildirim et al., 2014). Histone turnover has previously been described as a mechanism for establishing boundaries that prevent the lateral spread of epigenetic states, including the spread of heterochromatin (Dion et al., 2007; Mito et al., 2007). To address whether rapid histone turnover occurs for macroH2A, Yildirim and colleagues employed dox-inducible HA-tagged macroH2A2 expressing mESCs and MEFs. Using these cell lines, Yildirim et al. conducted a pulse-chase study in which anti-HA ChIP was performed over a time course to visualize kinetics of macroH2A2 genome-wide incorporation. Importantly, HA-tagged macroH2A2 was shown to not incorporate into ectopic genomic loci, as commercial macroH2A2 antibody ChIP was performed in parallel and yielded a nearly identical collection of macroH2A2 incorporation loci throughout the genome.

In comparison with the native macroH2A2 ChIP, the anti-HA ChIP revealed subsets of total macroH2A2-enriched loci that exhibited particularly rapid incorporation and turnover kinetics. An especially interesting subset of genes in mESCs exhibited dynamic macroH2A2 incorporation and turnover proximal to the transcriptional start sites (TSS), and this category of genes trended toward particularly high transcription when compared to genes with relatively little macroH2A turnover. Interestingly, the overall proportion of genes in MEFs that exhibited this particular TSS-proximal turnover quality was significantly reduced compared to mESCs, highlighting an important distinction

22

between pluripotent and somatic chromatin. Further, MEFs were also observed to acquire large domains of stable macroH2A incorporation compared to mESCs. These results in sum suggest that during the reprogramming of a somatic nucleus toward pluripotency, removal of stable-associated macroH2A from certain loci likely occurs in tandem with re-emergence of dynamic macroH2A incorporation and turnover at other loci. This study highlights the importance of distinguishing between stable histone incorporation versus dynamic incorporation and turnover, a distinction that standard ChIP-Seq assays alone typically overlook.

Another interesting observation is that macroH2A is actively removed from somatic chromatin during somatic cell nuclear transfer reprogramming independent of cell division (Chang et al., 2010). This study suggests that at least a subset of chromatin-bound macroH2A may be antagonistic to pluripotency. Additionally, macroH2A1 knockdown experiments in mESCs during retinoic acid induced differentiation demonstrated that that macroH2A facilitates differentiation at least in part by silencing pluripotency genes (Creppe et al., 2012). Indeed, it was also shown that macroH2A knockdown in various cells including murine dermal fibroblasts, adult neural stem cells, and human keratinocytes increased pluripotency induction efficiency and macroH2A overexpression reduced efficiency (Barrero et al., 2013a; Gaspar-Maia et al., 2013; Pasque et al., 2012), reinforcing the idea that macroH2A is an epigenetic barrier to pluripotency induction. However, the exact extent to which macroH2A is an epigenetic barrier to iPSC generation and the specific mechanisms by which macroH2A ostensibly impedes reprogramming remain somewhat nebulous.

One hint toward a mechanism of macroH2A's antagonism toward iPSC reprogramming was revealed by macroH2A ChIP-qPCR studies, which showed greater

macroH2A deposition at pluripotency genes Oct4 and Sox2 in mouse embryonic fibroblasts relative to ESCs (Pasque et al., 2012). However, macroH2A overexpression in ESCs did not drastically alter pluripotency gene expression or interfere with ESC maintenance (Pasque et al., 2012; Yildirim et al., 2014). Indeed, it's possible that macroH2A histone variants, while overexpressed, were simply not being stably incorporated into ESC chromatin to induce silencing. Indeed, the macroH2A-loading histone chaperone APLF – which is lowly expressed in ESCs – was shown to deposit macroH2A1 at pluripotency-related genes in MEFs (Syed et al., 2016). Additionally, it's possible that even if macroH2A were being incorporated into pluripotent gene-proximal chromatin, such incorporation might be insufficient or insufficiently stable to induce heterochromatin formation and subsequent transcriptional silencing of the robust ESC pluripotency gene expression network.

Another piece of insight into macroH2A's mechanism of pluripotency antagonism was demonstrated via examining UCSC Genome Browser ChIP-Seq profiles, which showed a broad presence of macroH2A1 and macroH2A2 domains that extend along and beyond the gene bodies of pluripotency network genes Oct4 and Nanog (Gaspar-Maia et al., 2013). These macroH2A-enriched domains were co-occupied with transcriptional silencing mark H3K27me3, and relatively depleted of transcriptional activating mark H3K27ac (Gaspar-Maia et al., 2013). Interestingly, however, the global H3K27me3 profile of macroH2A DKO genes in adult murine dermal fibroblasts was not strikingly different from that of macroH2A WT dermal fibroblasts, suggesting that other layers of epigenetic transcriptional silencing may be epistatic to macroH2A, and thus macroH2A knockout may be of little consequence (Gaspar-Maia et al., 2013), and under normal circumstances may not drastically alter gene expression.

Interestingly, Gaspar-Maia & colleagues also overlayed their macroH2A ChIP-Seq profiles in dermal fibroblasts with a published gene subset that exhibited aberrant H3K27me3 patterns upon depletion of the *Utx* histone demehtylase (Gaspar-Maia et al., 2013), a demethylase shown to be crucial for early iPSC reprogramming events (Mansour et al., 2012). A portion of these genes contained domains co-occupied by H3K27me3 as well as macroH2A, and included transcription factors activated early on in pluripotency induction including Sall1 and Sall4 (Gaspar-Maia et al., 2013). Strikingly, Sall1 and Sall4 activation kinetics following reprogramming factor infection were significantly accelerated in macroH2A DKO fibroblasts relative to WT (Gaspar-Maia et al., 2013), suggesting that one possible mechanism of macroH2A's blocking of reprogramming is the impediment of *Utx*-mediated demethylation of H3K27 and subsequent activation of these early pluripotency genes.

Another group suggests that macroH2A antagonizes iPSC reprogramming by preventing the regain of H3K4me2 at key genomic loci including pluripotency genes (Barrero et al., 2013a). Barrero and colleagues performed macroH2A1 ChIP-Seq in human keratinocytes and observed robust co-localization with the repressive H3K27me3 mark at lowly transcribed genes, and similar macroH2A enrichment at bivalent chromatin domains (Barrero et al., 2013b). Knockdown of macroH2A during iPSC reprogramming increased re-deposition of H3K4me2 at pluripotency genes and other bivalent domains, and concomitantly iPSC reprogramming efficiency was enhanced (Barrero et al., 2013b). Barrero and colleagues present an interesting mechanism in which macroH2A prevents acquisition of activating chromatin marks (H3K4me2/3) at certain bivalent loci, effectively guarding against otherwise aberrant cellular reprogramming or differentiation events.

This study further supports the increasingly apparent notion that macroH2A 'locks in' cell epigenetic identity and in turn upholds cell identity and function.

The intestinal epithelium

The mammalian intestinal epithelium is an especially attractive model for the study of adult stem cell dynamics. The tissue is effectively a single epithelial cell layer primarily tasked with nutrient absorption and highly compartmentalized into repeating units of fingerlike projections known as villi continuous with invaginations into surrounding mesenchyme known as crypts of Lieberkühn (crypts). Intestinal stem cells (ISCs) reside at the base of the crypt where they progressively migrate up the crypt-villus axis and differentiate as a result of Notch signaling input (Fre et al., 2005). Cells slated to become enterocytes first generate transit-amplifying (TA) intermediates, which rapidly divide to expand the numbers of absorptive cells that are produced from a single ISC. These absorptive progenitors migrate further upward and form enterocytes, which constitute the vast majority of differentiated villus cells.

Secretory progenitors result from Notch ligand *Dll1* expression, which in short order induces terminal differentiation and cell cycle exit (Stamataki et al., 2011). Secretory progenitors then migrate up the villus to form mucous-producing Goblet cells or hormone-producing enteroendocrine cells, or migrate back downward into the crypt to produce Paneth cells, which produce antimicrobial defenses including Lysozyme C. Excluding the long-lived crypt-resident Paneth cells, differentiating intestinal epithelial cells continually migrate upward into the villus where they terminally differentiate prior to ultimately undergoing apoptosis and sloughing off into the intestinal lumen. This process

qualifies the intestinal epithelium as the most highly proliferative solid tissue, with a complete turnover of cells from crypt to villus taking place over 3-5 days in the adult mouse.

Due to such high turnover and potential for tissue injury as a result of environmental perturbations and DNA replication errors, the intestinal epithelium relies on a robust and responsive ISC compartment with high proliferative capacity. This proliferative capacity is made possible by canonical Wnt signaling (Pinto et al., 2003), which is 'on' at the base of the intestinal crypt and 'off' further up toward the villus. The ISC niche – specifically the source of Wnt ligand – was originally proposed to be the Paneth cell (Sato et al., 2011). However, direct Paneth cell ablation was shown to not alter ISC function, and rather a population of Wnt ligand-secreting Fox1l^{+} subepithelial mesenchymal cells were elegantly shown to constitute the ISC niche (Aoki et al., 2016). This localized source of Wnt defines the intestinal stem cell zone, and therefore a Wnt[high] genetic signature and the proliferative capacity it bestows defines the most abundant and best characterized ISC subpopulation, the crypt-based columnar ISC.

Crypt-based columnar intestinal stem cells

The base of the intestinal crypt was originally thought to only contain the differentiated Paneth cells until slender cells interspersed between the Paneth cells were first observed (Cheng and Leblond, 1974). Cheng and Leblond termed these cells crypt-based columnar cells (CBCs) based upon their location and appearance, and observed that CBCs divided quite rapidly – about once a day – and appeared to self-renew and give rise to other cell types within the intestine, suggesting stem cell activity. In the

intervening years, the Clevers group has extensively characterized CBC ISCs via insertion of reporter genes into and under the control of the canonical Wnt target gene, *Lgr5* (Barker et al., 2007).

Lgr5[+] CBCs divide roughly daily and give rise to sufficient numbers of all differentiated intestinal cell types to accommodate the tissue's rapid turnover (Barker et al., 2007). CBCs undergoing differentiation migrate up the crypt-villus axis, initially producing transit-amplifying (TA) cells that divide rapidly prior to terminal differentiation and ultimate shedding into the intestinal lumen (Barker et al., 2007; Cheng and Leblond, 1974). These results suggest that CBCs, also termed 'active' ISCs, are responsible for much of the day-to-day homeostatic maintenance of the intestinal tissue. Interestingly, isolated whole intestinal crypts (which contain on average 15 Lgr5^{+} ISCs – significantly more than other putative ISC types), or even FACS-sorted single Lgr5 cells can be induced to produce organoid structures containing analogous *in vivo* structures *ex vivo*, demonstrating further that Lgr5 cells contain the capacity to recapitulate the intestinal tissue as a whole (Barker et al., 2010; Sato et al., 2009).

Through utilization of a Lgr5-driven Confetti reporter, Lgr5^{+} ISCs were also shown to clonally compete for crypt dominance, with CBCs at the Wnt[high] crypt base harboring a competitive advantage compared to CBCs at the Wnt[low] transit-amplifying zone (Ritsma et al., 2014). This result is strong evidence that CBCs are driven to proliferate and self-renew via canonical Wnt activity. Canonical Wnt activity was also shown to specifically sensitize CBCs to γ-irradiation-induced damage irrespective of cell cycle kinetics (Tao et al., 2015). Concomitantly, Lgr5^{+} CBCs have been largely characterized as radiosensitive with widespread CBC apoptosis observed at doses 12Gy and above (Asfaha et al., 2015; Barker et al., 2007; Hua et al., 2012; Metcalfe et al., 2014; Yan et al., 2012). As

such, whole-body irradiation is a useful tissue regeneration model to quantitatively ablate CBCs and test the regenerative capacity of non-CBC ISCs.

Significantly, although Lgr5$^+$ CBCs strongly contribute to homeostasis (Barker et al., 2007; Ritsma et al., 2014), they are dispensable for intestinal homeostasis as well (Metcalfe et al., 2014; Tian et al., 2011). This result strongly suggests the presence of a reserve ISC compartment or an otherwise compensatory cell population that can replenish the intestinal epithelium upon Lgr5$^+$ cell loss. Indeed, specific Lgr5$^+$ cell ablation leads to greater lineage tracing from cells marked with a *Bmi1-CreER* knock-in allele, one genetic marker of putative reserve ISCs, which I will discuss in detail below.

Reserve ISCs and their relationship with CBCs

The idea that the intestinal epithelium is host to a long-term, quiescent stem cell population that is resistant to genomic mutations has existed for decades. However, the notion that a reserve ISC population exists that is molecularly, functionally and positionally distinct from the relatively recently described Lgr5$^+$ CBC population has generated a modicum of controversy. In the 70s, Potten and colleagues described a label-retaining cell at position +4 with respect to the base of the crypt that was postulated to be a crypt stem cell population (Potten et al., 1974). Counter-intuitively, Potten's +4 label-retaining cell (LRC) was shown to be radiation-sensitive (Potten, 1977). However, several more recent reports have argued that there is at least one population of reserve, radioresistant stem cells at the +4 position (Montgomery et al., 2011; Sangiorgi and Capecchi, 2008; Takeda et al., 2011).

Sangiorgi and Capecchi originally described a +4-positioned crypt stem cell marked by insertion of a tamoxifen-inducible CreER into the locus of *Bmi1*, a Polycomb complex protein-encoding gene. The authors demonstrated that *Bmi1-CreER*^{+} cells are slow-cycling, give rise to all differentiated intestinal cells, and Bmi1 cell ablation results in crypt depletion (Sangiorgi and Capecchi, 2008). Importantly, another group revealed that unlike Lgr5^{+} CBCs, *Bmi1-CreER*[+] ISCs aren't dependent upon Wnt for survival, are highly radioresistant, and rarely divide during homeostasis (Yan et al., 2012). Importantly, upon Lgr5+ CBC ablation, greater lineage tracing is induced from *Bmi1-CreER*^{+} cells, suggesting that these cells may represent a reserve ISC population (Tian et al., 2011). It was further shown that single sorted *Bmi1-CreER*^{+} cells are capable of generating intestinal organoids containing Lgr5^{+} cells in vitro, suggesting that *Bmi1-CreER*[+] reserve ISCs sit at the top of the ISC hierarchy (Yan et al., 2012).

Another group revealed that a mouse telomerase reverse transcriptase (mTert)-driven tamoxifen-inducible CreER transgene could recapitulate many of the phenotypic properties of Bmi1-CreER-marked cells, including rare cell division, radioresistance, multipotent differentiation and contribution to post-irradiation regeneration (Montgomery et al., 2011). This result is particularly interesting, as telomerase is known to provide cellular senescence resistance by preventing the loss of telomerase ends during iterative rounds of cell division, a likely useful property for a putative long-lived reserve stem cell.

Another body of work led by Takeda and colleagues demonstrated that insertion of a tamoxifen-inducible CreER into the *Hopx* locus, which encodes the atypical homeobox protein Hopx, marks an ISC population at least partially functionally overlapping with *Bmi1-CreER*[+] ISCs. *Hopx-CreER*[+] reserve ISCs were further shown to be radioresistant and regenerate intestinal epithelium (Yousefi et al., 2016). These

results further suggest a hierarchical stem cell model for the intestinal crypt that places rare, quiescent, radioresistant reserve stem cells above the more abundant mitotically and radiosensitive active stem cells. Interestingly however, Lgr5^{+} cells were also shown to give rise to Hopx^{+} cells – suggesting that interconversion between ISC populations is possible and perhaps further suggests that ISC populations are relatively epigenetically plastic with respect to one another (Takeda et al., 2011).

The Clevers group has argued against the existence of functionally distinct ISC populations and interconversion thereof, and instead suggest a single or continuum ISC model by proposing that putative ISC subpopulations exhibit at least partial transcriptional and functional overlap (Itzkovitz et al., 2011; Muñoz et al., 2012). One study showed via fluorescent in-situ hybridization that Lgr5, mTert and Bmi1 mRNA co-localize within many intestinal crypt cells (Itzkovitz et al., 2011). Another study revealed via bulk transcriptome and proteome analysis of *Lgr5-CreER* derived cells that Bmi1, mTert and Hopx mRNA and protein were all present within at least a subpopulation of the aforementioned cells (Muñoz et al., 2012).

However, single-cell transcriptomic studies performed in the Lengner lab revealed that while indeed Hopx and Bmi1 mRNA was present to a higher degree in Lgr5^{high} cells versus Lgr5^{low}, *Hopx/Bmi1-CreER* nevertheless marked a molecularly and functionally distinct population of cells compared to *Lgr5-CreER[+]* CBCs (Li et al., 2014). While Li and colleagues place reserve ISCs marked by *Hopx/Bmi1-CreER* (in which *Hopx-CreER* marks a more uniform population) at the top of a hierarchical model, they and others acknowledge that Hopx[+] ISCs conduct at least some of their function, including post-irradiation intestinal regeneration through generation of Lgr5^{+} cells. This hypothesis is particularly supported by work from the de Sauvage group, which

employed an Lgr5-driven diptheria toxin ablation model to specifically eliminate Lgr5$^+$ cells. While Lgr5$^+$ cell destruction during homeostasis was inconsequential – suggesting a compensatory cell population (Tian et al., 2011), Lgr5$^+$ cell ablation in combination with intestinal irradiation led to complete tissue catastrophe (Metcalfe et al., 2014). This result supports the notion that reserve-ISC-driven intestinal regeneration depends on the generation of mitotically active and proliferative Lgr5$^+$ CBC intermediates, and reinforces the hierarchical model of ISC dynamics.

In sum, current literature underscores controversy in the field with respect to reserve ISCs and ISC delineation as a whole. However, all studies strongly argue in favor of a high degree of epigenetic plasticity within the intestinal epithelium – whether through interconversion of distinct ISC subtypes or a continuum of epigenetic identities within one large and highly heterogeneous ISC population. The specific epigenetic factors that govern ISC and intestinal epithelial cell identity at large require further characterization.

Epigenetics of the intestinal epithelium

The influences of epigenetic modifiers within ISCs and how chromatin organization relates to cell identity and function within the intestinal epithelium remain relatively understudied. Indeed, much remains to be characterized with respect to DNA modifications, histone modifications, and particularly histone variant substitution within the intestinal epithelium and the consequences thereof.

With respect to DNA modification, the DNA methyltransferase Dnmt1 was shown to be necessary for proper ISC differentiation and genomic stability in concert with the

de-novo DNA methyltransferase Dnmt3b (Elliott et al., 2016; Elliott et al., 2015). Additionally, DNA hydroxymethylation by the Tet1 enzyme was shown to be a critical process for governing expression of Wnt signaling related genes within ISCs (Kim et al., 2016), thus upholding ISC function.

Undoubtedly, a variety of histone modifications, histone modifying proteins and histone variant substitutions influence adult intestinal epithelial cell identity and function, yet few have been described in great detail. The DOT1L methyltransferase was shown to promote Wnt target gene transcriptional activation via deposition of the H3K79me2 mark in murine intestinal epithelial cells (Mahmoudi et al., 2010). In another study, the repressive histone mark H3K27me3 was shown to be acquired at key developmental genes in adult intestinal epithelial cells versus embryonic progenitors (Kazakevych et al., 2017). Further, Kazakevych and colleagues showed that the histone variant H2A.Z was shown to undergo broad depletion during ISC differentiation, suggesting that differential histone variant deposition may fine-tune intestinal epithelial cell identity.

Despite studies that point to the influence of epigenetic factors on intestinal cell identity, evidence interestingly also exists that at least a subset of intestinal epithelial cells' chromatin is quite epigenetically labile (Kim et al., 2014). Enhancers and regulatory elements for both secretory and absorptive progenitor lineage-specific genes were demonstrated to be 'primed' for activation within CBCs by the presence of activating chromatin marks H3K4me2 and H3K27ac, and these marks persisted during differentiation (Kim et al., 2014). In line with this finding, Dll1^{+} secretory progenitors were shown to be able to dedifferentiate into ISCs following irradiative damage (van Es et al., 2012), suggesting early ISC progeny retain considerable epigenetic plasticity. Even alkaline phosphatase expressing transit amplifying cells were shown to be able to

replenish ISCs upon Lgr5^{+} cell ablation (Tetteh et al., 2016), suggesting that a sizable population of differentiated intestinal epithelial cells may retain sufficient epigenetic plasticity to revert back to an ISC-like state when returned to a Wnt[high] niche.

In sum, many facets of the epigenome contribute to intricate chromatin rearrangements during cell state transitions in the intestinal epithelium and beyond, and the histone variant macroH2A has been described in several contexts to influence chromatin organization, remodeling, and cell state. In this work, we broadly sought to characterize the contributions of histone variant macroH2A to cell identity and epigenetic remodeling during iPSC reprogramming and adult ISC dynamics.

Chapter Two:

Materials and Methods

Mouse strains

All mouse experiments were performed under the purview of the University of Pennsylvania's Institutional Animal Care and Use Committee under protocol 803415 granted to Dr. Lengner. *Lgr5-eGFP-IRES-CreERT2* (JAX strain 008875) mice were acquired from The Jackson Laboratory. *Hopx-CreERT2* (JAX strain 017606) mice were a kind gift from Dr. Jon Epstein, and macroH2A DKO (JAX strain 025481) were kindly provided by Dr. John Pehrson. MacroH2A DKO and strain-matched 129S1/SvIm mice were crossed with *Lgr5-eGFP-IRES-CreERT2* or *Hopx-CreERT2::Rosa26-LSL-tdTomato* mice. *C57BL/6J-APC^{min}/J* mice were obtained from Jackson Laboratory (JAX strain 002020) and bred into a macroH2A DKO background in parallel with WT 129S1/SvIm mice.

Cell culture media

MEFs, 293Ts, PlatEs, CRCs, and most other general cell types unless otherwise stated were cultured in what I'll hereafter refer to as 'MEF media' – DMEM supplemented with 10% fetal bovine serum, penicillin/streptomycin, sodium pyruvate, nonessential amino acids and β-mercaptoethanol.

mESCs, iPSCs, and iPSC reprogramming experiments were cultured in what I'll hereafter refer to as 'ES media' – Knockout-DMEM/F12 media (Thermo Fisher) supplemented with 10% fetal bovine serum (Lonza), penicillin/streptomycin, l-glutamine, nonessential amino acids, β-mercaptoethanol and ESGRO LIF (Millipore).

Transfections and lenti/retroviral infections

For lentivirus production, 293T cells were grown to 60% confluence and transfected with 10 μg of backbone vector along with 7.5μg p-PAX2 and 2.5μg pMD.G packaging plasmids using Fugene HD transfection reagent (Promega) per manufacturer's instruction. Transfection media was changed the following morning and virus-containing media was strained through a 0.45-micron filter the following day. Viral media was then diluted 50/50 with fresh MEF media. MEFs were infected at 60% confluence and supplied 1x Polybrene (Millipore). Two consecutive days of infection were carried out followed by replacement of viral media.

For retrovirus production, platinum-E cells were transfected with 10μg backbone vector at 60% confluence using Lipofectamine transfection reagent (Thermo Fisher). Infection of target MEFs was carried out per method listed above for lentivirus.

iPSC reprogramming

MEFs were infected as described above with lentivirus encoding Yamanaka factors in a STEMCCA cassette – either 4F (OSKM) or 3F (OSK)-mCherry with either a Tet-inducible or constitutively active (CMV) promoter, experiment depending. Specific iPSC reprogramming experimental details are outlined within figure legends and diagrams in Chapter 3. BrdU incorporation assay was performed using BD Pharmingen BrdU Flow kit per manufacturer's instruction. Alkaline phosphatase positivity was determined using Vector Labs' Red AP kit per manufacturers' instructions on wells fixed with 4% paraformaldehyde. Images of AP-stained wells were captured using an iPhone 4S camera (Figures 3.4 & 3.6) or Samsung Galaxy S6 camera (Figure 3.7) – entirely

dependent upon which phone I had that particular year. Composite images of nanog immunofluorescence were taken using an EVOS FL Auto Imaging System (CDB microscopy core).

MacroH2A ChIP-Seq and ChIP-qPCR

In brief, Col1: TetO-macroH2A2-HA; Rosa26R: rTTA mESCs were trypsinized and plated onto gelatinized tissue culture plates. Subsequently, mESCs were exposed to 2 μg/mL doxycycline for 3, 6 and 12 hours after which they were crosslinked in 1% formaldehyde then lysed in SDS-Lysis Buffer with protease inhibitors. Chromatin was subsequently sonicated to 150-400 base pairs using a Bioruptor (UCD-200). Anti-HA (Abcam), anti-macroH2A2 (Abcam), anti-macroH2A1.2 (Abcam) or IgG control ChIP was then performed. ChIP-enriched chromatin was subsequently phenol-chloroform isoamyl alcohol and treated with RNAse (Qiagen) and CIP (NEB). Further in depth ChIP-Seq methods including library construction for deep sequencing, mapping and normalization and tile-based data analysis are further outlined in a previous report (Yildirim et al., 2014). Data is accessible via Gene Expression Omnibus Accession #GSE57665.

TetO-MacroH2A2-HA generation and mESC targeting

MacroH2A2 cDNA (MacroH2A2-MMM103-9201250, Open Biosystems) was subcloned in-frame with the HA-tag and then cloned via a unique *EcoRI* site into the pBS31 vector downstream of a PGK promoter and ATG start codon and an FRT recombination site along with a splice acceptor-double polyA cassette, tetracycline

operator (TetO) with a minimal CMV promoter, unique *EcoRI* site and an SV40 polyadenylation signal. This construct along with Flpe recombinase-expressing vector was then electroporated into KH2 mouse embryonic stem cells (which contain M2rtTA in the *Rosa26* locus and FRT-flanked *PGK-neomycinR* cassette upstream of promoterless ATG-less hygromycinR). Hygromycin-resistant colonies following flip-in reaction resulted in multiple iPSC clones that were verified for site-specific recombination at the *Coll1a1* locus via Southern blotting. The mESC products were functionally verified in Chapter 3, Figure 2.

Chimera generation and MEF isolation

mESC or iPSC clones for chimera generation were injected into BDF2 blastocysts and subsequently transplanted into pseudopregnant females. For MEF isolation, pregnant females were euthanized and E12.5 embryos were harvested, internal organs and brain tissue removed, and subsequently remaining embryo was diced and then trypsinized in 0.25% Trypsin-EDTA at 37ºC for 20 minutes. Digested embryos were then suspended in MEF media and plated onto two 15 cm plates per embryo. For further selection of transgenic MEFs, 2 μg/mL puromycin was added for 2 days and surviving MEFs were trypsinized for cryostorage.

Histology

Histology was performed at the Molecular Pathology & Imaging Core (MPIC) of the Penn Center for Molecular Studies in Digestive and Liver Diseases. In brief, mouse

small intestines were washed with DPBS and fixed overnight at 4°C in Zinc formalin (Polysciences Inc.). Following sectioning and tissue deparaffanization, antigen retrieval was performed with 10mM Tris base (pH 9.0) buffer using a pressure cooker.

For immunohistochemistry, sections were quenched of endogenous peroxidases by 3% H2O2, and sequentially blocked with Avidin D, biotin, and protein blocking reagents. Primary antibody incubation was conducted at 4°C overnight. Secondary biotinylated antibody was added at a dilution of 1:200, and incubated 2 hours at room temperature. Finally, sections were stained according to the ABC peroxidase protocol (Vector Laboratories) and counterstained with haematoxylin. Images were taken using an inverted Leica DM IRB microscope and analysis was performed using iVision software.

For immunofluorescence, sections were blocked with protein blocking reagent and incubated with primary antibody overnight at 4°C. Sections were washed in PBS and stained with fluorescent secondary antibodies (Jackson Laboratories) and counterstained with DAPI (Vector Laboratories). For immunofluorescence using mouse primary antibodies, a mouse-on-mouse (MOM) kit was employed (Vector Laboratories). Images were taken using a Nikon E600 microscope and fluorescent channel overlay and analysis was performed using iVision software. Specific primary antibodies and dilutions used were as follows: macroH2A1 (Abcam Ab37264, 1:200), macroH2A1.1 (CST #12455, 1:200), tdTomato (ClonTech 632392, 1:200), Ki67 (Abcam Ab15580, 1:200), Lysozyme C (Santa Cruz sc-27958, 1:200) ChgA (Abcam Ab15160, 1:1000), GFP (Abcam Ab6673, 1:200), cleaved caspase-3 (CST #9661) γ-H2AX (CST #9718, 1:200) and nanog (Bethyl laboratories # A300-397A, 1:100).

Isolation of intestinal epithelial cells

Mice were sacrificed and small intestine was dissected and cut open longitudinally. Villi were then scraped off using a microscope slide cover slip. Remaining tissue was then incubated with 5mM EDTA in HBSS for 30 min at 4°C to loosen crypts, and then manually pipetted up and down for mechanical dislodgement. Crypts were subsequently digested to single-cells with 0.66mg/ml Dispase (BD Biosciences).

Flow cytometry

Flow cytometry was performed on a BD LSR Fortessa cytometer (BD Biosciences). Single cells were selected by FSC height vs. FSC width and SSC height vs. SSC width plots. For *Hopx-CreERT2::Rosa26-LSL-tdTomato* mice, mice were injected with 2mg tamoxifen 18h prior to sacrifice and *tdTomato$^+$* cells were determined via a threshold established by an injected *Hopx-WT::Rosa26-LSL-tdTomato* negative control. For *Lgr5-eGFP-IRES-CreERT2* mice, eGFP+ threshold was established by an *Lgr5* WT mouse. All analysis was performed using FlowJo software. Cleaved-caspase 3 alexa-fluor 488 antibody (CST #9669) employed via BD Cytofix/Cytoperm (554714) kit per manufacturer's instructions. Fixable viability dye (Thermo Fisher 65-0865-14) was used to gate out dead cells.

Irradiation & regeneration, post-IR lineage tracing and apoptosis assays

For post-irradiation regeneration assessment, mice were treated with 12 Gy whole-body γ-irradiation and sacrificed 72h later at which point intestines were harvested and fixed overnight at 4°C in 4% paraformaldehyde, and processed for histology by the MPIC. Tissue sections were stained for proliferation marker Ki67. Ki67$^+$ crypts per 500μm were quantitated in each section.

For post-IR lineage tracing, macroH2A WT or DKO *Hopx-CreERT2::Rosa26-LSL-tdTomato* mice were injected with 2mg tamoxifen 48h and 24h prior to 12 Gy whole-body γ-irradiation, and 72h later they were sacrificed. Tissues were subsequently sectioned and stained for tdTomato using the MOM immunofluorescence kit (Vector Laboratories), and tdTomato$^+$ crypts were scored per 500μm.

For cleaved caspase-3 (CC3) flow cytometry, macroH2A WT or DKO *Hopx-CreERT2::Rosa26-LSL-tdTomato* mice were injected with 2mg tamoxifen 24h prior to 12 Gy whole-body γ-irradiation, and sacrificed 1 day later. Single crypt epithelial cells were isolated and stained with fixable viability dye (FVD) (eBioscience 65-0865-14) before BD Cytofix/Cytoperm fixation (554714) for 20 minutes at 4°C. Cells were then washed with BD Perm/Wash buffer before incubation with Pacific Blue-conjugated cleaved caspase-3 antibody (CST #8788S, 1:50) for 1 hour at 4°C. Hopx-tdTomato/CC3 double positive, FVD negative cells were then analyzed by flow cytometry.

In vitro organoid formation assay

Organoid culture was performed according to a published protocol(Sato et al., 2009). Crypt culture media consisted of Advanced DMEM/F12 supplemented with 1x B27 and N2 supplements (Invitrogen), 50 μM N-Acetylcysteine (Sigma-Aldrich), 50 ng ml^{-1} mouse EGF (Invitrogen), 1ug μL^{-1} R-Spondin (Wistar institute), 1ug μL^{-1} Noggin (Peprotech), and 3 μM GSK inhibitor CHIR99021 (Stemgent). After 7 days, intestinal organoids were qualitatively and quantitatively assessed. Organoid images were taken on a Nikon E600 microscope.

EdU incorporation assay

Hopx-Cre-ERT2::Rosa26-LSL-tdTomato mice were injected with 2mg of tamoxifen 18 hours prior to sacrifice, and then injected with 0.3mg of 5-EdU (Thermo Fisher) per 10g of body weight 2 hours prior to sacrifice. *Lgr5-eGFP-IRES-CreERT2* mice were injected with EdU 2 hours prior to sacrifice. Crypt epithelial cells were fixed and stained for EdU according to Click-iT® EdU Alexa Fluor® 647 protocol (Thermo Fisher). DNA was counterstained with DAPI. Flow cytometric analysis was performed as stated above on populations of *tdTomato*$^+$ or *GFP*$^+$ cells, comparing Alexa fluor 647 fluorescence to DNA content (DAPI).

Colorectal cancer cell proliferation (MTT) assay

RKO (ATCC stock number CRL-2577) or HCT116 (ATCC stock number CCL-247) cells were seeded in 6-well plates at 50,000 cells/well and cultured in DMEM with

10% FBS, 1% sodium pyruvate, and 1% L-glutamine 24 hours before siRNA transfection. The lipofectamine RNAiMax reagent (Invitrogen) was employed per manufacturer's instruction. Cell proliferation was assessed using Cell Proliferation kit I protocol (Roche). Absorbance of MTT assay was measured at 570 nm. The Stealth RNAis[TM] (Thermo Fisher) employed were siLuciferase control (Thermo Fisher 12935146), siH2AFY (Thermo Fisher HSS114259) and the macroH2A1 isoform-specific siRNAs used were of the following sequences:

siMacroH2A1.1: CACUGACUUCUACAUCGGUGGUGAA

siMacroH2A1.2: AGGCCAUAAUCAAUCCUACCAAUGC

Table 2.1: Sequences of qRT-PCR primers

Gene name	5'-3' forward sequence	5'-3' reverse sequence
Esrrb TSS	TAAGCTACGCCACTCAAGAAGCCA	ACGTGTCATGTATGGGCAAAGGG
hGAPDH	AGGGCTGCTTTTAACTCTGGT	CCCCACTTGATTTTGGAGGGA
hMacroH2A1.1	GGCCAAATCAATCCTACCAATG	TTCTCCAGCGTGTTTCCTAGGT
hMacroH2A1.2	GCCTCTTCCTTGGCCAGAA	CACTGTCGATCGAGGCAATGT
hMacroH2A2	CCATTCTGTCTTCTAAGAGCCTTGT	GGCTGATGTCACTCTGGGTTAAG
mActin	TGAACCCTAAGGCCAACC	AGGTCTCAAACATGATCTGGGTC
mMacroH2A1.1	GACATTGCCTCGATCGACAGT	CACCGGTGTAGAAGTCAGTGTTTG
mMacroH2A1.2	CCTCGGCCAGAAGCTGAA	TGGCCTCCACCTCAAAGC
mMacroH2A2	TGGCTGCGGTCATTGAGTAC	CAGCGTTCCCAGCCAACT

Table 2.2: Antibodies and dilutions

Antibody	Supplier, catalog #	Dilution/concentration	Applications
beta actin	Abcam, ab8227	1:1000	Western
CC3-AF-488	CST #9669	1:50	Flow cytometry
Chromogranin A	Abcam, ab15160	1:1000	IF
Cleaved caspase-3	CST #9661	1:200	IHC
GFP	Abcam, ab6673	1:200	IF
HA tag	Abcam, Ab18181	1:1000 ; 1:100	Western/IF ; ChIP
Histone H2A	Abcam, ab18255	5 μg/ml	ChIP
Ki67	Abcam, ab15580	1:200	IHC
Lysozyme C	Santa Cruz sc-27958	1:200	IF
MacroH2A1 (pan)	Abcam, ab37264	1:200	IHC
MacroH2A1.1 #1	John Perhson, Ph.D.	1:1000	Western, IHC
MacroH2A1.1 #2	CST #12455	1:200	IHC
MacroH2A1.2	John Perhson, Ph.D.	1:1000	Western, IHC
MacroH2A2	John Perhson, Ph.D.	1:1000	Western, IHC
mGAPDH	Abcam, ab9485	1:2000	Western
Nanog	Bethyl #A300-397A	1:100	IF
tdTomato	ClonTech, 632392	1:200	IF
γ-H2AX	CST #9718	1:200	IF

Chapter Three:

The histone variant macroH2A imposes a subtle

epigenetic barrier to pluripotency induction

Abstract

Epigenetic remodeling mechanisms are at the core of cellular transitions during development, differentiation and induced reprogramming. Induced pluripotent stem cells (iPSCs) show great promise for applications in regenerative medicine, yet questions remain about whether iPSCs are epigenetically similar or distinct from embryonic stem cells (ESCs). Furthermore, much remains to be known about which factors contribute to pluripotency at the epigenetic level, and how such epigenetic factors could be manipulated to increase efficiency of iPSC generation and therapeutic quality of the resulting cells. Studies of the epigenetics of pluripotency have placed much emphasis on differential epigenetic marks such as histone and DNA modifications, and the enzymes that catalyze the addition or removal of these modifications, but little investigation has been carried out with respect to the functional consequences of substituting canonical core histones for structural variants. One histone variant in particular, macroH2A, has been implicated in reinforcing a cell's epigenetic state during development, differentiation, and epigenetic reprogramming by somatic cell nuclear transfer (SCNT). Here, we develop and employ a macroH2A2 overexpression system to study macroH2A dynamics during iPSC reprogramming. We also generate 'secondary' macroH2A DKO MEFs with genome-integrated doxycycline-inducible iPSC reprogramming cassettes to determine whether addback of individual macroH2A isoforms alters reprogramming efficiency. We strikingly find that macroH2A undergoes significant dynamic incorporation and turnover behavior proximal to transcriptional start sites in mESCs compared to MEFs, and this behavior is associated with greater gene expression. We surprisingly observe little consequence as a result of macroH2A manipulation during iPSC

reprogramming, excluding a slight but statistically significant difference in macroH2A DKO MEFs achieving Yamanaka factor transgene independence at an earlier time point than comparable WT MEFs. In sum, we demonstrate that macroH2A imposes a subtle, but significant epigenetic barrier to acquisition of pluripotency, a more nuanced outlook than current literature suggests.

Introduction

Pluripotent stem cells have unlimited self-renewal capacity and are able to differentiate into any cell type within an organism. Understanding this unique quality is paramount to harnessing the power of pluripotency for applications ranging from disease modeling to regenerative medicine. While it's possible to derive patient-specific pluripotent cells through ectopic expression of transcription factors (Takahashi and Yamanaka, 2006), many challenges remain before induced pluripotent stem cells (iPSCs) may be used in the clinic. One such challenge is whether iPSCs are identical or similar to ESCs at the genetic and epigenetic level (Dai and Rasmussen, 2007; Hanna et al., 2010). Much attention in the field of the epigenetics of cellular developmental potency has been placed on studying histone and DNA modifications, yet an important and poorly understood facet of a cell's epigenetic signature is the substitution of canonical core histones for structural variants. One histone variant implicated in establishing or reinforcing specific epigenetic states is macroH2A.

MacroH2A is about three times the size of canonical core histone H2A (Pehrson and Fried, 1992), and is highly conserved from mammals to fish (Chakravarthy et al., 2005; Changolkar and Pehrson, 2006). In mammals, macroH2A exists as two genes

encoding three isoforms: macroH2A1.1, macroH2A1.2 and macroH2A2 (Costanzi and Pehrson, 2001; Pehrson et al., 1997). During development, macroH2A chromatin content progressively increases, particularly within transcriptionally silent domains (Chang et al., 2010; Chang et al., 2005; Nashun et al., 2010) such as the female silent X chromosome (Xi) (Changolkar and Pehrson, 2006; Hernández-Muñoz et al., 2005). Concomitantly, macroH2A content is markedly enriched within differentiated cells compared to pluripotent ESCs (Dai and Rasmussen, 2007; Hernández-Muñoz et al., 2005). MacroH2A content also increases with cell age and during senescence (Kreiling et al., 2011), consistent with the loss of overall cell and tissue proliferative capacity during ageing. MacroH2A was further shown in human pluripotent cell differentiation experiments to localize to both pluripotency and developmentally related genes during differentiation concomitant with their silencing (Barrero et al., 2013b). Thus, macroH2A may play a role in cell specialization via heterochromatin formation and gene silencing.

Studies of MacroH2A in different epigenetic states suggest that macroH2A is crucial for developmental processes but antagonistic to pluripotency. MacroH2A was shown to have a role in fine-tuning the spatiotemporal expression of HoxA genes upon RA-induced ESC differentiation (Buschbeck et al., 2009), suggesting that macroH2A guides and fine-tunes gene expression and chromatin orgaization during development. Conversely, in somatic cell nuclear transfer reprogramming, macroH2A is removed from somatic donor nuclei prior to the onset of cell division (Chang et al., 2010), implying that macroH2A removal may be an epigenetic roadblock to pluripotency acquisition. Further, macroH2A1 was shown to regulate the balance of self-renewal and differentiation in mouse ESCs (mESCs) (Creppe et al., 2012), specifically by potentiating stem cell differentiation at the expense of self-renewal. Correspondingly, macroH2A1 depletion in

mESCs impaired both RA-induced neural lineage differentiation and the formation of embryoid bodies, while simultaneously reducing the ability of differentiating cells to silence pluripotency genes (Creppe et al., 2012). This is strong evidence that macroH2A has a role in establishing epigenetic cell states, and specifically that macroH2A maintains cell differentiation at the expense of overall cell potency. Therefore, it's tempting to speculate that artificial maintenance of high macroH2A chromatin content during induced pluripotency of somatic cells may indeed impair the reprogramming efficiency.

Here, we show that although macroH2A exhibits differential genome localization and turnover patterns at key pluripotency genes in mESCs vs. MEFs consistent with the degree of transcription, macroH2A overexpression during iPSC reprogramming surprisingly doesn't significantly alter reprogramming efficiency. Further, macroH2A DKO MEFs do not reach certain early pluripotency hallmarks at an elevated rate than macroH2A WT counterparts when sex was not accounted for. Additionally, addback of individual macroH2A isoforms in macroH2A DKO MEFs did not significantly alter reprogramming efficiency relative to control. Intriguingly, we did observe a slight but significant increase in early pluripotency acquisition when comparing macroH2A WT female MEFs, which contain the macroH2A-rich Xi, to macroH2A DKO male MEFs. Finally, we determined that female macroH2A DKO MEFs have the capacity to achieve transgene-independent pluripotency at a slightly but significantly earlier time point than female macroH2A WT MEFs. In sum, our results suggest that the histone variant macroH2A has a minor influence on iPSC generation efficiency, and corroborate literature that suggests macroH2A removal is a key epigenetic remodeling event that occurs during induced pluripotency. However, our data caution against the notion that

relatively high macroH2A chromatin content in and of itself is a significant barrier to pluripotency induction, as in our hands the degree of macroH2A's retardation of reprogramming was determined to be quite subtle.

Results:

MacroH2A deposition at pluripotency genes in MEFs and mESCs

To gain insight into whether macroH2A content may influence both iPSC reprogramming efficiency and differential gene expression in mESCs and MEFs, we collaborated with Dr. Oliver Rando's lab at The University of Massachusetts Medical School to perform macroH2A2 chromatin immunoprecipitation followed by deep sequencing (ChIP-Seq) in MEFs and mESCs. Strikingly, we observed significant macroH2A2 enrichment in MEFs and concomitant depletion in mESCs across the bodies of genes that encode key pluripotency factors including including Oct4 (*Pou5f1*), alkaline phosphatase (*Alp1*), Nanog (*Nanog*) and Esrrb (*Esrrb*) (Figure 3.1 A). Of note, we observed particularly stronger peaks proximal to the promoters of *Pou5f1* and *Esrrb* in MEFs but not mESCs (Figure 3.1 A). *Esrrb* encodes a nuclear receptor critical for pluripotency that can substitute for Klf genes as a reprogramming factor (Feng et al., 2009). Next, wildtype mESCs and MEFs underwent ChiP for macroH2A2 or macroH2A1.2, and qPCR for the *Esrrb* transcription start site (TSS) was performed on resulting enriched DNA fragments (Figure 3.1 B). MacroH2A2, but not macroH2A1.2, was enriched at the *Esrrb* TSS in MEFs compared to ESCs. Since *Esrrb* undergoes lower transcription in MEFs versus ESCs, it's tempting to speculate that macroH2A2's *Esrrb* localization confers transcriptional silencing, and could suggest one mechanism by

which macroH2A may serve as an epigenetic barrier to pluripotency. Thus, macroH2A2 removal from *Esrrb* may be an important epigenetic bottleneck that a somatic cell must pass through during iPSC reprogramming. Conversely, macroH2A2 overexpression during iPSC reprogramming may hinder *Esrrb* activation and thus delay pluripotency.

Generation of a doxycycline-indcible macroH2A2 overexpression system

In order to test whether maintaining high macroH2A2 expression levels during iPSC reprogramming impairs reprogramming efficiency, we first generated drug-inducible macroH2A2-expressing mESCs to derive somatic cells for reprogramming experiments. Embryonic stem cells harboring a reverse tetracycline transactivator (M2rtTA) at the constitutively active ROSA26 locus were targeted with a tetracycline operator (TetO)-macroH2A2-HA cassette in safe-haven chromatin downstream of the Collagen I locus (Beard et al., 2006). We initially confirmed that these ESCs overexpress transgenic HA-tagged macroH2A2 protein upon doxycycline (dox) administration (Figure 3.2 A). Further, ESCs overexpressing macroH2A2 were morphologically and phenotypically normal (Figure 3.2 B). ESCs were injected into blastocysts and introduced into pseudopregnant mice, and MEFs were harvested from E12.5 embryos. The resulting MEFs exhibited robust dox-induced macroH2A2 overexpression and were morphologically normal (Figure 3.2 C).

Genome-wide macroH2A dynamic incorporation and turnover in mESCs.

In processes dependent on epigenetic remodeling such as iPSC reprogramming, studying stable histone variant deposition may be insufficient without taking into account the dynamic histone incorporation and turnover that occurs during epigenetic transitions. It has been shown in yeast that histone turnover is not random, and that high turnover regions flanking promoters enable chromatin architecture amenable to active transcription (Dion et al., 2007). Such a mechanism could account for macroH2A's less understood ability to protect a subset of its target genes from transcriptional silencing (Creppe et al., 2012; Gamble et al., 2010). To address this possibility, we took advantage of our mESCs with dox-inducible expression of HA-epitope-tagged macroH2A2 (Figure 3.2 A) to study macroH2A turnover dynamics.

MacroH2A2 overexpression in mESCs was induced for 3, 6, and 12 hours by dox addition. Anti-HA ChIP pulled down induced macroH2A2 protein, and sequencing identified sites of macroH2A2 incorporation into chromatin during these time intervals (Figure 3.3 A). Importantly, ChIP performed in parallel with a commercial anti-macroH2A2 antibody revealed a nearly identical macroH2A localization profile (Yildirim et al., 2014), strongly suggesting that transgenic macroH2A2 does not incorporate into any ectopic genomic loci. Patterns of macroH2A2 incorporation divided the genome into four groups: those with little incorporation, those with robust incorporation proximal to genes' TSS, and those with incorporation up- or downstream of the TSS (Figure 3.3 A). Transcriptome profiling determined the average gene expression levels for each category (Figure 3.3 B).

We observed clear transcriptional trends among distinct macroH2A2 turnover categories. Genes with little macroH2A2 turnover were the least expressed (however, these genes may contain high levels of stable endogenous macroH2A2, undetectable in this assay). Interestingly, genes with robust macroH2A2 incorporation near the TSS were the most transcribed on average (Figure 3.3 C), and included the pluripotency factor *Esrrb* (data not shown). These observations suggest that macroH2A2 turnover may maintain open promoter chromatin and thus enable transcription of at least some mESC genes. Interestingly, macroH2A2 turnover at promoters within more differentiated MEFs was shown to be significantly reduced compared to mESCs (Yildirim et al., 2014). Concomitantly, additional macroH2A2 was acquired in stable association with gene-poor regions of the MEF genome compared to mESCs (Yildirim et al., 2014). In sum, these results strongly suggest that the histone variant macroH2A exhibits distinct dynamic and stable deposition patterns within mESCs and MEFs, and further highlights the possibility that artificial macroH2A2 overexpression during iPSC reprogramming may disrupt the epigenetic transition from MEF to mESC.

Overexpression or knockdown of macroH2A during iPSC reprogramming.

To determine whether maintaining macroH2A2 expression levels high during iPSC reprogramming disturbs pluripotency acquisition, we initiated reprogramming via lentiviral infection with a STEMCCA-3F-mCherry cassette (Carey et al., 2009; Sommer et al., 2009) in our doxycycline-inducible macroH2A2 overexpressing MEFs (Figure 3.4 A). In parallel, we also reprogrammed MEFs isolated from mice without macroH2A histones (macroH2A DKO) (Pehrson et al., 2014). To assess induction of pluripotency, we stained

for early pluripotency marker alkaline phosphatase (AP) (Brambrink et al., 2008; Stadtfeld et al., 2008; Wernig et al., 2007) and strikingly noticed little difference in AP induction irrespective of macroH2A overexpression or absence (Figure 3.4 B). This could suggest that macroH2A has little to no influence on reprogramming efficiency, or perhaps that the effect is so subtle that it cannot be ascertained by this method. To further test this, we next infected macroH2A WT or DKO MEFs with STEMCCA-3F-mCherry, performed FACS to select for cells infected with lentivirus, plated infected cells at low density onto inactivated MEF feeders, and observed reprogramming efficiency over 2 weeks (Figure 3.4 C-D). Once again, reprogramming efficiency was not significantly altered by macroH2A presence or absence (Figure 3.4 E). These results in sum suggest that macroH2A has no significant effects on iPSC reprogramming efficiency.

Reprogramming efficiency is proportional to not only the rate of epigenetic remodeling events, but also the number of cell divisions a cell undergoes (Hanna et al., 2009). To rule out the possibility that macroH2A presence, absence or overexpression alters the cell division rate and thus confounds iPSC reprogramming efficiency assessment, we performed BrdU-incorporation assays on MEFs prior to infection with reprogramming factors. MacroH2A2 overexpressing, macroH2A DKO, and macroH2A WT MEFs were subjected to a 45-minute BrdU pulse, then stained with an anti-BrdU antibody and counterstained for total DNA with 7-AAD followed by flow cytometry analysis (Figure 3.5). All samples showed similar distribution of cells within each phase of the cell cycle (Figure 3.5), demonstrating that neither macroH2A2 overexpression nor macroH2A germline knockout alters cell division rate. This suggests that any further

observed effects of macroH2A overexpression or knockdown on reprogramming kinetics are independent of effects on cell cycling.

The influence of individual macroH2A isoforms on iPSC reprogramming efficiency.

Thus far, we've shown that total macroH2A knockout and overexpression of the macroH2A2 isoform within MEFs does not significantly alter iPSC reprogramming efficiency. To rule out the possibility that individual macroH2A isoforms, particularly the splice variants of *H2AFY* – macroH2A1.1 and macroH2A1.2 have unique and perhaps opposing influence on iPSC reprogramming, we performed a macroH2A isoform addback experiment (Figure 3.6 A). In brief, 'secondary' macroH2A DKO MEFs were generated with a genomically-inserted doxycycline-induclbe STEMCCA-3F-mCherry cassette (Nakagawa et al., 2008; Wernig et al., 2008). These MEFs were then supplied with macroH2A-mCherry overexpression retrovirus or FUW-GFP control, FACS-purified to select for this infection, plated at low density onto feeder MEFs and lastly reprogramming was initiated via dox addition (Figure 3.6 A-B). We observed robust maintenance of FUW-GFP expression within resulting iPSC colonies concomitant with STEMCCA-3F-mCherry expression (Figure 3.6 C), suggesting that macroH2A-mCherry[+] expression was maintained throughout iPSC reprogramming as well. However, irrespective of the macroH2A isoform added back to macroH2A DKO MEFs, no significant effects on iPSC reprogramming efficiency were observed (Figure 3.6 D), suggesting that presence or absence of even single macroH2A isoforms has no major effect on the epigenetic remodeling events during iPSC reprogramming.

Nuanced analysis of macroH2A's influence on iPSC reprogramming efficiency

Although our studies thus far indicate that macroH2A presence, absence, overexpression or addback have no discernable effects on iPSC reprogramming efficiency, we next took a more nuanced approach to assessing pluripotency induction. We isolated single-embryo-derived and thus sex-segregated MEFs from macroH2A DKO and strain-matched WT mice. We then initiated iPSC reprogramming via infection with STEMCCA-4F. Once again, macroH2A presence or absence did not have markedly distinct outcomes on reprogramming efficiency in most comparisons (Figure 3.7 A). However, when we compared macroH2A DKO male to macroH2A WT female MEF efficiency, we noticed a slight but statistically significant increase in pluripotency induction of the DKO male compared to the WT female (Figure 3.7 A). While the difference was subtle, this could indicate that macroH2A removal from the WT female somatic chromatin, particularly from the macroH2A-rich Xi, may represent a more significant barrier to pluripotency acquisition than in the case of macroH2A WT male MEFs, which lack the Xi. Next, we took female MEFs of macroH2A WT or DKO background, simultaneously infected with TetO-STEMCCA-4F and FUW-rTTA and supplied dox to initiate reprogramming (Figure 3.7 B). We then withdrew dox at different time points during iPSC reprogramming to assess for differential attainment of Yamanaka factor transgene independence as gauged by expression of *Nanog*, an important protein for maintenance of late-stage pluripotency (Mitsui et al., 2003). Pluripotent, *Nanog*+ iPSCs begin to emerge following approximately 8-10 days of transgenic Yamanaka factor expression (Brambrink et al., 2008; Hanna et al., 2009; Stadtfeld et al., 2008), thus we chose to withdraw dox and thus withdraw Yamanaka factor expression around these time points (Figure 3.7 B). Strikingly, dox withdrawl at

day 8 revealed that significantly more macroH2A DKO MEFs had achieved *Nanog* positivity by this time point than macroH2A WT, but interestingly this differential was progressively less significant when dox was withdrawn at day 10 (p = 0.116) and day 12 (p = 0.606) (Figure 3.7 C). This result indicates that macroH2A DKO MEFs indeed do achieve Yamanaka factor transgene independence with slightly quicker kinetics compared to macroH2A WT MEFs. However, these results in sum also indicate that while macroH2A removal from chromatin during iPSC reprogramming may indeed be a necessary epigenetic remodeling event, macroH2A removal is ostensibly not significantly rate-limiting overall to warrant being considered an epigenetic 'bottleneck' to pluripotency acquisition.

Discussion

Our study revealed a number of insights that refine our understanding of the histone variant macroH2A's contribution toward epigenetic identity and iPSC reprogramming efficiency. While macroH2A overexpression, knockout, and individual isoform addback each did not significantly alter reprogramming kinetics on their own, macroH2A DKO male MEFs interestingly did reprogram at a quicker rate than macroH2A WT female MEFs when this particular comparison was made. In addition, female macroH2A DKO MEFs achieved a slightly but significantly greater degree of Yamanaka transgene-independence at an earlier time point compared to macroH2A WT MEFs, furthering evidence that macroH2A's influence on iPSC reprogramming is quite subtle. Further, macroH2A is known to be expressed within pluripotent ESCs, and macroH2A2 was shown to undergo a greater degree of dynamic incorporation and turnover in

mESCs compared to MEFs at the promoters of highly-transcribed genes including *Esrrb*. Thus, it's possible that overall macroH2A levels may not be especially influential when it comes to determining a given cell's epigenetic state, and entirely possible that epigenetic mechanisms epistatic to macroH2A determine the degree, stability and location of macroH2A incorporation.

It's particularly interesting that macroH2A WT female MEFs reprogrammed into pluripotency at a slightly, but significantly slower rate than macroH2A DKO male MEFs. One study indicated that upon macroH2A depletion, a slight but significant increase in an Xi-linked reporter gene expression was observed, indicating that macroH2A removal from the Xi may be a epigenetic rate-limiting step that occurs during nuclear reprogramming (Pasque et al., 2011). Indeed, Xi reactivation is a hallmark epigenetic remodeling event during reprogramming of female somatic cells toward pluripotency (Maherali et al., 2007; Pasque et al., 2014). Thus, it's not difficult to imagine that macroH2A removal from the Xi is an epigenetic remodeling event that must occur in a somatic nucleus transitioning toward pluripotency. Interestingly, however, macroH2A itself is not necessary for X chromosome inactivation during ESC differentiation (Tanasijevic and Rasmussen, 2011), further suggesting that macroH2A removal from the Xi during reprogramming may only be a relatively minor and perhaps not rate-limiting epigenetic remodeling event. Additionally, male and female macroH2A DKO mice are viable and fertile, and macroH2A DKO female pups are birthed and survive to adulthood at normal ratios (Pehrson et al., 2014). Thus, while macroH2A removal may pose a minor challenge to pluripotency induction, undoubtedly other epigenetic factors, which unlike macroH2A are necessary for X chromosome silencing, are more likely to impose

epigenetic bottlenecks with respect to their removal from the Xi during iPSC reprogramming.

Interestingly, several other studies have suggested in stronger terms than we suggest here that macroH2A acts as an epigenetic barrier to induced pluripotency (Barrero et al., 2013a; Gaspar-Maia et al., 2013; Pasque et al., 2012). Our results, which indicate that macroH2A exerts minor influence on iPSC reprogramming, are not entirely inconsistent with these studies. In our work we initiated iPSC reprogramming in MEFs, which are less differentiated and perhaps contain less stably-deposited macroH2A (Chang et al., 2010; Chang et al., 2005; Nashun et al., 2010; Yildirim et al., 2014) than the dermal fibroblasts reprogrammed by Gaspar-Maia and colleagues. Thus, it's perhaps not surprising that macroH2A knockdown or overexpression had a more pronounced effect on iPSC reprogramming efficiency over a greater developmental distance. Further, one methodology employed by Gaspar-Maia and colleagues that could account at least in part for an exaggerated iPSC reprogramming differential was the process of trypsinizing and replating dermal fibroblasts undergoing reprogramming 4-6 days after STEMCCA-4F infection. Replating at this time could select for clones successfully undergoing reprogramming at this intermediate stage and thus amplify the number of total colonies that result upon pluripotency marker assessment.

Pasque and colleagues performed iPSC reprogramming of adult neural stem cells (NSCs), which contained demonstrably more macroH2A than MEFs, under macroH2A knockdown conditions (Pasque et al., 2012). Thus, it's perhaps not surprising that macroH2A knockdown in a cell type with more macroH2A, would have a more pronounced effect on iPSC reprogramming efficiency. Interestingly, Pasque and colleagues also reported a marked reduction in iPSC reprogramming efficiency upon

macroH2A overexpression when reprogramming epiblast stem cells (EpiSCs) into iPSCs (Pasque et al., 2012). EpiSCs contain demonstrably less macroH2A than MEFs (Pasque et al., 2012) and thus one might expect macroH2A overexpression to have a more pronounced influence on iPSC reprogramming in this cell type than in MEFs. Peculiarly, Pasque and colleagues subjected EpiSCs infected with Nanog and macroH2A overexpression cassettes to a 2-week selection process (Pasque et al., 2012). It's possible that this queer selection process for Nanog and macroH2A resulted in greater and iteratively inherited epigenetic changes within dual macroH2A-Nanog selected EpiSCs compared to Nanog and empty vector selected clones and thus exaggerated any observed differential iPSC reprogramming.

Lastly, Barrero and colleagues demonstrated that macroH2A knockdown increased iPSC generation efficiency and conversely macroH2A overexpression reduced reprogramming of human keratinocytes (Barrero et al., 2013a). The authors demonstrated that macroH2A1 in particular was robustly differentially expressed upon ESC differentiation and further enriched within human keratinocytes (Barrero et al., 2013a). The upward efficiency trend for macroH2A knockdown and downward efficiency trend for macroH2A overexpression were quite remarkable within each individual experiment (Barrero et al., 2013a). Peculiarly, however, the negative controls – empty vector and shRD for the overexpression and knockdown experiments respectively – yielded ostensibly drastically different alkaline phosphatase staining patterns by themselves when compared across experiments (Barrero et al., 2013a). Nevertheless, it's entirely possible that macroH2A may reduce reprogramming efficiency to different degrees across distinct species and in different cell types. Overall, our results remain

consistent with the notion that macroH2A imposes an epigenetic bottleneck, albeit in our

hands a minor one, to induced pluripotency.

A

B

Essrb TSS
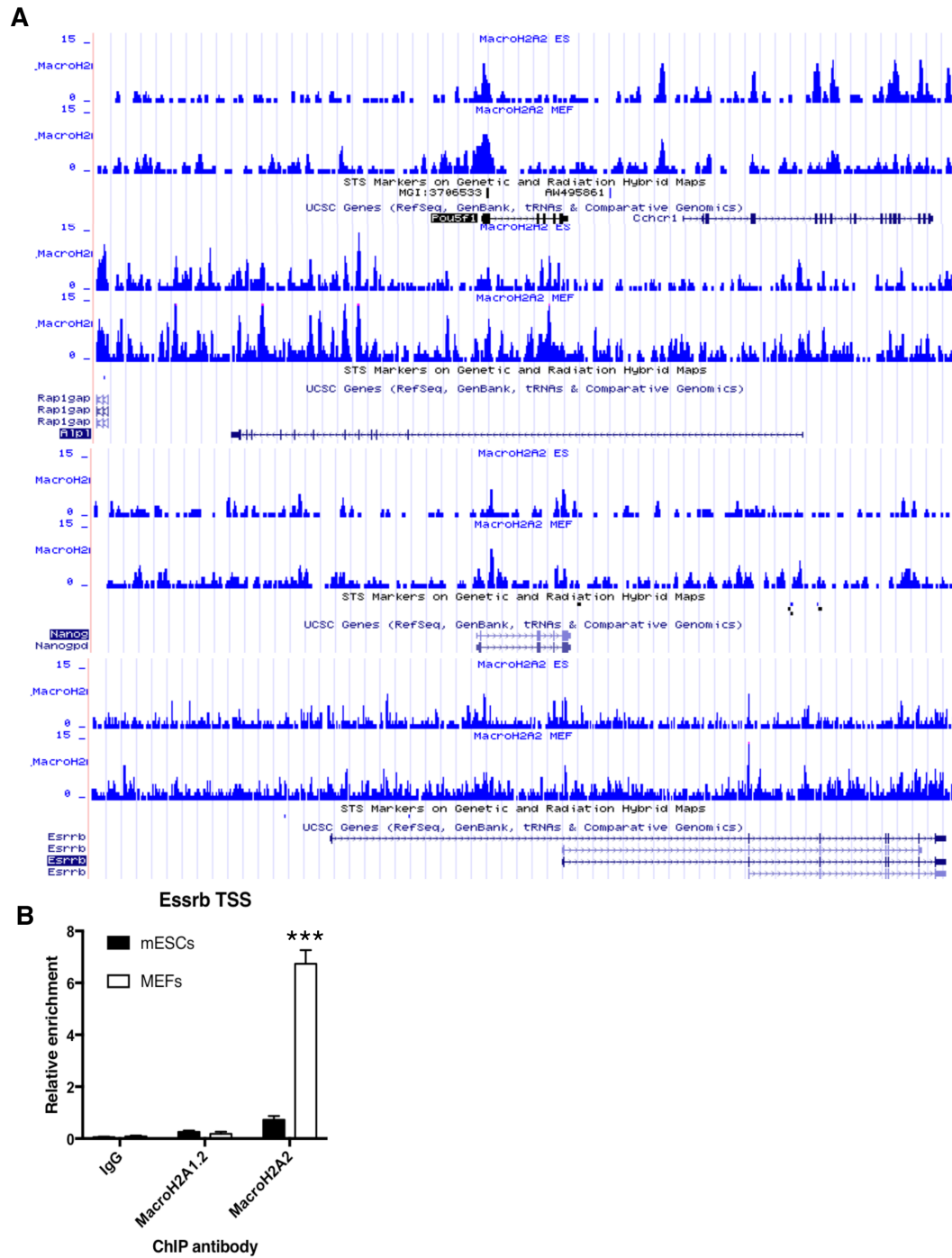
Figure 3.1: MacroH2A deposition at pluripotency genes in mESCs and MEFs.

Figure 3.1: MacroH2A deposition at pluripotency genes in mESCs and MEFs. (A) Genome browser subsets of macroH2A2 ChIP-Seq reads proximal to pluripotency genes in mESCs and MEFs. Four genes are depicted: *Pou5f1* (Oct4), *Alp1* (alkaline phosphatase), *Nanog* and *Esrrb* respectively ordered top to bottom. For each gene, reads from mESCs and MEFs are shown in the bottom and top orientations respectively. (B) ChIP-qPCR results for dox-induced TetO-macroH2A1.2-HA and TetO-macroH2A2-HA incorporation in mESCs and MEFs. Anti-HA or IgG control ChIP was performed in aforementioned cells !xh after 2 μg/mL doxycycline administration and PCR was performed using *Esrrb* TSS-proximal primers. N=3 per condition, ***p<0.0005, Student's *t*-test.

A

Dox (hrs)

0   2   4   6   8   12

44 kDa

Coll1: TetO- MacroH2A2-HA

Rosa26R: rttA

B

- Dox   + Dox

DAPI   MacroH2A2

Oct4   Oct4

C

DAPI   α-HA-MacroH2A2   Merge

-Dox

24h
Dox

96h
Dox
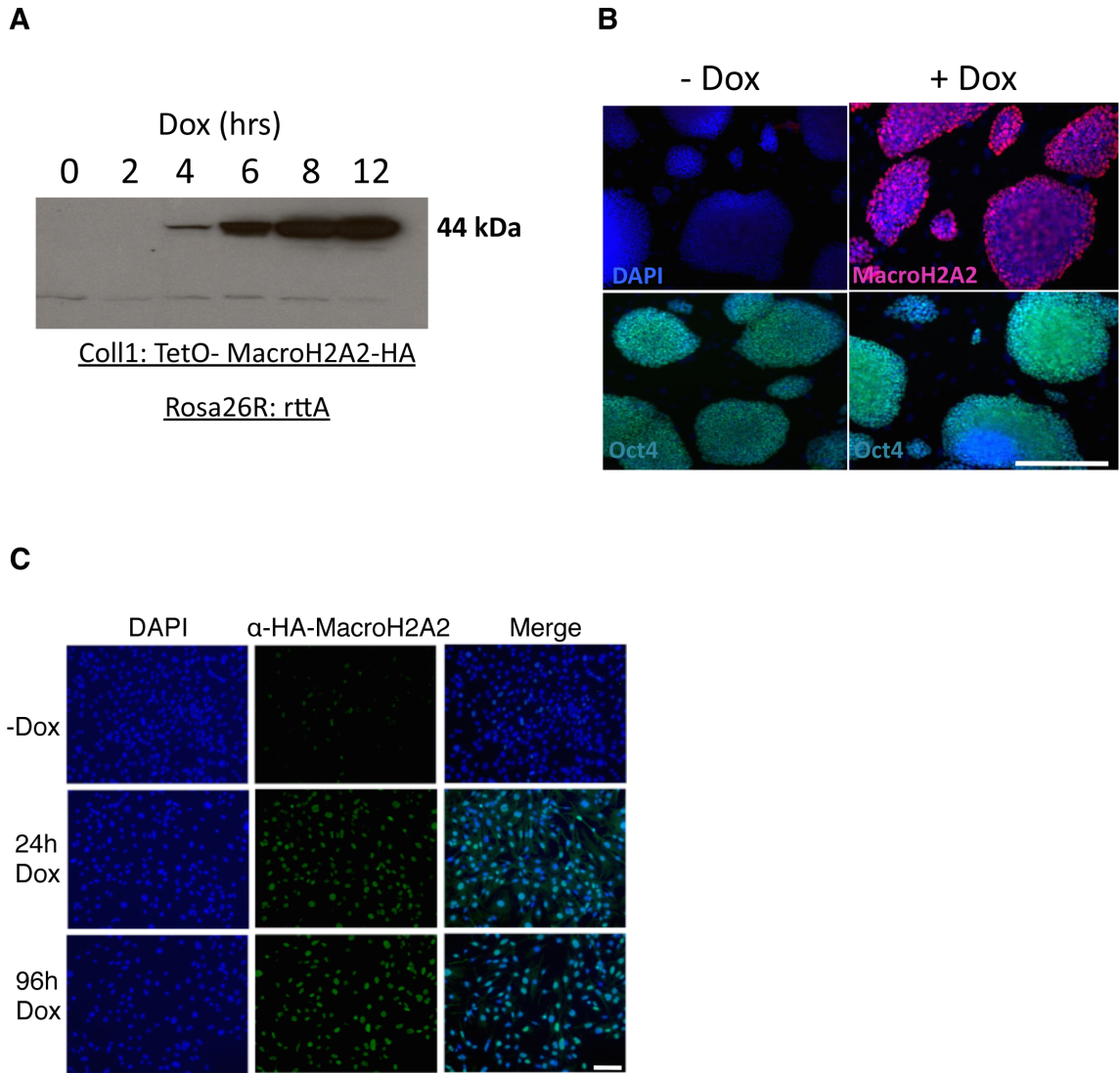
Figure 3.2: Generation of a doxycycline-inducible macroH2A2 overexpression system.

Images in A-B courtesy of Dr. Ozlem Yildirim.

Figure 3.2: Generation of a doxycycline-inducible macroH2A2 overexpression system. (A) Anti-HA immunoblot depicting time course of TetO-macroH2A2-HA induction in Col1: TetO-macroH2A2-HA; Rosa26R: rTTa mESCs following 2 μg/mL doxycycline administration. (B) Representative immunofluorescence images of Col1: TetO-macroH2A2-HA; Rosa26R: rTTa mESCs !xh before and after 2 μg/mL doxycycline administration, stained with anti-HA (top) and anti-Oct4 (bottom) antibodies. (C) Representative immunofluorescence images of Col1: TetO-macroH2A2-HA; Rosa26R: rTTa MEFs !xh before and after 2 μg/mL doxycycline administration, stained with DAPI (left) and anti-HA (middle) antibody. Merged channels shown at right. Scale bars = 100μm.
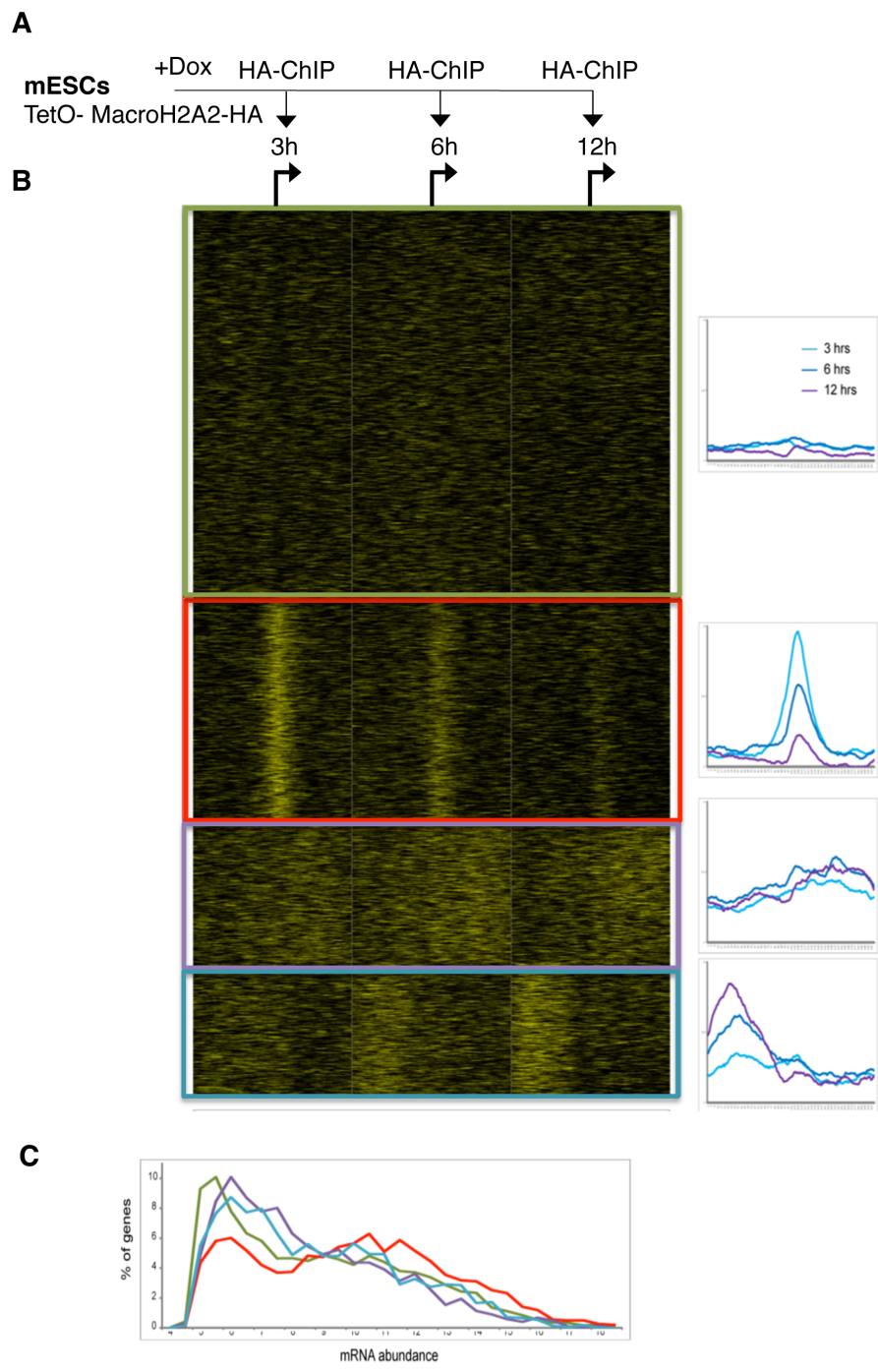
Figure 3.3: Genome-wide macroH2A dynamic incorporation and turnover in

mESCs.

Modified courtesy of Ozlem Yildirim (Yildirim et al., 2014).

Figure 3.3: Genome-wide macroH2A dynamic incorporation and turnover in

mESCs. (A) Scheme depicting TetO-macroH2A2-HA induction and subsequent anti-HA

ChIP-Seq timepoints (3, 6, and 12 hours after dox administration) in mESCs. (B) Left:

Heat map showing four categories of macroH2A2-HA incorporation (yellow traces) of

genes with respect to TSS locus. Category I (green box) exhibited diffuse macroH2A2-

HA incorporation across the body of genes, category II (red box) exhibited greatest

macroH2A2-HA incorporation directly flanking genes' TSS, and categories III and IV

(purple and blue boxes) exhibited greatest incorporation upstream or downstream,

respectively, of genes' TSS. Right: Graphical traces of heatmap densities proximal to

TSS, with indicated colors highlighting traces for 3, 6 and 12 hour induction times. TSS is

situated in the middle for both heatmaps & heatmap traces. (C) Graphical depiction of

the four aforementioned categories of macroH2A2 incorporation and turnover related to

the relative number of genes with a given transcriptional level within each category.

MacroH2A2 incorporation category colors are as described in (B).

A

TetO-macroH2A2-HA MEFs; MacroH2A DKO MEFs

+ STEMCCA 3F-mCherry

2 days

Trypsinized, plated 10k/well +/- dox;

2 weeks

Analysis: AP

B

MacroH2A o/e (+ Dox)

MacroH2A WT (- Dox)

MacroH2A DKO

ns

AP$^+$ colonies per well

MacroH2A2 o/e
MacroH2A WT
MacroH2A DKO

C

MacroH2A WT MEFs; MacroH2A DKO MEFs

+ STEMCCA 3F-mCherry

2 days

FACS for mCherry, Plate 1k MEFs/well onto feeders

2 weeks

Analysis: AP

D

+ STEMCCA-3F-mCherry

FACS for mCherry onto feeders

mCherry (native)

E

MacroH2A WT

MacroH2A DKO

ns

AP$^+$ colonies, Day 10

MacroH2A WT
MacroH2A DKO

Figure 3.4: Overexpression or knockdown of macroH2A during iPSC reprogramming

Figure 3.4: Overexpression or knockdown of macroH2A during iPSC reprogramming. (A) iPSC reprogramming scheme for TetO-macroH2A2 MEFs ± macroH2A2 overexpression and macroH2A DKO MEFs. MEFs were infected with STEMCCA 3F-mCherry lentivirus, trypsinized 2 days later and seeded at 10,000 cells per 6-well plate well with or without 2 μg/mL doxycycline. 2 weeks later, cultures were fixed with PFA and assessed for alkaline phosphatase (AP) positivity. (B) Left: images of AP$^+$ colonies in assayed wells. Right: quantitation of AP$^+$ colonies per well. N=1 well per condition. (C) iPSC reprogramming scheme for macroH2A WT or DKO MEFs. MEFs were infected with STEMCCA 3F-mCherry lentivirus, and FACS-sorted 2 days later onto inactivated feeder MEFs at a density of 1,000 cells per 6-well plate. 2 weeks later, cultures were fixed with PFA and assessed for alkaline phosphatase (AP) positivity. (D) Representative phase contrast (top) fluorescence (native) images of pre (left) and post (right) FACS-sorted cultures. (E) Left: representative images of AP$^+$ colonies in assayed wells. Right: quantitation of AP$^+$ colonies per well. Scale bars = 100μm. N=3 wells per condition. ns = not significant, Student's *t*-test.
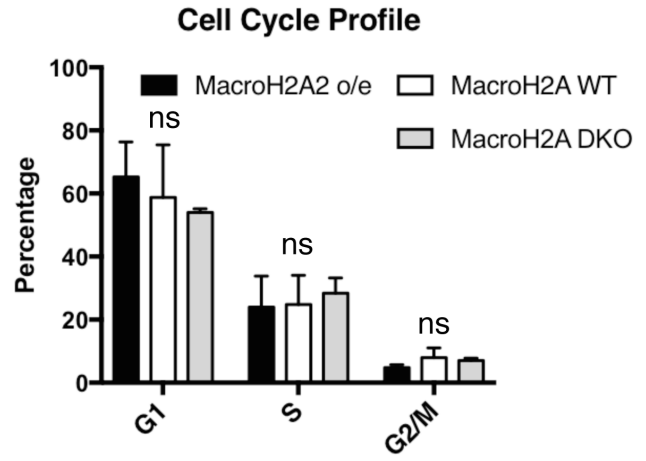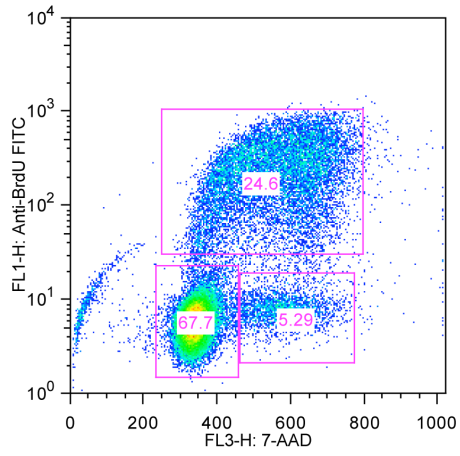
Figure 3.5: Cell cycle parameters of MEFs with altered macroH2A expression.

Figure 3.5: Cell cycle parameters of MEFs with altered macroH2A expression. Left:

representative flow cytometry plots of BrdU content vs. 7-AAD within MEFs. Right:

quantitation of cell cycle subpopulations within TetO-macroH2A2-HA; Rosa26R: rTTa

MEFs ± doxycycline (macroH2A2 o/e and macroH2A WT respectively) and macroH2A

DKO MEFs. N = 3 wells per condition, mean ± SD, ns = not significant, Student's *t*-test.
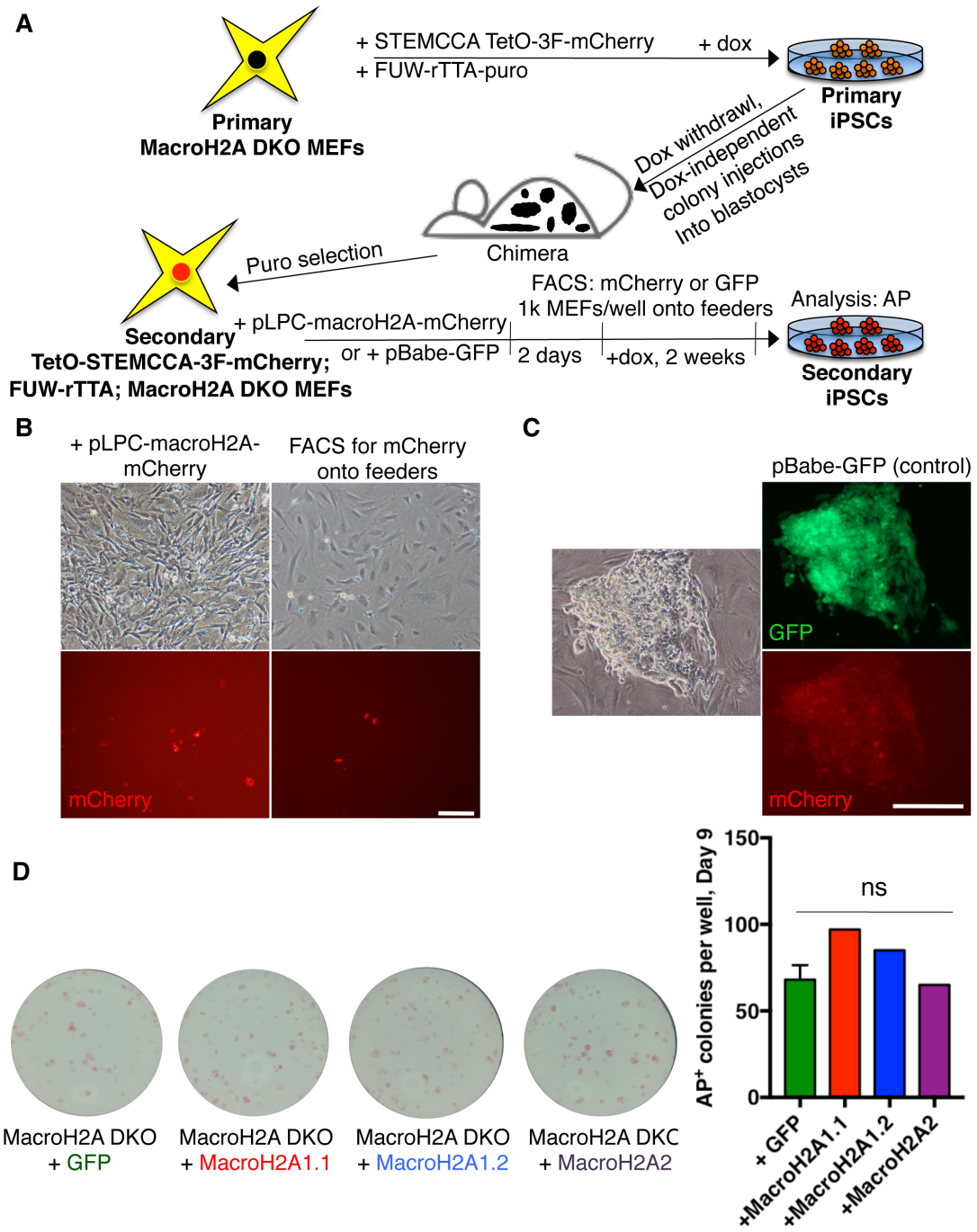
Figure 3.6: The influence of individual macroH2A isoforms on iPSC reprogramming efficiency.

Figure 3.6: The influence of individual macroH2A isoforms on iPSC reprogramming efficiency. (A) General scheme for secondary reprogrammable TetO-STEMCCA-3F-mCherry; FUW-rTTA; macroH2A DKO MEF generation followed by iPSC reprogramming. MacroH2A DKO MEFs were infected with STEMCCA-TetO-3F-mCherry in parallel with FUW-rTTA-puro lentivirus and iPSC reprogramming was induced via 2 μg/mL doxycycline administration. Successful iPSC colonies were then picked, expanded, and dox was withdrawn to further select for transgene-independent stable pluripotent clones. Said clones were then injected into blastocysts which were subsequently injected into pseudopregnant female mice for chimeric embryo generation. MEFs from chimeric pups were then isolated and subjected to 2 days of 2 μg/mL puromycin selection to eliminate non-transgenic MEFs. At this point, these 'secondary' MEFs were infected with pLPC-macroH2A-mCherry or pBabe-GFP retroviruses and two days later FACS-sorted for mCherry or GFP and plated at 1,000 cells/well onto 6-well plates with inactivated feeder MEFs. At this point, iPSC reprogramming of secondary MEFs was initiated by 2 μg/mL doxycycline administration, and 2 weeks later AP$^+$ colonies per well were scored. (B) Representative phase contrast (top) fluorescence (native) images of pre (left) and post (right) FACS-sorted cultures. (C) Representative iPSC colony from GFP infection displayed in phase contrast (left), native GFP fluorescence (top right), and native mCherry expression (bottom right). (D) Left: Representative images of AP$^+$ colonies in assayed wells. Right: quantitation of AP$^+$ colonies per well. N=2 wells GFP condition, N=1 all other conditions. Scale bars = 100μm. ns = not significant, Student's *t*-test.
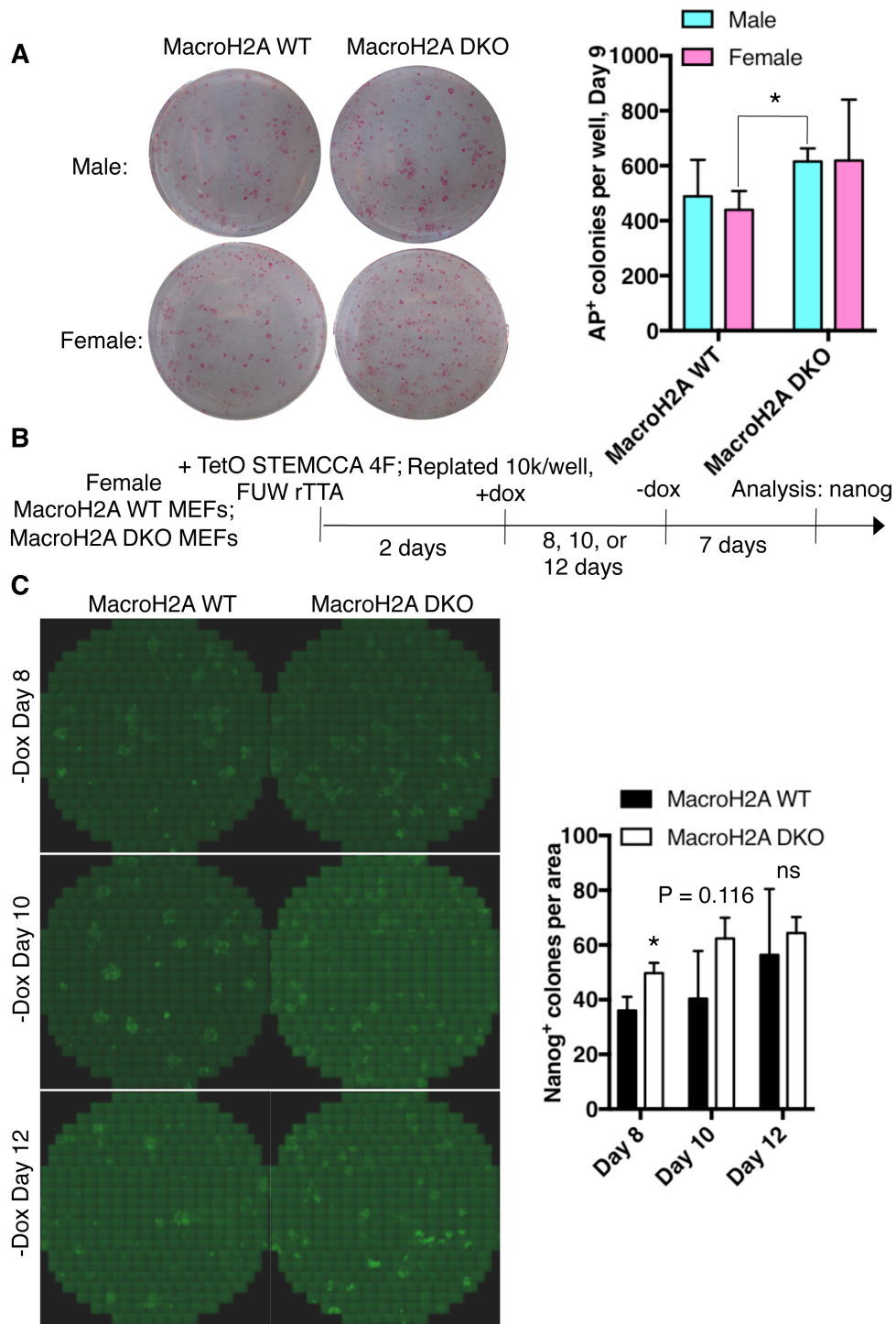
Figure 3.7: Nuanced analysis of macroH2A's influence on iPSC reprogramming efficiency.

Figure 3.7: Nuanced analysis of macroH2A's influence on iPSC reprogramming efficiency. (A) Male or female macroH2A DKO or strain-matched WT MEFs were infected simultaneously with STEMCCA-TetO-4F and FUW-rTTA and 2 days later were seeded at 10,000 cells / 6-well plate well. iPSC reprogramming was subsequently initiated by 2 μg/mL doxycycline administration. Left: Representative images of AP$^+$ colonies in assayed wells. Right: quantitation of AP$^+$ colonies per well. N=3 wells per condition. (B) iPSC reprogramming scheme for female macroH2A WT or DKO MEFs. MEFs were infected with both STEMCCA-TetO-4F and FUW-rTTA and 2 days later were trypsinized and seeded at 10,000 cells / 6-well plate well. iPSC reprogramming was subsequently initiated by 2 μg/mL doxycycline administration and 8-12 days from this point doxycycline was withdrawn from cultures for exactly one week prior to fixation of wells with PFA and nanog immunofluorescence. (C) Left: Representative composite images of nanog immunofluorescence in center partitions of 6-well plate wells one week following dox withdrawl. Right: quantitation of nanog$^+$ colonies per well partition. *p<0.05, p = 0.116, ns = not significant, Student's *t*-test.

Chapter Four:

The histone variant macroH2A confers functional

robustness to the intestinal stem cell compartment

Abstract:

A stem cell's epigenome directs cell fate during development, homeostasis, and regeneration. Epigenetic dysregulation can lead to inappropriate cell fate decisions, aberrant cell function, and even cancer. The structural histone variant macroH2A has been shown to influence gene expression, guide cell fate, and safeguard against genotoxic stress. Interestingly, mice lacking functional macroH2A histones (hereafter referred to as macroH2A DKO) are viable and fertile; yet suffer from increased perinatal death and reduced weight and size compared to wildtype (WT). We set out to investigate whether the ostensible reduced vigor of macroH2A DKO mice extends to intestinal stem cell (ISC) function during homeostasis, post-injury regeneration, and oncogenesis. *Lgr5-eGFP-IRES-CreERT2* or *Hopx-CreERT2::Rosa26-LSL-tdTomato* ISC reporter strains or the *C57BL/6J-APC^{min}/J* murine intestinal adenoma model were bred into a macroH2A DKO or strain-matched WT background and assessed for macroH2A DKO versus WT ISC functionality, regeneration and tumorigenesis. High-dose (12Gy) whole-body γ-irradiation was used as an injury model. MacroH2A was dispensable for intestinal homeostasis and macroH2A DKO mice had similar numbers of active crypt-base columnar ISCs (CBCs). MacroH2A DKO intestine had impaired regeneration following injury, despite having significantly more putative reserve ISCs. DKO reserve ISCs disproportionately underwent apoptosis compared to WT after DNA damage infliction. Interestingly, a macroH2A DKO background did not increase tumorigenesis in the *APC^{min}* model of intestinal adenoma. MacroH2A influences ISC number and function during homeostasis and regeneration. These data support a model in which macroH2A enhances ISC survival after DNA damage and thus confers functional robustness to the intestinal epithelium.

79

Introduction:

The intestinal epithelium is the most highly proliferative mammalian tissue. Its rapid turnover and tremendous regenerative capacity following injury necessitate a robust and highly organized ISC compartment. ISCs are located within the intestinal crypt where they self-renew and produce progenitors, which in turn proliferate and terminally differentiate along the crypt-villus axis prior to being shed into the lumen. To accommodate this rapid turnover and respond to environmental cues, the intestine is served by at least two functionally distinct ISC populations, including the fast-cycling CBCs and slow-cycling reserve ISCs (Li and Clevers, 2010).

CBCs are marked by expression of Wnt-responsive G-protein coupled receptor Lgr5, are driven to actively proliferate by canonical Wnt pathway activity, strongly contribute to intestinal homeostasis (Barker et al., 2007; Cheng and Leblond, 1974) and are ablated by γ-irradiation (Asfaha et al., 2015; Barker et al., 2007; Hua et al., 2012; Metcalfe et al., 2014; Yan et al., 2012). In contrast, reserve ISCs are rare, largely quiescent, radioresistant, and can be marked by *CreER* reporter genes inserted into the *Bmi1, or Hopx* loci, as well as by transgenes driven by the *mTert* and *Lrig1* promoters (Li et al., 2016; Li et al., 2014; Montgomery et al., 2011; Powell et al., 2012; Sangiorgi and Capecchi, 2008; Takeda et al., 2011; Tian et al., 2011; Yan et al., 2012). Following DNA damage and CBC loss, reserve ISCs awaken en masse and play a critical role in epithelial regeneration – in part by producing CBCs (Tao et al., 2015; Yan et al., 2012; Yousefi et al., 2016). Epigenetic mechanisms governing the identities of these two classes of ISCs have not been investigated.

An underappreciated facet of epigenetic control is the substitution of canonical core histones for structural variants. One such variant – macroH2A (Pehrson and Fried, 1992), is highly conserved (Pehrson et al., 2014; Pehrson and Fuji, 1998) and is implicated in reinforcing cell identity *in vitro* (Buschbeck et al., 2009; Changolkar et al., 2007; Grigoryev et al., 2004; Pehrson et al., 1997). Structurally, macroH2A consists of a histone domain, a linker, and a large globular non-histone domain that renders macroH2A about three times the size of canonical core histone H2A (Pehrson and Fried, 1992). MacroH2A is enriched at both facultative and constitutive heterochromatin including the Xi, (Chadwick and Willard, 2002; Changolkar and Pehrson, 2006; Costanzi and Pehrson, 1998; Costanzi et al., 2000; Hernández-Muñoz et al., 2005; Mermoud et al., 1999) senescence-associated heterochromatin foci, (Kreiling et al., 2011; Zhang et al., 2005) the nuclear lamina (Douet et al., 2017; Fu et al., 2015), and other transcriptionally silent chromatin (Changolkar and Pehrson, 2006; Gamble et al., 2010; Mermoud et al., 2001). MacroH2A has been implicated in transcriptional silencing via mechanisms including blocking recruitment of the SWI/SNF nucleosome remodeling complex, (Angelov et al., 2003; Chang et al., 2008) repressing p300 and Gal-VP16-driven RNA pol II transcriptional initiation, (Doyen et al., 2006) and modulating Parp-1 (Chen et al., 2014; Ouararhni et al., 2006) and by simply physically blocking transcription factors from accessing chromatin (Angelov et al., 2003). Interestingly, some active chromatin domains also contain macroH2A, (Gamble et al., 2010) but at least a subset of these sites undergo dynamic macroH2A incorporation and turnover (rather than long-term, stable deposition) and remain transcriptionally accessible (Yildirim et al., 2014).

In mammals, macroH2A exists as 3 isoforms encoded by 2 genes – *H2afy* encodes splice variants macroH2A1.1 and macroH2A1.2, and *H2afy2* encodes

macroH2A2 (Chadwick and Willard, 2001b; Costanzi and Pehrson, 2001; Pehrson et al., 1997). MacroH2A1.1 facilitates chromatin remodeling by binding Parp-1 and ADP-ribosylated chromatin, a property the other macroH2As lack (Karras et al., 2005; Kustatscher et al., 2005). Global macroH2A chromatin content increases during development, (Chang et al., 2005; Pasque et al., 2012; Pehrson et al., 1997) and macroH2A removal has been described as an epigenetic bottleneck to induced pluripotency (Gaspar-Maia et al., 2013; Pasque et al., 2011; Pasque et al., 2012). Interestingly, macroH2A chromatin content also increases with tissue age, (Kreiling et al., 2011) coincident with the known loss of stem cell vigor in aging. Similarly, macroH2A overexpression limits stem cell self-renewal *in vitro* (Creppe et al., 2012). Interestingly, germline macroH2A DKO mice are viable and fertile during homeostasis, yet are peculiarly less robust than WT as evidenced by increased perinatal death and reduced body weight and size throughout life compared to WT (Pehrson et al., 2014). In line with a role for macroH2A in conferring robustness, macroH2A has been shown in cell lines to provide resistance against varied forms of genotoxic stress (Khurana et al., 2014; Lavigne et al., 2015; Ouararhni et al., 2006; Timinszky et al., 2009; Xu et al., 2012). These *in vitro* studies suggest that macroH2A, while perhaps dispensable during homeostasis, may similarly provide cells and even tissues at large with stress resistance *in vivo*.

Here, we show that macroH2A DKO mice have normal intestinal epithelial function during homeostasis. However, macroH2A DKO intestine exhibits reduced regeneration following γ-irradiation injury. Seemingly paradoxically, macroH2A DKO intestine contains markedly more reserve ISCs, but these ISCs are significantly more radiosensitive than WT counterparts. Lastly, we observe no elevated levels of intestinal

adenoma formation in the $APC^{min/+}$ intestinal transformation model in a macroH2A DKO background, corroborating the observed lack of spontaneous tumorigenesis in macroH2A DKO mice (Pehrson et al., 2014) despite evidence that suggests macroH2As may have tumor suppressive properties (Cantariño et al., 2013; Kapoor et al., 2010; Novikov et al., 2011; Sporn and Jung, 2012; Sporn et al., 2009). Our study demonstrates that the histone variant macroH2A, despite being dispensable during intestinal homeostasis and of limited overall influence on intestinal adenoma growth, nevertheless bestows the ISC compartment with functional robustness, specifically by providing resistance to genotoxic stress.

Results:

MacroH2A expression within the intestinal epithelium

We first sought to characterize the expression of macroH2A isoforms within the intestinal epithelium. While macroH2A expression was at least 4-fold lower in the intestine relative to the macroH2A-rich liver,(Costanzi and Pehrson, 2001; Pehrson et al., 1997) *H2AFY* splice variants macroH2A1.1 and macroH2A1.2 were robustly expressed within the crypt and villus (Figure 4.1 A). In contrast, *H2AFY2* – which encodes macroH2A2 – was not appreciably transcribed within the small intestine (Figure 4.1 A). Of note, the PAR-binding macroH2A1.1 was slightly enriched within the crypt versus villus (Figure 4.1 A). Next, we FACS-purified CBCs and reserve ISCs by using the *Lgr5-eGFP-IRES-CreER(Barker et al., 2007)* and *Hopx-CreERT2::Rosa26-LSL-tdTomato* reporter strains respectively (Takeda et al., 2011). We use *Hopx-CreERT2* to mark reserve ISCs as we and others have shown this population to be molecularly and

functionally overlapping with other reserve ISC markers including *Bmi1-CreER* and *mTert-CreER*, and single cell expression profiles indicate that the *Hopx-CreERT2* population is more homogenous that the commonly used *Bmi1-CreER* marker (Li et al., 2014; Montgomery et al., 2011; Sangiorgi and Capecchi, 2008; Takeda et al., 2011; Tian et al., 2011; Yan et al., 2012). Interestingly, the non PAR-binding macroH2A1.2 was slightly but significantly enriched within CBCs compared to reserve ISCs (Figure 4.1 B). Further, both macroH2A1 isoforms were readily detectable at the protein level in FACS-purified ISCs (Figure 4.1 C), and macroH2A1.1 and/or macroH2A1.2 protein was observed within most cells along the crypt-villus axis (Figure 4.1 D). These data together suggest that macroH2A variant expression and deposition may guide or fine-tune intestinal epithelial cell identity and function.

MacroH2A DKO intestine during homeostasis

Next, we examined macroH2A DKO intestinal epithelia under steady-state conditions compared to WT. No gross architectural abnormalities were observed within the proximal or distal small intestine of DKO versus WT mice (Figure 4.2 A). The epithelial height from crypt base to villus tip in both DKO and WT intestine was nearly identical (Figure 4.2 B), as was the total crypt height (Figure 4.2 C). Both DKO and WT intestine had comparable placement and numbers of Paneth, enterocyte, enteroendocrine, and goblet cells (Figure 4.2 D, Figure 4.3 A-C). These results suggest that the intestinal epithelium does not require macroH2A histones for homeostatic maintenance.

CBC frequency and activity in macroH2A DKO intestine

In order to assess macroH2A DKO intestinal stem cell functionality, we isolated whole intestinal crypts from DKO and WT mice for *in vitro* organoid formation assays. Organoid growth is driven by ISCs, and both active CBCs and reserve ISCs are capable of initiating organoid formation (Li et al., 2016; Sato et al., 2009). Phenotypically normal organoids were robustly generated from macroH2A DKO crypts (Figure 4.4 A) at a strikingly greater frequency than macroH2A WT crypts (Figure 4.4 B), suggesting that macroH2A DKO crypts may harbor more ISCs per crypt that are able to contribute to organoid genesis. This result was reproduced in crypts isolated from 2-year old macroH2A DKO and WT mice (Figure 4.4 B) with 2-year old macroH2A DKO crypts trending toward retaining nearly more organoid formation capacity during aging compared to WT (Figure 4.4 C). This result is intriguing as macroH2A chromatin deposition is known to increase with age (Kreiling et al., 2011), thus the nearly greater drop-off of WT organoid formation capacity during aging compared to DKO may be due to continued macroH2A histone deposition in WT ISCs over time.

We next sought to determine whether macroH2A DKO mice have different numbers of active CBCs. To this end we bred macroH2A DKO and strain-matched WT mice into the *Lgr5-eGFP-IRES-CreERT2* reporter strain. Surprisingly, macroH2A DKO crypts contained equal numbers of CBCs per crypt as WT (Figure 4.4 D) with functionally identical cell cycle profiles (Figure 4.4 E). These data suggest that the increased DKO organoid formation was neither due to increased CBC numbers nor increased CBC proliferation.

Reserve ISC frequency and activity in macroH2A DKO intestine

To interrogate the reserve ISC compartment in mice without macroH2A, we bred macroH2A DKO and strain-matched WT mice into the *Hopx-Cre-ERT2::Rosa26-LSL-tdTomato* reporter strain (Li et al., 2014; Takeda et al., 2011). Remarkably, macroH2A DKO crypts contained significantly more putative Hopx-CreER[+] reserve ISCs than WT (Figure 4.5 A), suggesting macroH2A may limit reserve ISC numbers. MacroH2A DKO reserve ISCs also exhibited significantly greater steady-state lineage tracing compared to WT reserve ISCs (Figure 4.5 B-C). However, this increased tracing could not be attributed to increased reserve ISC cycling, as although a slight trend in increased EdU incorporation in macroH2A DKO reserve ISCs was observed, this result was not statistically significant (Figure 4.5 D). Furthermore, the increased tracing appeared to be largely a reflection of the increased size of the reserve ISC pool, as normalization of tracing events to reserve ISC cell numbers revealed no significant difference between macroH2A DKO and WT cohorts (Figure 4.5 C). Importantly, FACS-isolated macroH2A DKO *Hopx-tdTomato[+]* reserve ISCs were able to produce comparable quantities of organoids *in vitro* compared to their WT counterparts when controlled for cell number (Figure 4.5 E), suggesting that the increased organoid formation capacity of macroH2A DKO mice is at least in part due to the expanded reserve ISC pool. In sum, these results reveal that macroH2A DKO reserve ISCs are almost 3 times as abundant as WT, are not significantly more proliferative than WT, and contribute equally on a cell-to-cell basis to lineage tracing and *in vitro* organoid formation.

Regeneration and DNA damage response in macroH2A DKO intestine

Reserve ISCs are known to be resistant to DNA damage and required for epithelial regeneration following exposure to high-dose γ-radiation that quantitatively ablates actively cycling cells including CBCs (Asfaha et al., 2015; Metcalfe et al., 2014; Tao et al., 2015; Tian et al., 2011; Yan et al., 2012; Yousefi et al., 2016). To test the contribution of macroH2A DKO reserve ISCs to intestinal regeneration following injury, we subjected macroH2A WT and DKO mice to high-dose (12Gy) γ-radiation. Strikingly, macroH2A DKO intestine exhibited a significantly worse regenerative response compared to WT (Figure 4.6 A). Somewhat paradoxically, macroH2A DKO and WT intestine neither showed a significant difference in crypt apoptosis at large (Figure 4.6 B, C) nor DNA damage signal clearance in the crypt 1 day after irradiation (Figure 4.6 D). This is perhaps not surprising, as macroH2A was shown to neither affect H2AX phosphorylation nor γ-H2AX signal clearance *in vitro* (Timinszky et al., 2009). However, irradiation of mice two days after Hopx-CreER[+] lineage tracing initiation revealed comparable numbers of clonal tracing events between macroH2A DKO and WT (Figure 4.7 A-B). This observation reveals a significant decrease in tracing from macroH2A DKO reserve ISCs versus WT on a per-cell basis (Figure 4.7 B), and suggests that macroH2A DKO reserve ISCs have increased DNA damage sensitivity. To further test this, we assayed macroH2A DKO reserve ISCs for apoptosis one day after irradiation. Indeed, macroH2A DKO reserve ISCs exhibited a higher incidence of cleaved caspase-3 immunoreactivity (Figure 4.7 C), indicating that macroH2A DKO reserve ISCs disproportionately undergo apoptosis and are aberrantly radiosensitive. Importantly, macroH2A DKO crypt epithelium at large was not significantly more apoptotic than WT (Figure 4.7 C), corroborating our previous results (Figure 4.6 B-C). Taken together, these

data suggest that macroH2A bestows reserve ISCs with resistance to radiation-induced DNA damage.

Influence of macroH2A on intestinal tumorigenesis

Colorectal cancer (CRC) progression is directly correlated with an increase in the expression of an ISC transcriptional signature, and both Wnt[High] CBCs and Wnt[Negative] radioresistant cells have been implicated as potential cells-of-origin in colorectal tumorigenesis (Asfaha et al., 2015; Barker et al., 2009; Merlos-Suárez et al., 2011; Yanai et al., 2017). Our findings thus far indicate that macroH2A DKO crypts exhibit increased ISC activity in organoid formation assays (Figure 4.4 A-C), increased reserve ISC numbers (Figure 4.5 A), and reduced reserve ISC DNA damage tolerance (Figure 4.7 C). Given that macroH2A has been implicated as a tumor suppressor in several cancers including CRC (Cantariño et al., 2013; Kapoor et al., 2010; Novikov et al., 2011; Sporn and Jung, 2012; Sporn et al., 2009), this prompted us to ask whether macroH2A absence might influence intestinal tumorigenesis.

Consistent with a prior report (Sporn and Jung, 2012), we observed decreased macroH2A1.1 expression in several human CRC cell lines relative to healthy human intestinal crypt epithelium (Figure 4.8 A). Concomitantly, the non-PAR binding macroH2A1.2 exhibited greater expression in several CRC lines, suggesting selection for increased macroH2A1.2 vs. macroH2A1.1 isoform splicing disparity in these cancers (Figure 4.8 A). MacroH2A1.2 and macroH2A1.1 are produced by mutually exclusive exon inclusion spicing events (Figure 4.8 B) (Rasmussen et al., 1999), therefore our data corroborate literature that suggests that the PAR-binding isoform macroH2A1.1 has

tumor suppressive activity (Cantariño et al., 2013; Novikov et al., 2011; Sporn and Jung, 2012; Sporn et al., 2009).

To simulate the transcriptional environment of macroH2A DKO ISCs in human CRCs, we used RNAi to knock down macroH2A within two CRC lines that exhibited both a pronounced increase in macroH2A1.2 and a prominent decrease in macroH2A1.1. Surprisingly, knockdown of either macroH2A1.1 or macroH2A1.2 modestly but significantly reduced proliferation (Figure 4.8 C-F). While the siRNA knockdowns were robust and specific, particularly in RKOs (Figure 4.8 C), we cannot rule out the possibility of altered macroH2A1 isoform genomic deposition following reciprocal splice variant depletion, and the functional consequences thereof. Interestingly, pan-*H2AFY* knockdown resulted in a modest increase in RKO and HCT116 CRC proliferation (Figure 4.8 D, F) suggesting that total macroH2A loss may increase CRC proliferation slightly and contribute subtly to oncogenesis.

Finally, to test the influence of macroH2A absence on intestinal tumorigenesis in a more physiological setting, we bred macroH2A DKO and WT mice into the *APC$^{min/+}$* mouse model of intestinal transformation (Su et al., 1992) and quantified adenoma formation. On average, macroH2A DKO mice did not develop more tumors compared to WT (Figure 4.9), indicating that macroH2A absence does not hypersensitize the intestinal epithelium to oncogenic stress caused by loss of heterozygosity in the APC$^{min/+}$ model. This finding is consistent with prior work which observed no increase in spontaneous tumor formation in ageing macroH2A DKO mice (Pehrson et al., 2014). Thus, these data suggest that macroH2A has no significant tumor suppressive function in the intestinal epithelium.

Discussion

This study identified for the first time a role for the histone variant macroH2A in the function of somatic stem cells *in vivo*. In spite of the observed radiosensitivity within macroH2A DKO reserve ISCs, macroH2A is ostensibly dispensable during intestinal homeostasis (Figure 4.10). This is perhaps not surprising, as macroH2A DKO mice are ordinarily healthy, yet at the same time are described as smaller, more perinatal death-prone, and less vigorous overall than WT counterparts (Pehrson et al., 2014). It is therefore interesting that macroH2A DKO mice are more sensitive to genotoxic γ-irradiation, as this is further evidence that macroH2A DKO mice are less robust.

As with our *in vivo* study, macroH2A perturbation alongside genotoxic stress has been of great consequence in a number of *in vitro* studies. In one example, simultaneous macroH2A knockdown and viral challenge increased the 'transcriptional noise' of many genes (Lavigne et al., 2015). In another study, macroH2A1.1 and PARP-1 were shown to coordinate proper hsp70 expression following heat-shock induction (Ouararhni et al., 2006). Further, two notable studies highlight roles for both macroH2A1.1 and macroH2A1.2 in directing DNA damage response (DDR) element localization following targeted double strand break (DSB) induction. PAR-binding macroH2A1.1 knockdown was shown to impair PARP-1 recruitment to DSB sites, a key early step in the DDR (Timinszky et al., 2009). Additionally, knockdown of non-PAR-binding macroH2A1.2 significantly reduced BRCA1 recruitment to break sites and in turn reduced DSB resolution via homology-directed repair (HDR) (Khurana et al., 2014).

Based on the literature and our study's observed increase in cleaved caspase-3 staining within macroH2A DKO reserve ISCs compared to WT, it's tempting to speculate

that macroH2A DKO reserve ISCs are less effective at DNA repair than WT, and thus excessively undergo apoptosis after suffering DNA damage. Specific DDR deficiencies within macroH2A DKO reserve ISCs remain unknown, but possibilities include reduced Chk2 kinase phosphorylation, a DDR signaling hallmark shown to be disrupted upon macroH2A knockdown (Xu et al., 2012). Another possibility is that macroH2A DKO reserve ISCs are less able to recruit BRCA1 to DSB sites and thus disproportionately undergo non-homologous end joining rather than the less error-prone HDR (Khurana et al., 2014). Further studies are needed to determine which DDR deficiencies macroH2A DKO reserve ISCs may suffer from.

In our study, we discovered that macroH2A DKO intestine has almost 3 times as many reserve ISCs than WT under steady-state conditions and these DKO reserve ISCs are at least as able as WT reserve ISCs to contribute to lineage tracing and *in vitro* organoid formation. This result is perhaps not surprising as it's been shown that macroH2A knockdown can increase somatic stem cell self-renewal *in vitro* (Creppe et al., 2012). Interestingly, macroH2A DKO reserve ISCs are not significantly more proliferative than WT. This could suggest that more DKO reserve ISCs are established early in development, or alternatively that DKO reserve ISCs undergo more frequent self-renewal versus commitment divisions. Additionally, we cannot rule out the possibility of non cell-autonomous influences on ISC numbers, including from the macroH2A DKO ISC niche. Future experiments aimed at understanding macroH2A's role in ISC development and specification are needed to further characterize the macroH2A DKO reserve ISC.

Our research has shed light on macroH2A's purported tumor suppressive role. Since macroH2A has been shown to provide functional robustness against genotoxic

stress in several studies (Khurana et al., 2014; Lavigne et al., 2015; Ouararhni et al., 2006; Timinszky et al., 2009; Xu et al., 2012) including our own, it follows that macroH2A may also insulate against oncogenesis, at least in part by bolstering DNA repair. It is therefore interesting that macroH2A DKO in an $APC^{min/+}$ background does not result in increased tumorogenesis relative to WT, yet this result is in agreement with the observation that macroH2A DKO mice are not more susceptible to spontaneous cancer (Pehrson et al., 2014). Another nuance to the study of macroH2A in cancer is that macroH2A1.1 and macroH2A1.2 may have distinct influences on oncogenesis. MacroH2A1.1 has more often than macroH2A1.2 been described as a bona-fide tumor suppressor (Cantariño et al., 2013; Novikov et al., 2011; Sporn and Jung, 2012; Sporn et al., 2009; Zhang et al., 2005). Interestingly, another study found that macroH2A1 can potentiate silencing, heterochromatin formation, and hypermethylation of the tumor suppressor p16 in CRC, but the work did not distinguish between macroH2A1.1 and macroH2A1.2 (Barzily-Rokni et al., 2011). These insights highlight the importance of developing tools that distinguish between the individual effects of macroH2A isoforms, particularly the macroH2A1 splice variants – both in terms of variant expression as well as subgenomic localization. Understanding the individual roles of the macroH2A isoforms will indeed prove critical to further characterizing the role of macroH2A in cancer, in ISCs, and undoubtedly in other adult stem cell systems as well.
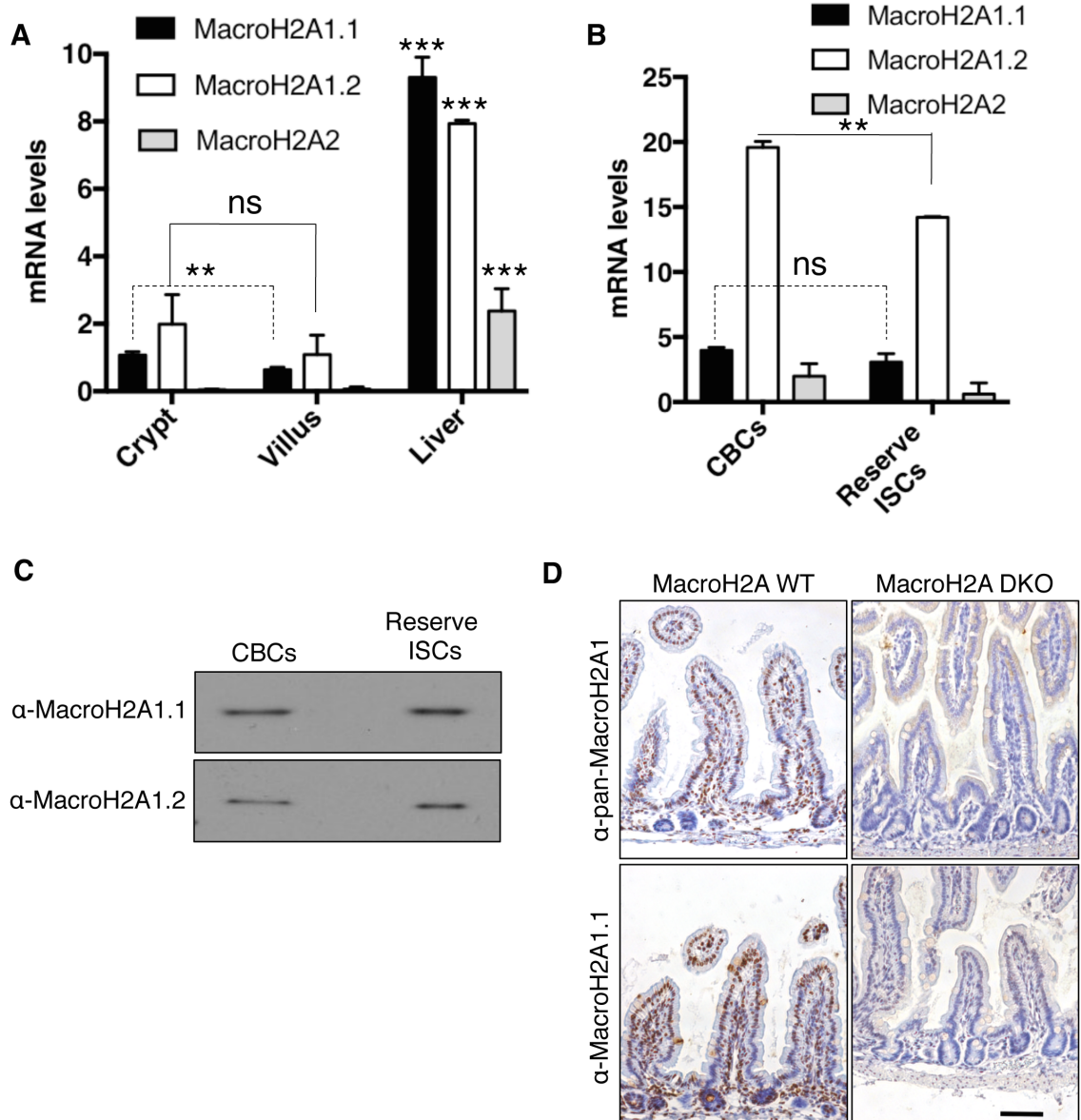
Figure 4.1: MacroH2A expression within the intestinal epithelium.

Figure 4.1: MacroH2A expression within the intestinal epithelium. (A) Analysis of intestinal jejunum crypt or villus tissue fractions for macroH2A variant mRNA levels compared to mouse liver. ΔΔCT method, values normalized to *Actb*, N=3 per condition, mean ± SD. (B) MacroH2A isoform mRNA level analysis within Lgr5-eGFP^high CBCs or Hopx-tdTomato^+ reserve ISCs FACS-purified from *Lgr5-eGFP-IRES-CreERT2* or *Hopx-CreERT2 Rosa26R-LSL-tdTomato* mice. ΔΔCT method, values normalized to *Actb*, N=3 per condition, mean ± SD. (C) Western blot showing macroH2A1 isoform protein level within FACS-purified populations of CBCs (again, Lgr5-eGFP^high from *Lgr5-eGFP-IRES-CreERT2* mice) or reserve ISCs (Hopx-tdTomato^+ from *Hopx-CreERT2 Rosa26R-LSL-tdTomato* mice). Entire protein lysate from 30,000 CBCs or 20,000 reserve ISCs loaded into each well of gel corresponding to indicated samples on blot. (D) Immunohistochemical straining of pan-macroH2A1 or macroH2A1.1 in macroH2A WT or macroH2A DKO proximal small intestine. 10x objective. Scale bars = 100μm. **p<0.005, ***p<0.0005, ns = not significant, Student's *t*-test.
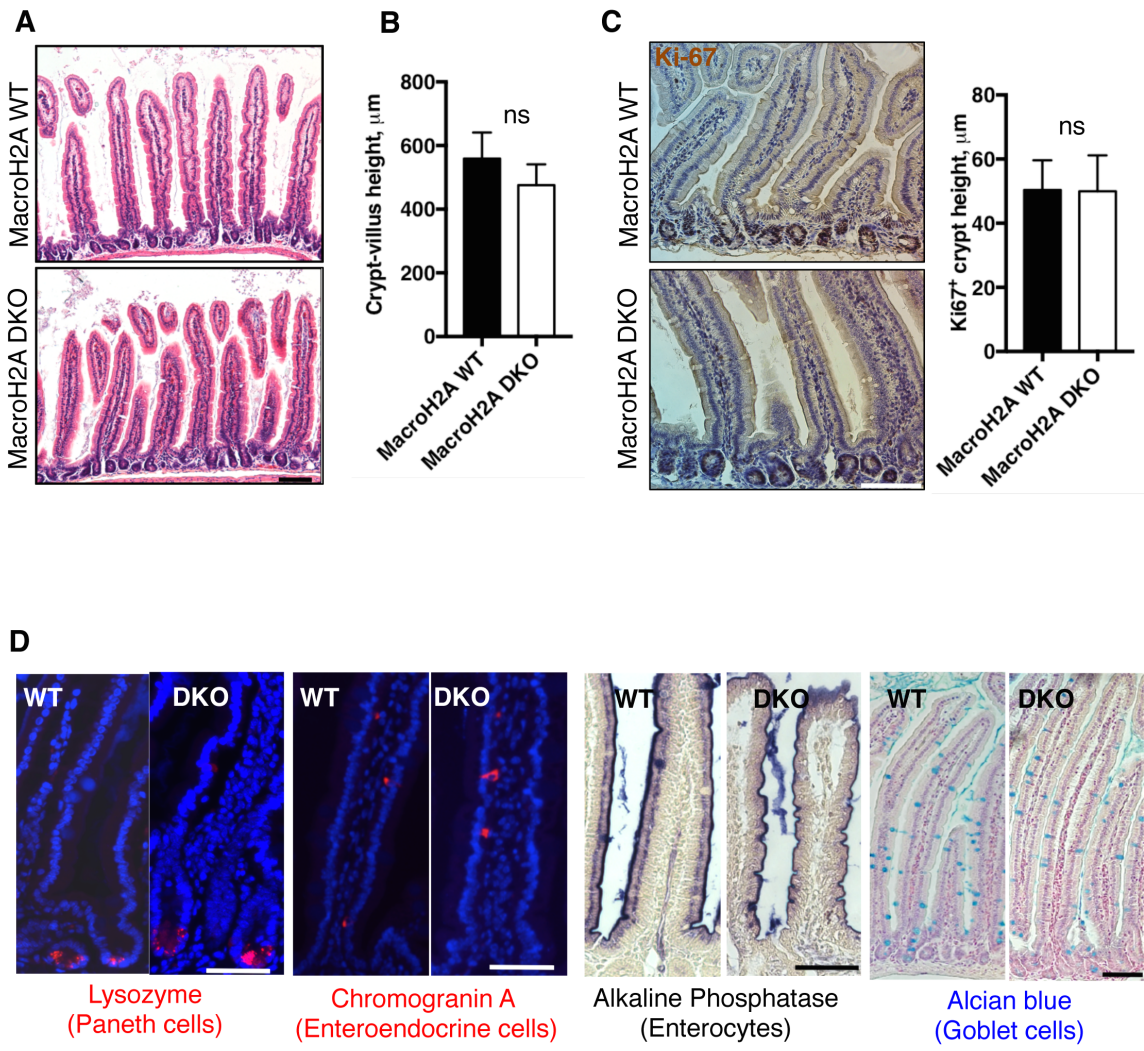
Figure 4.2: MacroH2A DKO intestine during homeostasis.

Figure 4.2: MacroH2A DKO intestine during homeostasis. (A) Representative H&E sections of macroH2A WT and DKO proximal small intestine. 4x objective. (B) Average height in microns of crypt-villus axis (distance from base of crypt to tip of villus) of macroH2A WT vs. DKO proximal small intestine. N = 3 mice per condition, mean ± SD (C) Left: Representative Ki67 immunohistochemistry of macroH2A WT and DKO proximal small intestine. 10x objective. Right: Average Ki67$^+$ crypt height in microns of macroH2A WT vs. DKO proximal small intestine. N = 3 mice per condition, medians, quartiles and ranges of values shown. (D) Representative immunofluorescence and immunohistochemical images of proximal small intestines of macroH2A WT or DKO mice stained for lysozyme (Paneth cells), chromogranin A (enteroendocrine cells), alkaline phosphatase (enterocytes), or alcian blue (goblet cells). Lysozyme, chromogranin A and alkaline phosphatase: 20x objective, alcian blue: 10x objective. Scale bars = 100μm. ns = not significant, Student's *t*-test.
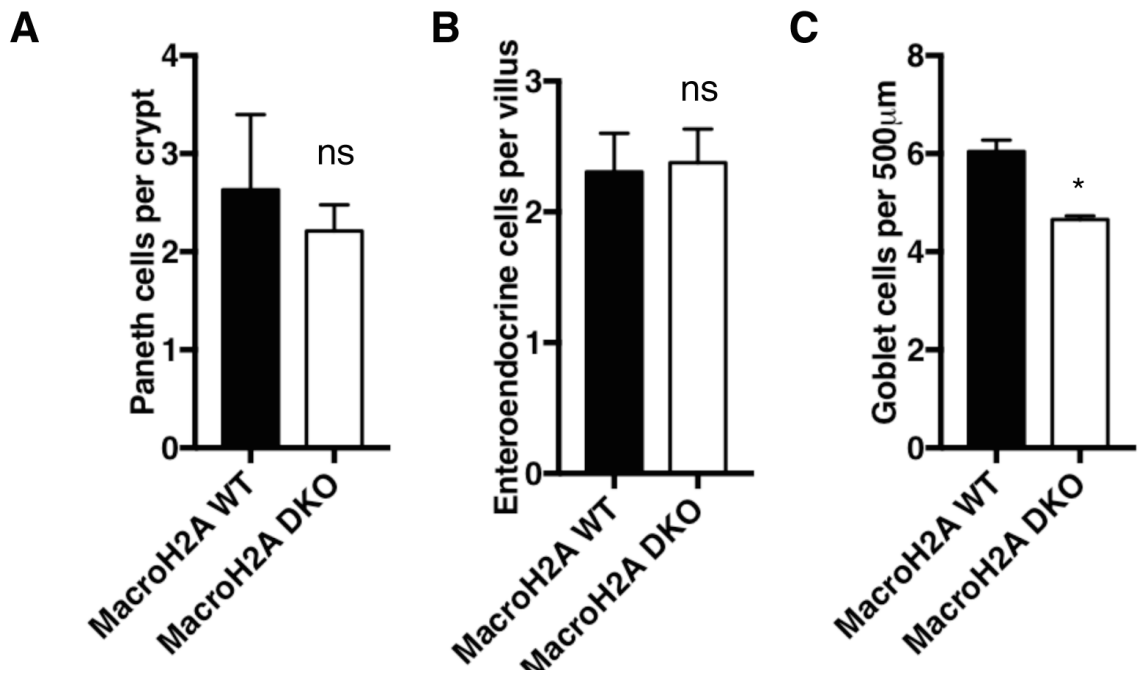
Figure 4.3: Differentiated intestinal epithelial cell quantitations.

Figure 4.3: Differentiated intestinal epithelial cell quantitations. (A) Quantitation of

Lysozyme C$^+$ Paneth cells per crypt, N=3 per condition, mean ± SD. (B) Quantitation of

chromogranin A$^+$ enteroendocrine cells per villus, N=3 per condition, mean ± SD. (C)

Quantitation of Alcian Blue stained goblet cells per 500 microns, N=3 per condition,

mean ± SD. *p<0.05, ns = not significant, Student's *t*-test.
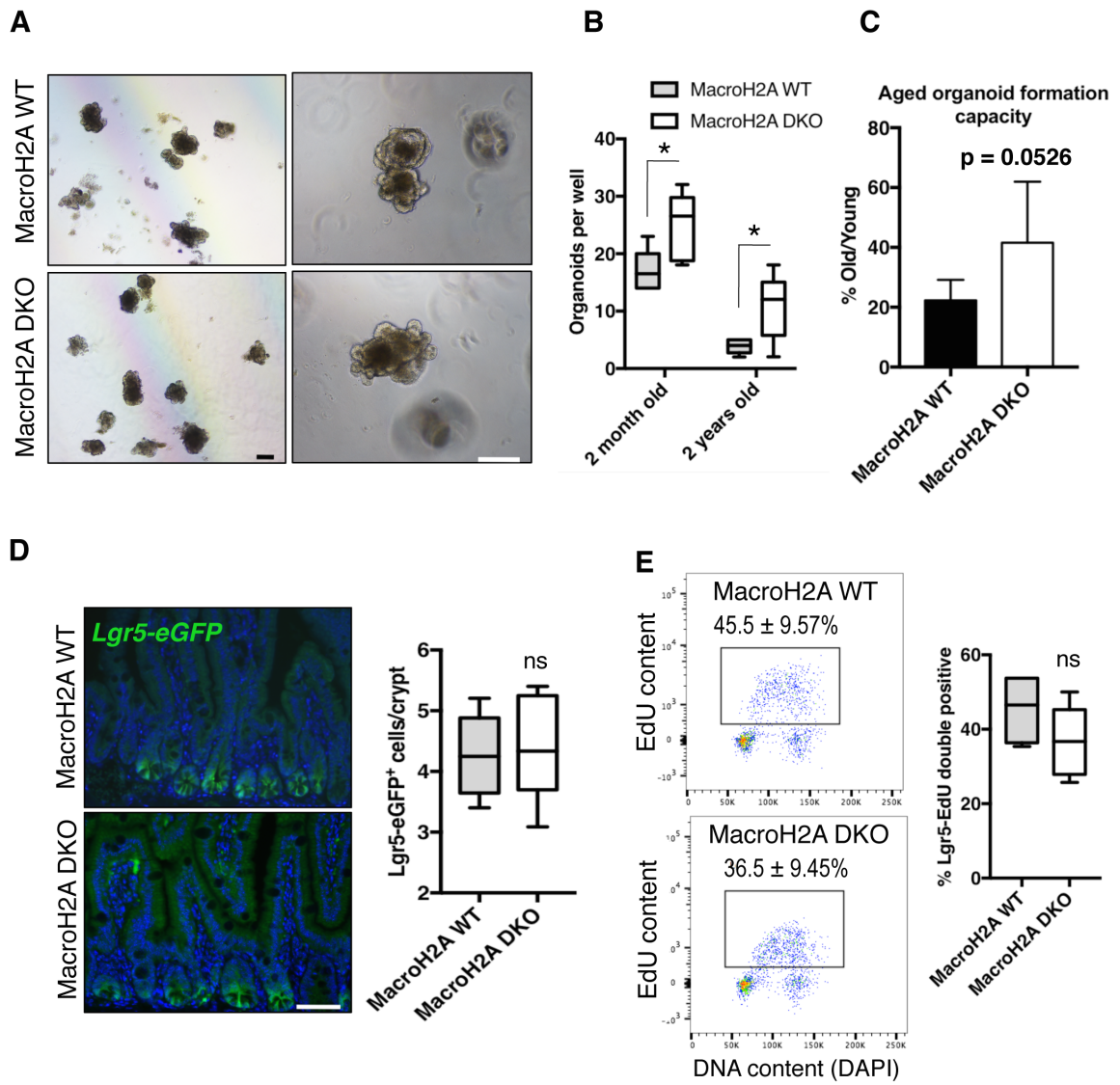
Figure 4.4: CBC frequency and activity in macroH2A DKO intestine.

Figure 4.4: CBC frequency and activity in macroH2A DKO intestine. (A)

Representative phase contrast images of macroH2A WT and DKO crypt-derived

organoids, 7 days into culture. Left: 4x objective. Right: 10x objective. (B) Average

resulting organoids per well (24-well tissue culture plate) from 100 crypts from

macroH2A WT or DKO proximal small intestine from 2-month or 2-year old mice. N=6

mice per condition, medians, quartiles and ranges of values shown. (C) Aged organoid

formation capacity as defined by the average number of organoids that formed as a

percent of the number of corresponding organoids that formed from 2-month old crypts

per genotype. 10x objective. (D) Left: representative anti-eGFP immunofluorescence of

macroH2A WT and DKO proximal small intestine. Right: average Lgr5-eGFP$^+$ cells per

crypt. N = 6 mice per condition, medians, quartiles and ranges of values shown. (E) Left:

representative flow cytometry plots of EdU content vs. DAPI of within *Lgr5-eGFP$^+$*

subpopulations of macroH2A WT and DKO proximal small intestinal crypt cells. Right:

quantitation of *Lgr5-eGFP*/EdU double positivity as defined by boxed subpopulation on

left. N=4 mice per condition, medians, quartiles and ranges of values shown. *p<0.05, ns

= not significant, Student's *t*-test. Scale bars = 100μm.
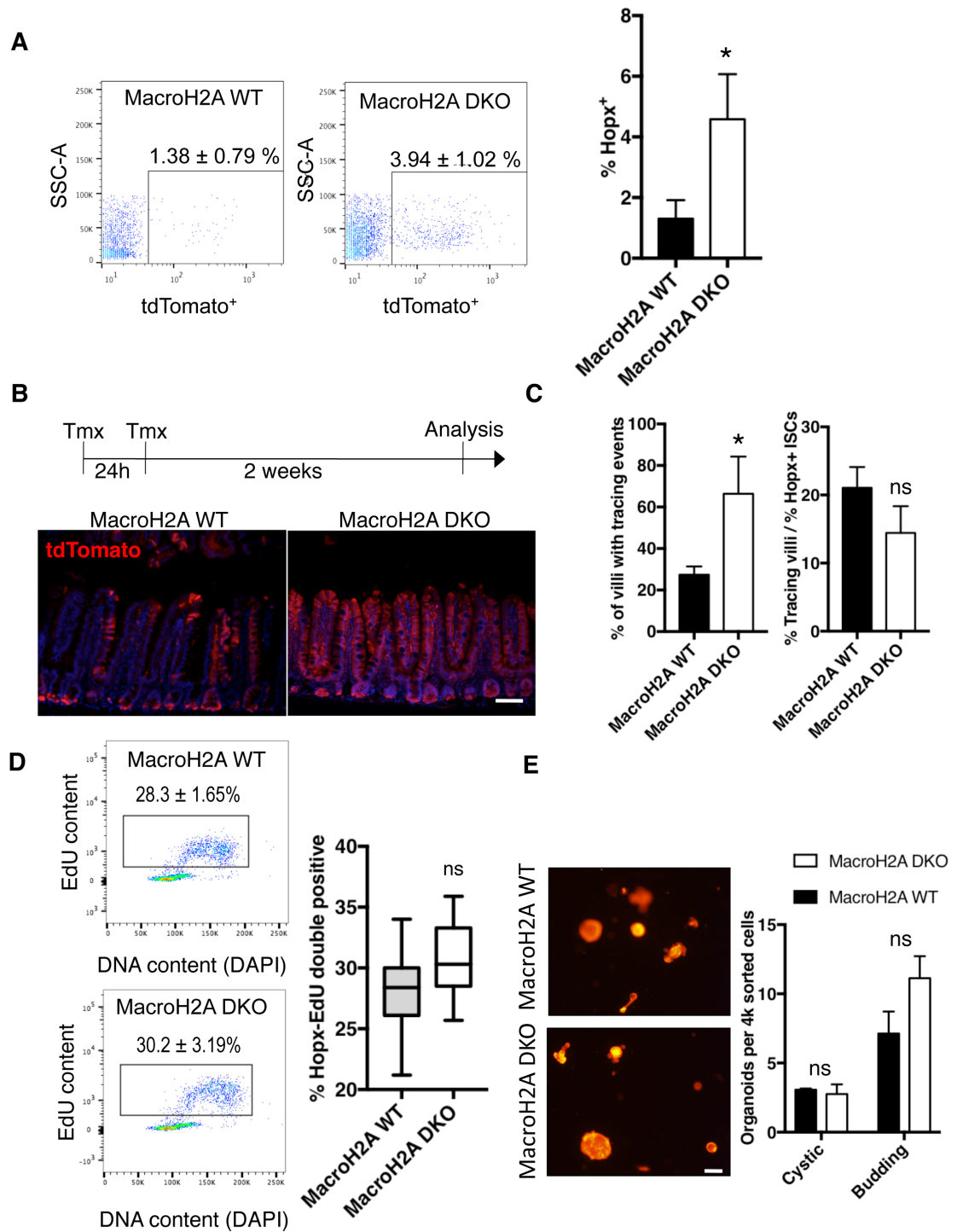
Figure 4.5: Reserve ISC frequency and activity in macroH2A DKO intestine.

Figure 4.5: Reserve ISC frequency and activity in macroH2A DKO intestine. (A) Left: representative flow cytometry plots of SSC-A vs. *Hopx-tdTomato*$^+$ signal in proximal small intestine crypt cells from macroH2A WT or DKO mice. Right: quantitation of *Hopx-tdTomato*$^+$ population as a percentage of crypt epithelial cells. N=5 mice per condition, mean ± SD. (B) Top: homeostatic lineage-tracing scheme: macroH2A WT and DKO *Hopx-CreERT2::Rosa26-LSL-tdTomato* mice were injected with 2mg tamoxifen for 2 consecutive days followed by a 2-week chase. Bottom: representative anti-tdTomato immunofluorescence of macroH2A WT and DKO proximal small intestine 2-weeks after induction of *Hopx-tdTomato* lineage tracing. 4x objective. (C) Left: quantitation of percentage of villi with tracing events after 2 week chase, N=3 mice per condition, mean ± SD. Right: percentage of villi with tracing events normalized to percentage of *Hopx-tdTomato*$^+$ ISCs during homeostasis (values in Figure 4A). N=3 mice per condition, mean ± SD. (D) Left: representative flow cytometry plots of EdU content vs. DAPI of within *Hopx-tdTomato*$^+$ subpopulations of macroH2A WT and DKO proximal small intestinal crypt cells. Right: quantitation of *Hopx-tdTomato*/EdU double positivity as defined by boxed subpopulation on left. N=7 mice per condition, medians, quartiles and ranges of values shown. (E) Left: representative Hopx-tdTomato$^+$ immunofluorescence of organoids after 7 days culture. Right: Quantitation of cystic and budding organoids per 4000 FACS-sorted Hopx-tdTomato$^+$ cells plated, day 7, N = 2 mice per condition, mean ± SD, *p<0.05, ns = not significant, Student's *t*-test. Scale bars = 100μm.
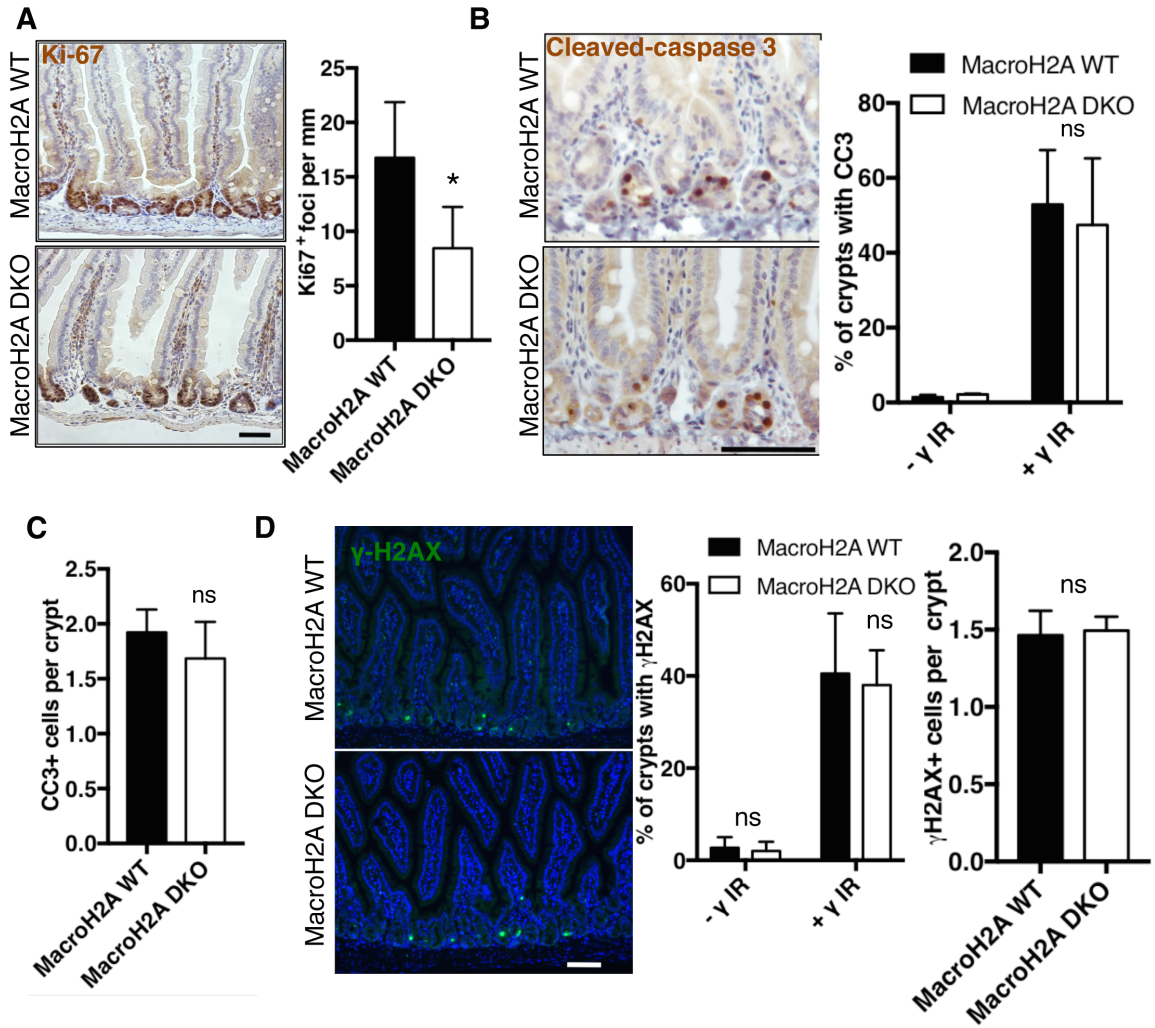
Figure 4.6: Regeneration and DNA damage response in macroH2A DKO intestine.

Figure 4.6: Regeneration and DNA damage response in macroH2A DKO intestine.

(A) Left: representative images of Ki-67 immmunohistochemistry within macroH2A WT and DKO proximal small intestine 3 days after exposure of mice to 12 Gy whole body γ-irradiation. 10x objective. Right: quantitation of Ki67$^+$ nascent crypt foci per mm. N = 3 mice per condition, mean ± SD. (B) Left: representative images of cleaved-caspase 3 (CC3) immunohistochemistry within macroH2A WT and DKO proximal small intestine 24 hours after exposure to 12 Gy. 40x objective. Right: quantitation of percent of crypts with CC3 signal during homeostasis or 24 hours after 12Gy. N = 3 mice per condition, mean ± SD. (C) Quantitation of average CC3$^+$ cells per crypt with at least one CC3$^+$ cell 24 hours after γ-irradiation. N=3 per condition, mean ± SD. (D) Left: representative images of γH2AX immunofluorescence within macroH2A WT and DKO proximal small intestine 24 hours after exposure to 12 Gy. 10x objective. Middle: quantitation of percent of crypts with γH2AX signal during homeostasis or 24 hours after 12Gy. N = 3 mice per condition, mean ± SD. Right: quantitation of average γH2AX cells per crypt with at least one CC3$^+$ cell 24 hours after γ-irradiation. N=3 per condition, mean ± SD. Scale bar = 100μm. ns = not significant, Student's *t*-test.

A

Tmx   Tmx   γ-IR   Analysis

24h   24h   72h

MacroH2A WT   MacroH2A DKO

tdTomato

B

Tracing foci per 500um

MacroH2A WT   MacroH2A DKO   ns

Foci per 500um / % Hopx+ ISCs

MacroH2A WT   MacroH2A DKO   ***

C

MacroH2A WT   MacroH2A DKO

Total crypt epithelium:

SSC-A — 15.7 ± 3.11 % — Comp-450 50 Violet-A

SSC-A — 15.1 ± 4.81 % — Comp-450 50 Violet-A

Hopx-tdTomato+ subpopulation:

SSC-A — 8.69 ± 0.61 % — Cleaved Caspase-3

SSC-A — 15.63 ± 2.13 % — Cleaved Caspase-3

% CC3 positive

■ MacroH2A WT   □ MacroH2A DKO

Total crypt epithelium   ns

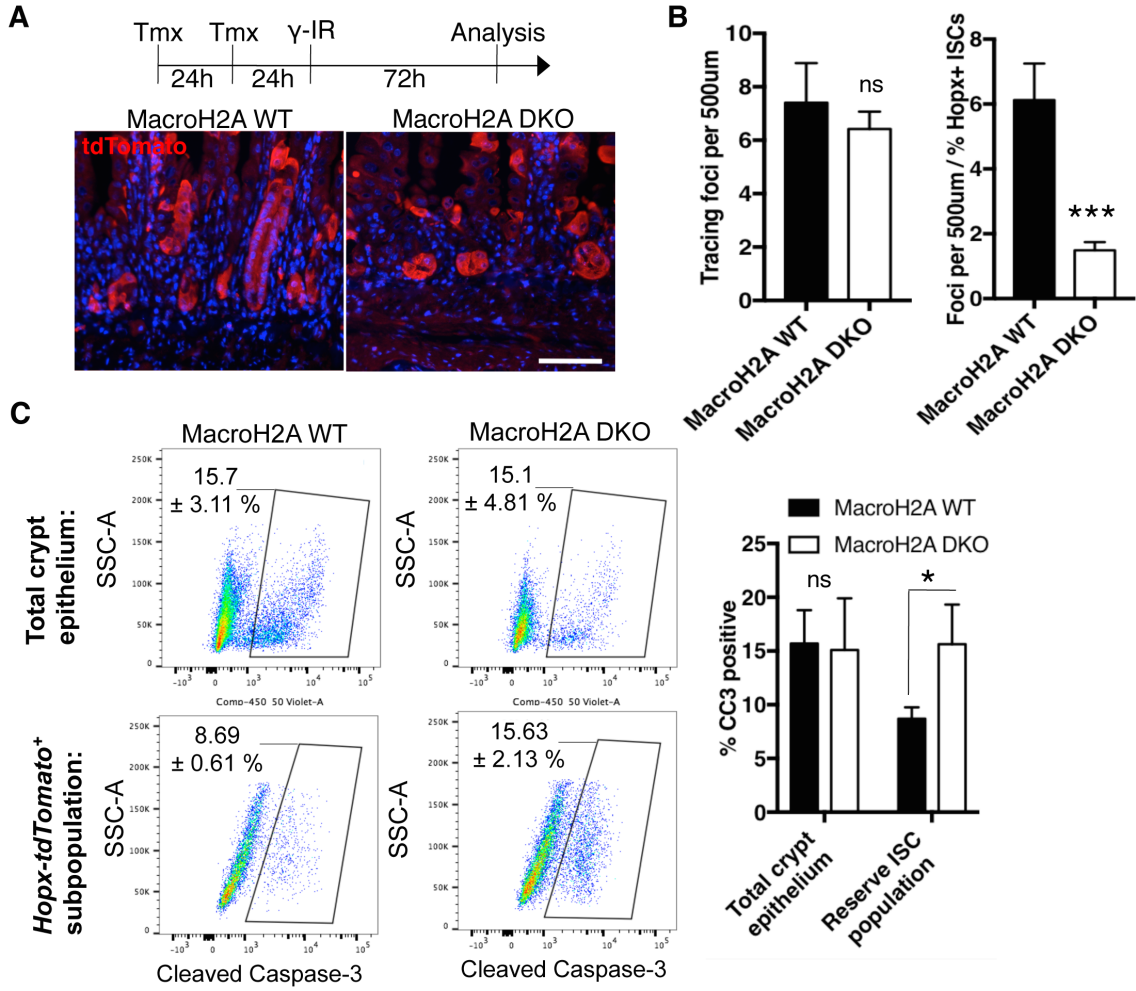Reserve ISC population   *

Figure 4.7: Radiosensitivity of macroH2A WT and DKO reserve ISCs.

Figure 4.7: Radiosensitivity of macroH2A WT and DKO reserve ISCs. (A) Top: post-IR lineage tracing scheme: macroH2A WT or DKO *Hopx-CreERT2::Rosa26-LSL-tdTomato* mice were injected with 2mg tamoxifen 48h and 24h prior to treatment with 12 Gy whole-body gamma irradiation, and 72h later sacrificed for analysis. Bottom: representative immunofluorescence of tdTomato lineage tracing within macroH2A WT and DKO crypts 120 hours after initial *Hopx-tdTomato* induction and 72 hours after γ-irradiation. 30x objective (B) Left: quantitation of tdTomato tracing events per 500μm, N=3 mice per condition, mean ± SD. Right: quantitation of tdTomato tracing events per 500μm normalized to percentage of *Hopx-tdTomato$^+$* ISCs during homeostasis (values in Figure 4A), N=3 mice per condition, mean ± SD. (C) Left: flow cytometry plots of SSC-A vs. cleaved caspase-3 content within total crypt epithelium or *Hopx-tdTomato$^+$* subpopulations of macroH2A WT and DKO proximal small intestinal crypt cells 24 hours after γ-irradiation. Right: quantitation of total crypt epithelium CC3 positivity and *Hopx-tdTomato$^+$/*CC3 double positivity as defined by boxed subpopulation on left. N=3 mice per condition, mean ± SD. *p<0.05, ***p<0.0005, ns = not significant, Student's *t*-test. Scale bars = 100μm.
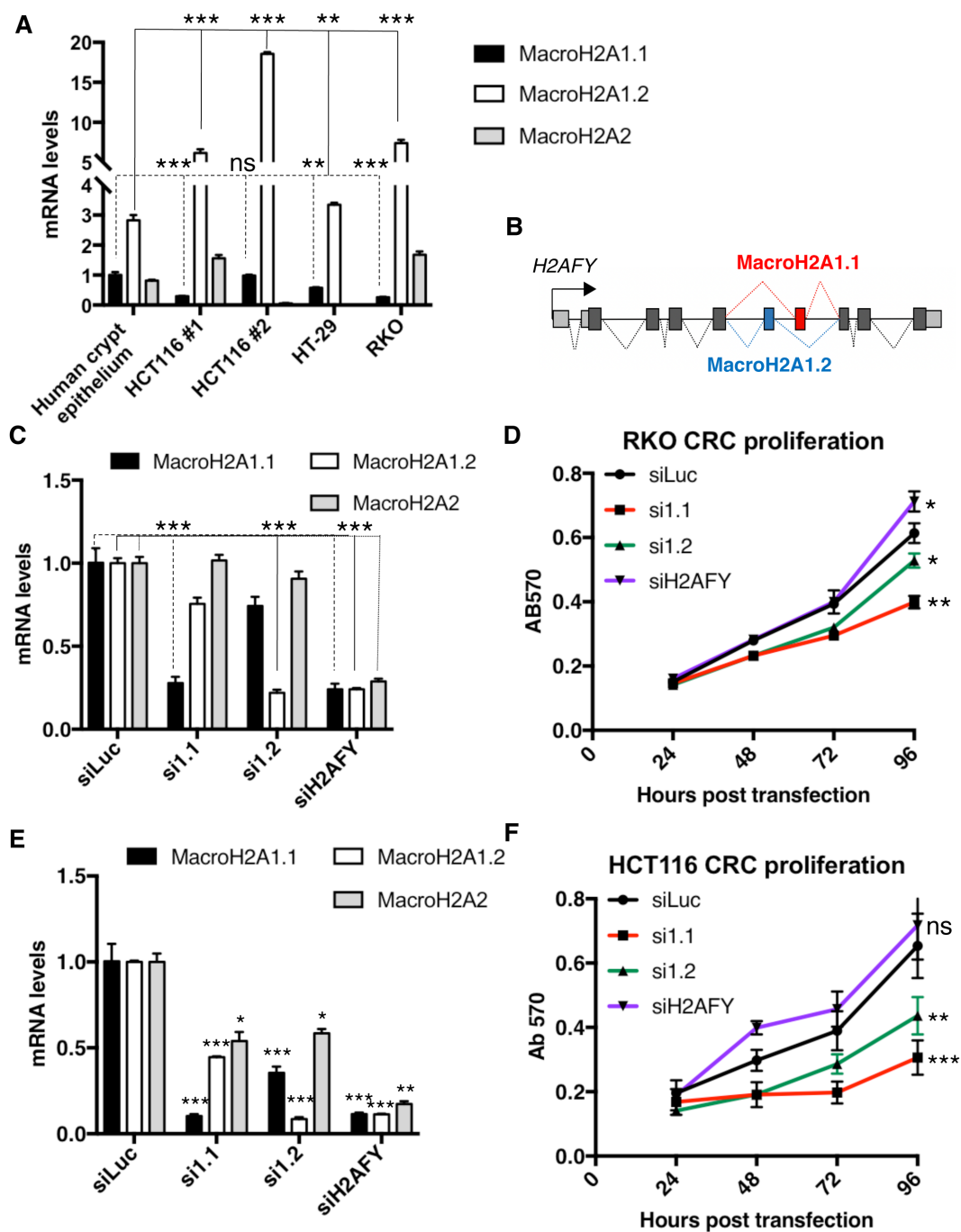
Figure 4.8: MacroH2A's influence on human colorectal cancer.

Figure 4.8: MacroH2A's influence of human colorectal cancer. (A) MacroH2A

mRNA level analysis of healthy human intestinal crypt epithelium and human CRC cell

lines. ΔΔCT method, values normalized to *GAPD*. N=3 per condition, mean ± SD. (B)

Graphical depiction of the *H2AFY* gene and its exons, including the mutually-exclusive

exons of the macroH2A1.1 and macroH2A1.2 splice variants. (C) MacroH2A siRNA

knockdown validation in RKO CRC cell line. ΔΔCT method, values normalized to *GAPD*

independently per macroH2A primer relative to luciferace knockdown control. N=3 per

condition, mean ± SD. (D) MTT cell proliferation assay of RKO cell line during

macroH2A1.1, 1.2, *H2AFY*, or control luciferace RNAi knockdown. N=3 per condition,

mean ± SD. (E) MacroH2A siRNA knockdown validation in HCT116 CRC cell line. ΔΔCT

method, values normalized to *GAPD* independently per macroH2A primer relative to

luciferace knockdown control. N=3 per condition, mean ± SD. (F) MTT cell proliferation

assay of HCT116 cell line during macroH2A1.1, 1.2, *H2AFY*, or control luciferace RNAi

knockdown. N=3 per condition, mean ± SD. *p<0.05, **p<0.005, ***p<0.0005, ns = not

significant, Student's *t*-test.
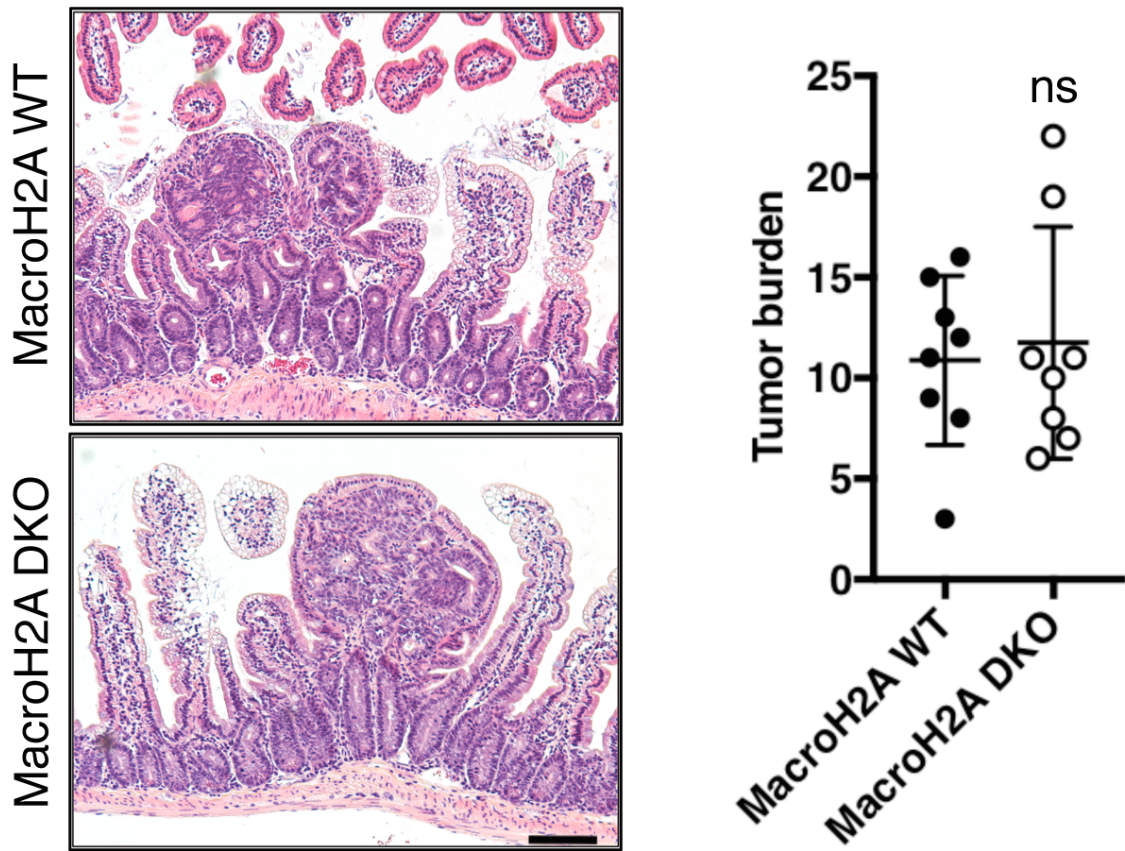
Figure 4.9: MacroH2A's effect on murine intestinal adenoma.

Figure 4.9: MacroH2A's effect on murine intestinal adenoma. Left: representative H&E images of macroH2A WT and DKO APC^{min} derived tumors within proximal small intestine. 4x objective. Right: quantitation of average total tumors within entire small intestine of macroH2A WT and DKO. N=8 mice per condition, mean ± SD, ns = not significant, Student's *t*-test. Scale bars = 100μm.
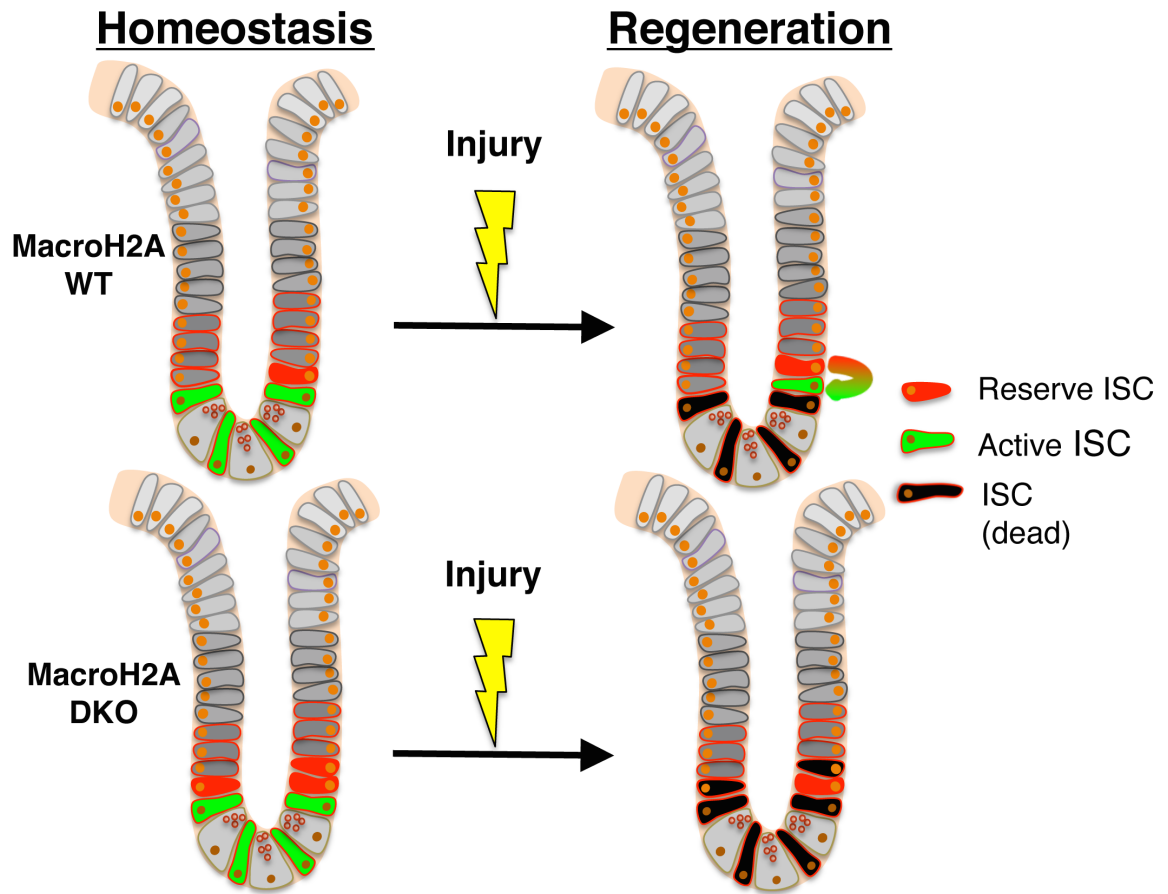
Figure 4.10: Model: Histone variant macroH2A confers intestinal fortitude.

Original intestinal crypt-villus image courtesy of Sarah Rauers

Figure 4.10: Model: Histone variant macroH2A confers intestinal fortitude. In sum, we show that macroH2A DKO intestine has approximately 3 times as many Hopx-tdTomato[+] reserve ISCs compared to WT, yet the DKO intestinal epithelium is otherwise normal and healthy during homeostasis. However, following 12 Gy γ-irradiation, macroH2A DKO intestinal epithelium is notably radiosensitive. The radiosensitivity phenotype is particularly evident within the macroH2A DKO Hopx-tdTomato[+] reserve ISCs, which disproportionately undergo apoptosis following irradiative damage compared to WT. We thus conclude that macroH2A confers intestinal fortitude by promoting reserve ISC survival and improving regeneration following γ-irradiation damage.

Chapter Five:

Conclusions and future directions

In the preceding chapters, I have extensively described the histone variant macroH2A's contributions to cellular identity and function. In my own work, I have employed two models of stem cell dynamics: induced pluripotent stem cell reprogramming and the murine intestinal stem cell system. Using these tools, I have contributed to the field of stem cell epigenetics by answering fundamental questions about the role macroH2A plays in governing stem cell homeostasis, post-injury regeneration, oncogenesis, and transgene-driven cell reprogramming. I broadly conclude that macroH2A confers epigenomic stability to cells by 'locking in' cell epigenetic identity, limiting stem cell pool size, safeguarding against genotoxic stress, and overall resisting epigenetic changes including those of both malignant transformations such as during oncogenesis and artificial transitions as a result of induced reprogramming.

My work, while largely in agreement with what others in the field observe, significantly is the first of its kind to describe the consequence of macroH2A germline knockout on stem cell dynamics *in vivo*. It is especially interesting that I observe that macroH2A DKO intestine is more radiosensitive than WT (Figure 4.6, 4.7), since several studies reveal that macroH2A contributes to the DNA damage response (Timinszky et al., 2009; Xu et al., 2012) despite the known fact that macroH2A DKO mice are viable and fertile (Pehrson et al., 2014). This result is even more interesting as many other studies indicate that macroH2A isn't necessary for many processes its implicated in, yet macroH2A is thought to provide epigenetic reinforcement over a range of conditions. One example is X-inactivation, which at baseline doesn't depend on macroH2A (Csankovszki et al., 1999), yet evidence exists that macroH2A is necessary for 'stable' X-inactivation (Hernández-Muñoz et al., 2005). Another example is the fact that macroH2A is not necessary for development (Pehrson et al., 2014), yet macroH2A is

necessary for proper spatiotemportal expression of key developmental genes (Buschbeck et al., 2009). It's therefore tempting to speculate that macroH2A provides an additional layer of epigenetic reinforcement or even redundancy, which increases the stability of chromatin architecture and thus gene expression.

It's also interesting that macroH2A has been implicated in regulating cell cycle kinetics (Kim et al., 2013; Kim et al., 2012), despite the fact that I do not observe differences in cell proliferation with and without macroH2A (Figures 3.5, 4.4, 4.5). It could be that acute macroH2A disruption in the aforementioned studies may elicit more profound effects on the cell cycle than my methodology, which utilizes germline macroH2A knockout, potentially allowing adaptation back to baseline cell cycle kinetics long-term. Nevertheless, it's especially interesting that I observe nearly 3 times as many reserve ISCs in macroH2A DKO mice, despite not observing significant differences in reserve ISC proliferation. This result, while consistent with a prior report that suggests macroH2A limits stem cell self-renewal (Creppe et al., 2012), could indicate that in macroH2A DKO mice reserve ISC numbers are specified earlier in development or are otherwise influenced by a macroH2A DKO niche. Further studies should employ targeted macroH2A deletion regimens, including using a Hopx-driven Cre, to determine whether the observed increased reserve ISC number is cell autonomous.

I observe that macroH2A confers a slight epigenetic barrier to iPSC reprogramming, consistent with prior reports (Barrero et al., 2013a; Gaspar-Maia et al., 2013; Pasque et al., 2012). However, I contend that those studies exaggerate the degree to which macroH2A is an actual epigenetic barrier, and I discuss such nuances in detail in Chapter 3. Further, our data highlight that the notion that macroH2A is removed from somatic chromatin during the epigenetic transition toward a macroH2A-depleted

pluripotent state is too simplistic an overall view, since it doesn't take into account differential incorporation patterns of the functionally distinct macroH2A isoforms. Others and we have shown that macroH2A does indeed function in mESCs, where among other tasks it localizes to lineage-specific genes (Yildirim et al., 2014). We have also shown that macroH2A2 engages in dynamic behavior in mESCs to a greater extent than MEFs, and such rapid macroH2A2 incorporation and turnover proximal to mESC promoters correlates with high transcription (Yildirim et al., 2014) (Figure 3.3). It would be interesting to determine whether this phenomenon also exists for other macroH2A isoforms, and determine which genes exhibit differential macroH2A incorporation patterns in mESCs vs. MEFs and the functional consequences thereof.

Another interesting theme with respect to macroH2A's influence on gene expression is the reported metabolic gene disruption that mice with altered macroH2A expression experience, particularly with respect to fatty acid metabolism and lipid storage (Boulard et al., 2010; Changolkar et al., 2007; Pazienza et al., 2014; Sheedfar et al., 2015). It's especially curious that macroH2A mice tend to be smaller in body dimensions and lighter in weight than WT counterparts (Pehrson et al., 2014), and that liver macroH2A1 expression increases substantially during the transition of neonatal mice into young adulthood (Changolkar et al., 2007). It's tempting to further speculate that macroH2A may influence nutrient absorption or other metabolic functions within the intestinal epithelium as well as the liver. It would be interesting to determine whether macroH2A DKO mice respond similarly as WT to varied diets, including calorie restriction, as gauged by functional outputs such as activation of the mTOR pathway – a known sensor of growth factors and nutrient availability. It would also be interesting to

determine whether the gut microbiome of macroH2A DKO mice differs from WT, and whether macroH2A DKO mice may be more sensitive to disruption of intestinal flora.

My observation that macroH2A DKO mice bred into the APC[min] model of intestinal adenoma do not experience increased tumor burden relative to WT, despite literature evidence that suggests that macroH2A is a tumor suppressor is somewhat surprising (Figure 4.9). Nevertheless, this result is consistent with the notion that macroH2A-deficient mice are not more prone to spontaneous cancer than WT (Pehrson et al., 2014) and macroH2A's tumor suppression has mostly been described in human patient samples and cell lines (Barzily-Rokni et al., 2011; Cantariño et al., 2013; Kapoor et al., 2010; Novikov et al., 2011; Sporn and Jung, 2012; Sporn et al., 2009). Interestingly, I see in human CRC lines that distinct macroH2A isoform selection patterns are prevalent – enrichment of the macroH2A1.2 isoform and loss of macroH2A1.1. This result could suggest that loss of both macroH2A1.1 and macroH2A1.2, as is the case for my macroH2A DKO mice, may be zero-sum with respect to tumorogenesis. Development of tools to selectively express or knockdown individual H2AFY isoforms is paramount for fully characterizing macroH2A's role in cancer. Another possibility is that the epigenetic interspecies differences between mouse and human gastrointestinal tumorogenesis are sufficiently distinct with respect to macroH2A influence that attempting to model macroH2A loss in humans using mice is ultimately uninformative.

My work has uncovered many interesting facets of histone variant macroH2A, particularly properties of the macroH2A DKO reserve ISC, which create opportunities for additional experiments to address novel and ongoing questions. An important question is whether there exist key differences in the transcriptome of macroH2A DKO vs. WT reserve ISCs – therefore RNA-Seq on sorted Hopx-tdTomato[+] populations would be

especially informative. Further, it would be interesting to relate this information to which genomic loci macroH2A localizes to in WT reserve ISCs, and relate this behavior to gene expression. Another interesting experiment to perform would be single-cell multiplexed qRT-PCR on sorted DKO and WT Hopx-tdTomato$^+$ populations using the Fluidigm platform for principle component analysis. This would enable population-wide visualization of cell-to-cell mRNA variability within Hopx-tdTomato$^+$ cells, and cross-comparison of this population to the Lgr5-eGFP$^+$ active ISC population within macroH2A DKO and WT mice. Given that macroH2A DKO reserve ISCs are more abundant and radiosensitive than WT, I hypothesize that DKO Hopx-tdTomato$^+$ ISCs are more 'CBC-like' than their WT counterparts. This result would be interesting as it would suggest that macroH2A might play a role in 'locking down' reserve ISC identity and function in the intestinal epithelium, that macroH2A loss may effectively blur the line between the epigenetic identity of at least these two stem cell populations.

While the Lgr5-eGFP$^+$ CBCs of macroH2A WT and DKO mice do not differ in number or heretofore observed function, nevertheless it would be interesting to compare the transcriptome of these populations and perform the same experiments on these cells as described above for the Hopx-tdTomato$^+$ reserve ISC population. It would be interesting to determine whether macroH2A deposition within this cell type as well as reserve ISCs differs with age, since macroH2A has been shown to increase with age. If so, it may be possible that macroH2A DKO and WT active ISCs experience differential degrees of stem cell exhaustion over time, yet the observation that macroH2A DKO CBCs do not proliferate quicker than WT suggest against this notion. It would also be interesting to determine whether single-sorted Lgr5-eGFP^{high} DKO CBCs can outcompete their WT counterparts in organoid formation assays. Despite my current

data strongly suggesting that observed increased organoid genesis originates from greater numbers of Hopx-tdTomato$^+$ reserve ISCs, it's important to rule out whether DKO CBCs disproportionately contribute as well. Further experiments will need to be performed to determine whether there are indeed any differences in macroH2A DKO CBCs that thus far have gone unnoticed.

Another interesting intersection between macroH2A and reserve ISCs is that macroH2A is enriched on heterochromatin, and reserve ISCs are largely quiescent and mitotically inactive. Staining sorted Hopx-tdTomato$^+$ ISCs for total DNA and RNA content using Hoescht and Pyronin would indicate the relative degree of G0 occupancy that macroH2A DKO and WT reserve ISCs experience. One might also hypothesize that macroH2A DKO reserve ISC chromatin is less heterochromatic than WT, and thus more accessible to various transcription factors and other DNA-binding proteins. Chromatin accessibility assays including micrococcal nuclease sensitivity and ATAQ-Seq assays should be employed to determine whether this idea holds merit.

It would also be interesting to further analyze the DNA damage hypersensitivity phenotype of macroH2A DKO reserve ISCs. MacroH2A has been shown to direct genomic deposition of DNA damage repair effectors such as BRCA1 to double-strand break sites (Khurana et al., 2014). Thus, it would be particularly interesting to perform BRCA1/γ-H2AX co-localization assays within sorted Hopx-tdTomato$^+$ reserve ISCs at various time points after γ-irradiation. It could be that macroH2A absence within reserve ISCs reduces BRCA1 localization and subsequent recruitment of downstream homology-directed repair factors. It would also be interesting to determine whether other hallmarks of DDR and apoptosis are detectable and exhibit differential expression within DKO and WT reserve ISCs after γ-irradiation. One potential example is the Chk2 kinase, whose

phosphorylation and activation was shown to be slightly diminished following macroH2A knockdown (Xu et al., 2012). It would also be informative to generate a γ-irradiation dose-response curve for DKO and WT organoids i*n vitro*, with the anticipation that macroH2A DKO organoids are more sensitive to even lower doses than WT.

In conclusion, I have shown that while the histone variant macroH2A imposes only a minor barrier to iPSC reprogramming efficiency and is dispensable for intestinal homeostasis, macroH2A nevertheless maintains intestinal fortitude in response to genotoxic stress. MacroH2A confers this resilience through maintaining robust DNA damage resistance and promoting survival within the reserve ISC compartment. This study represents to the best of our knowledge the first time that functional consequences of macroH2A absence within an adult stem cell compartment have been demonstrated *in vivo*. Despite macroH2A ostensibly improving genomic stability, macroH2A DKO mice are no more sensitive to tumorogenesis via APC loss of heterozygosity. In collaboration with the Rando lab, we have also shown for the first time that histone variant macroH2A2 undergoes dynamic incorporation and turnover at diverse loci in the genome in addition to stable incorporation, and relate this behavior to gene expression. In sum, we broadly characterize histone macroH2A as an epigenetic reinforcer that upholds cell identity and function by multiple mechanisms including protecting chromatin from DNA damage, directing repair, maintaining robust gene expression control, and limiting aberrant drift of cell epigenetic identity. Our study opens the door to future research aimed at further characterizing macroH2A within the intestinal crypt, during iPSC reprogramming, within other stem cell systems, in other forms of malignant cell transformation, and during other forms of directed cellular reprogramming for regenerative medicine.

Chapter Six:

Bibliography

Bibliography

Ahmad, K., and S. Henikoff, 2002, The histone variant H3.3 marks active chromatin

by replication-independent nucleosome assembly: Mol Cell, v. 9, p. 1191-200.

Angelov, D., A. Molla, P. Y. Perche, F. Hans, J. Côté, S. Khochbin, P. Bouvet, and S.

Dimitrov, 2003, The histone variant macroH2A interferes with transcription

factor binding and SWI/SNF nucleosome remodeling: Mol Cell, v. 11, p. 1033-

41.

Aoki, R., M. Shoshkes-Carmel, N. Gao, S. Shin, C. L. May, M. L. Golson, A. M. Zahm, M.

Ray, C. L. Wiser, C. V. Wright, and K. H. Kaestner, 2016, Foxl1-expressing

mesenchymal cells constitute the intestinal stem cell niche: Cell Mol

Gastroenterol Hepatol, v. 2, p. 175-188.

Asfaha, S., Y. Hayakawa, A. Muley, S. Stokes, T. A. Graham, R. E. Ericksen, C. B.

Westphalen, J. von Burstin, T. L. Mastracci, D. L. Worthley, C. Guha, M. Quante,

A. K. Rustgi, and T. C. Wang, 2015, Krt19(+)/Lgr5(-) Cells Are Radioresistant

Cancer-Initiating Stem Cells in the Colon and Intestine: Cell Stem Cell, v. 16, p.

627-38.

Bannister, A. J., and T. Kouzarides, 2011, Regulation of chromatin by histone

modifications: Cell Res, v. 21, p. 381-95.

Bannister, A. J., P. Zegerman, J. F. Partridge, E. A. Miska, J. O. Thomas, R. C. Allshire,

and T. Kouzarides, 2001, Selective recognition of methylated lysine 9 on

histone H3 by the HP1 chromo domain: Nature, v. 410, p. 120-4.

Barker, N., M. Huch, P. Kujala, M. van de Wetering, H. J. Snippert, J. H. van Es, T. Sato, D. E. Stange, H. Begthel, M. van den Born, E. Danenberg, S. van den Brink, J. Korving, A. Abo, P. J. Peters, N. Wright, R. Poulsom, and H. Clevers, 2010, Lgr5(+ve) stem cells drive self-renewal in the stomach and build long-lived gastric units in vitro: Cell Stem Cell, v. 6, p. 25-36.

Barker, N., R. A. Ridgway, J. H. van Es, M. van de Wetering, H. Begthel, M. van den Born, E. Danenberg, A. R. Clarke, O. J. Sansom, and H. Clevers, 2009, Crypt stem cells as the cells-of-origin of intestinal cancer: Nature, v. 457, p. 608-11.

Barker, N., J. H. van Es, J. Kuipers, P. Kujala, M. van den Born, M. Cozijnsen, A. Haegebarth, J. Korving, H. Begthel, P. J. Peters, and H. Clevers, 2007, Identification of stem cells in small intestine and colon by marker gene Lgr5: Nature, v. 449, p. 1003-7.

Barrero, M. J., B. Sese, B. Kuebler, J. Bilic, S. Boue, M. Martí, and J. C. Izpisua Belmonte, 2013a, Macrohistone variants preserve cell identity by preventing the gain of H3K4me2 during reprogramming to pluripotency: Cell Rep, v. 3, p. 1005-11.

Barrero, M. J., B. Sese, M. Martí, and J. C. Izpisua Belmonte, 2013b, Macro histone variants are critical for the differentiation of human pluripotent cells: J Biol Chem, v. 288, p. 16110-6.

Barzily-Rokni, M., N. Friedman, S. Ron-Bigger, S. Isaac, D. Michlin, and A. Eden, 2011, Synergism between DNA methylation and macroH2A1 occupancy in epigenetic silencing of the tumor suppressor gene p16(CDKN2A): Nucleic Acids Res, v. 39, p. 1326-35.

Beard, C., K. Hochedlinger, K. Plath, A. Wutz, and R. Jaenisch, 2006, Efficient method to generate single-copy transgenic mice by site-specific integration in embryonic stem cells: Genesis, v. 44, p. 23-8.

Black, B. E., L. E. Jansen, P. S. Maddox, D. R. Foltz, A. B. Desai, J. V. Shah, and D. W. Cleveland, 2007, Centromere identity maintained by nucleosomes assembled with histone H3 containing the CENP-A targeting domain: Mol Cell, v. 25, p. 309-22.

Boulard, M., S. Storck, R. Cong, R. Pinto, H. Delage, and P. Bouvet, 2010, Histone variant macroH2A1 deletion in mice causes female-specific steatosis: Epigenetics Chromatin, v. 3, p. 8.

Brambrink, T., R. Foreman, G. G. Welstead, C. J. Lengner, M. Wernig, H. Suh, and R. Jaenisch, 2008, Sequential expression of pluripotency markers during direct reprogramming of mouse somatic cells: Cell Stem Cell, v. 2, p. 151-9.

Buschbeck, M., and S. B. Hake, 2017, Variants of core histones and their roles in cell fate decisions, development and cancer: Nat Rev Mol Cell Biol, v. 18, p. 299-314.

Buschbeck, M., I. Uribesalgo, I. Wibowo, P. Rué, D. Martin, A. Gutierrez, L. Morey, R. Guigó, H. López-Schier, and L. Di Croce, 2009, The histone variant macroH2A is an epigenetic regulator of key developmental genes: Nat Struct Mol Biol, v. 16, p. 1074-9.

Cantariño, N., J. Douet, and M. Buschbeck, 2013, MacroH2A--an epigenetic regulator of cancer: Cancer Lett, v. 336, p. 247-52.

Carey, B. W., S. Markoulaki, J. Hanna, K. Saha, Q. Gao, M. Mitalipova, and R. Jaenisch, 2009, Reprogramming of murine and human somatic cells using a single polycistronic vector: Proc Natl Acad Sci U S A, v. 106, p. 157-62.

Chadwick, B. P., and H. F. Willard, 2001a, A novel chromatin protein, distantly related to histone H2A, is largely excluded from the inactive X chromosome: J Cell Biol, v. 152, p. 375-84.

Chadwick, B. P., and H. F. Willard, 2001b, Histone H2A variants and the inactive X chromosome: identification of a second macroH2A variant: Hum Mol Genet, v. 10, p. 1101-13.

Chadwick, B. P., and H. F. Willard, 2002, Cell cycle-dependent localization of macroH2A in chromatin of the inactive X chromosome: J Cell Biol, v. 157, p. 1113-23.

Chakravarthy, S., S. K. Gundimella, C. Caron, P. Y. Perche, J. R. Pehrson, S. Khochbin, and K. Luger, 2005, Structural characterization of the histone variant macroH2A: Mol Cell Biol, v. 25, p. 7616-24.

Chakravarthy, S., A. Patel, and G. D. Bowman, 2012, The basic linker of macroH2A stabilizes DNA at the entry/exit site of the nucleosome: Nucleic Acids Res, v. 40, p. 8285-95.

Chang, C. C., S. Gao, L. Y. Sung, G. N. Corry, Y. Ma, Z. P. Nagy, X. C. Tian, and T. P. Rasmussen, 2010, Rapid elimination of the histone variant MacroH2A from somatic cell heterochromatin after nuclear transfer: Cell Reprogram, v. 12, p. 43-53.

Chang, C. C., Y. Ma, S. Jacobs, X. C. Tian, X. Yang, and T. P. Rasmussen, 2005, A

maternal store of macroH2A is removed from pronuclei prior to onset of

somatic macroH2A expression in preimplantation embryos: Dev Biol, v. 278,

p. 367-80.

Chang, E. Y., H. Ferreira, J. Somers, D. A. Nusinow, T. Owen-Hughes, and G. J. Narlikar,

2008, MacroH2A allows ATP-dependent chromatin remodeling by SWI/SNF

and ACF complexes but specifically reduces recruitment of SWI/SNF:

Biochemistry, v. 47, p. 13726-32.

Changolkar, L. N., C. Costanzi, N. A. Leu, D. Chen, K. J. McLaughlin, and J. R. Pehrson,

2007, Developmental changes in histone macroH2A1-mediated gene

regulation: Mol Cell Biol, v. 27, p. 2758-64.

Changolkar, L. N., and J. R. Pehrson, 2006, macroH2A1 histone variants are depleted

on active genes but concentrated on the inactive X chromosome: Mol Cell

Biol, v. 26, p. 4410-20.

Chen, H., P. D. Ruiz, L. Novikov, A. D. Casill, J. W. Park, and M. J. Gamble, 2014,

MacroH2A1.1 and PARP-1 cooperate to regulate transcription by promoting

CBP-mediated H2B acetylation: Nat Struct Mol Biol, v. 21, p. 981-9.

Cheng, H., and C. P. Leblond, 1974, Origin, differentiation and renewal of the four

main epithelial cell types in the mouse small intestine. V. Unitarian Theory of

the origin of the four epithelial cell types: Am J Anat, v. 141, p. 537-61.

Cong, R., S. Das, J. Douet, J. Wong, M. Buschbeck, F. Mongelard, and P. Bouvet, 2014,

macroH2A1 histone variant represses rDNA transcription: Nucleic Acids Res,

v. 42, p. 181-92.

Costanzi, C., and J. R. Pehrson, 1998, Histone macroH2A1 is concentrated in the inactive X chromosome of female mammals: Nature, v. 393, p. 599-601.

Costanzi, C., and J. R. Pehrson, 2001, MACROH2A2, a new member of the MARCOH2A core histone family: J Biol Chem, v. 276, p. 21776-84.

Costanzi, C., P. Stein, D. M. Worrad, R. M. Schultz, and J. R. Pehrson, 2000, Histone macroH2A1 is concentrated in the inactive X chromosome of female preimplantation mouse embryos: Development, v. 127, p. 2283-9.

Creppe, C., P. Janich, N. Cantariño, M. Noguera, V. Valero, E. Musulén, J. Douet, M. Posavec, J. Martín-Caballero, L. Sumoy, L. Di Croce, S. A. Benitah, and M. Buschbeck, 2012, MacroH2A1 regulates the balance between self-renewal and differentiation commitment in embryonic and adult stem cells: Mol Cell Biol, v. 32, p. 1442-52.

Creyghton, M. P., S. Markoulaki, S. S. Levine, J. Hanna, M. A. Lodato, K. Sha, R. A. Young, R. Jaenisch, and L. A. Boyer, 2008, H2AZ is enriched at polycomb complex target genes in ES cells and is necessary for lineage commitment: Cell, v. 135, p. 649-61.

Csankovszki, G., B. Panning, B. Bates, J. R. Pehrson, and R. Jaenisch, 1999, Conditional deletion of Xist disrupts histone macroH2A localization but not maintenance of X inactivation: Nat Genet, v. 22, p. 323-4.

D'Amours, D., S. Desnoyers, I. D'Silva, and G. G. Poirier, 1999, Poly(ADP-ribosyl)ation reactions in the regulation of nuclear functions: Biochem J, v. 342 (Pt 2), p. 249-68.

Dai, B., and T. P. Rasmussen, 2007, Global epiproteomic signatures distinguish embryonic stem cells from differentiated cells: Stem Cells, v. 25, p. 2567-74.

Dardenne, E., S. Pierredon, K. Driouch, L. Gratadou, M. Lacroix-Triki, M. P. Espinoza, E. Zonta, S. Germann, H. Mortada, J. P. Villemin, M. Dutertre, R. Lidereau, S. Vagner, and D. Auboeuf, 2012, Splicing switch of an epigenetic regulator by RNA helicases promotes tumor-cell invasiveness: Nat Struct Mol Biol, v. 19, p. 1139-46.

David, K. K., S. A. Andrabi, T. M. Dawson, and V. L. Dawson, 2009, Parthanatos, a messenger of death: Front Biosci (Landmark Ed), v. 14, p. 1116-28.

de Murcia, J. M., C. Niedergang, C. Trucco, M. Ricoul, B. Dutrillaux, M. Mark, F. J. Oliver, M. Masson, A. Dierich, M. LeMeur, C. Walztinger, P. Chambon, and G. de Murcia, 1997, Requirement of poly(ADP-ribose) polymerase in recovery from DNA damage in mice and in cells: Proc Natl Acad Sci U S A, v. 94, p. 7303-7.

Dell'Orso, S., A. H. Wang, H. Y. Shih, K. Saso, L. Berghella, G. Gutierrez-Cruz, A. G. Ladurner, J. J. O'Shea, V. Sartorelli, and H. Zare, 2016, The Histone Variant MacroH2A1.2 Is Necessary for the Activation of Muscle Enhancers and Recruitment of the Transcription Factor Pbx1: Cell Rep, v. 14, p. 1156-68.

Dion, M. F., T. Kaplan, M. Kim, S. Buratowski, N. Friedman, and O. J. Rando, 2007, Dynamics of replication-independent histone turnover in budding yeast: Science, v. 315, p. 1405-8.

Douet, J., D. Corujo, R. Malinverni, J. Renauld, V. Sansoni, M. P. Marjanović, N. Cantari'o, V. Valero, F. Mongelard, P. Bouvet, A. Imhof, M. Thiry, and M.

Buschbeck, 2017, MacroH2A histone variants maintain nuclear organization and heterochromatin architecture: J Cell Sci.

Doyen, C. M., W. An, D. Angelov, V. Bondarenko, F. Mietton, V. M. Studitsky, A. Hamiche, R. G. Roeder, P. Bouvet, and S. Dimitrov, 2006, Mechanism of polymerase II transcription repression by the histone variant macroH2A: Mol Cell Biol, v. 26, p. 1156-64.

Efroni, S., R. Duttagupta, J. Cheng, H. Dehghani, D. J. Hoeppner, C. Dash, D. P. Bazett-Jones, S. Le Grice, R. D. McKay, K. H. Buetow, T. R. Gingeras, T. Misteli, and E. Meshorer, 2008, Global transcription in pluripotent embryonic stem cells: Cell Stem Cell, v. 2, p. 437-47.

Elliott, E. N., K. L. Sheaffer, and K. H. Kaestner, 2016, The 'de novo' DNA methyltransferase Dnmt3b compensates the Dnmt1-deficient intestinal epithelium: Elife, v. 5.

Elliott, E. N., K. L. Sheaffer, J. Schug, T. S. Stappenbeck, and K. H. Kaestner, 2015, Dnmt1 is essential to maintain progenitors in the perinatal intestinal epithelium: Development, v. 142, p. 2163-72.

Feng, B., J. Jiang, P. Kraus, J. H. Ng, J. C. Heng, Y. S. Chan, L. P. Yaw, W. Zhang, Y. H. Loh, J. Han, V. B. Vega, V. Cacheux-Rataboul, B. Lim, T. Lufkin, and H. H. Ng, 2009, Reprogramming of fibroblasts into induced pluripotent stem cells with orphan nuclear receptor Esrrb: Nat Cell Biol, v. 11, p. 197-203.

Fernandez-Capetillo, O., H. T. Chen, A. Celeste, I. Ward, P. J. Romanienko, J. C. Morales, K. Naka, Z. Xia, R. D. Camerini-Otero, N. Motoyama, P. B. Carpenter, W. M. Bonner, J. Chen, and A. Nussenzweig, 2002, DNA damage-induced G2-M

checkpoint activation by histone H2AX and 53BP1: Nat Cell Biol, v. 4, p. 993-7.

Fischle, W., B. S. Tseng, H. L. Dormann, B. M. Ueberheide, B. A. Garcia, J. Shabanowitz, D. F. Hunt, H. Funabiki, and C. D. Allis, 2005, Regulation of HP1-chromatin binding by histone H3 methylation and phosphorylation: Nature, v. 438, p. 1116-22.

Foltz, D. R., L. E. Jansen, B. E. Black, A. O. Bailey, J. R. Yates, and D. W. Cleveland, 2006, The human CENP-A centromeric nucleosome-associated complex: Nat Cell Biol, v. 8, p. 458-69.

Fre, S., M. Huyghe, P. Mourikis, S. Robine, D. Louvard, and S. Artavanis-Tsakonas, 2005, Notch signals control the fate of immature progenitor cells in the intestine: Nature, v. 435, p. 964-8.

Fu, Y., P. Lv, G. Yan, H. Fan, L. Cheng, F. Zhang, Y. Dang, H. Wu, and B. Wen, 2015, MacroH2A1 associates with nuclear lamina and maintains chromatin architecture in mouse liver cells: Sci Rep, v. 5, p. 17186.

Gamble, M. J., K. M. Frizzell, C. Yang, R. Krishnakumar, and W. L. Kraus, 2010, The histone variant macroH2A1 marks repressed autosomal chromatin, but protects a subset of its target genes from silencing: Genes Dev, v. 24, p. 21-32.

Gaspar-Maia, A., Z. A. Qadeer, D. Hasson, K. Ratnakumar, N. A. Leu, G. Leroy, S. Liu, C. Costanzi, D. Valle-Garcia, C. Schaniel, I. Lemischka, B. Garcia, J. R. Pehrson, and E. Bernstein, 2013, MacroH2A histone variants act as a barrier upon reprogramming towards pluripotency: Nat Commun, v. 4, p. 1565.

Goshima, T., M. Shimada, J. Sharif, H. Matsuo, T. Misaki, Y. Johmura, K. Murata, H.
Koseki, and M. Nakanishi, 2014, Mammal-specific H2A variant, H2ABbd, is
involved in apoptotic induction via activation of NF-κB signaling pathway: J
Biol Chem, v. 289, p. 11656-66.

Grigoryev, S. A., T. Nikitina, J. R. Pehrson, P. B. Singh, and C. L. Woodcock, 2004,
Dynamic relocation of epigenetic chromatin markers reveals an active role of
constitutive heterochromatin in the transition from proliferation to
quiescence: J Cell Sci, v. 117, p. 6153-62.

Gupte, R., Z. Liu, and W. L. Kraus, 2017, PARPs and ADP-ribosylation: recent
advances linking molecular functions to biological outcomes: Genes Dev, v.
31, p. 101-126.

Hanna, J., K. Saha, B. Pando, J. van Zon, C. J. Lengner, M. P. Creyghton, A. van
Oudenaarden, and R. Jaenisch, 2009, Direct cell reprogramming is a
stochastic process amenable to acceleration: Nature, v. 462, p. 595-601.

Hanna, J. H., K. Saha, and R. Jaenisch, 2010, Pluripotency and cellular
reprogramming: facts, hypotheses, unresolved issues: Cell, v. 143, p. 508-25.

Hernández-Muñoz, I., A. H. Lund, P. van der Stoop, E. Boutsma, I. Muijrers, E.
Verhoeven, D. A. Nusinow, B. Panning, Y. Marahrens, and M. van Lohuizen,
2005, Stable X chromosome inactivation involves the PRC1 Polycomb
complex and requires histone MACROH2A1 and the CULLIN3/SPOP ubiquitin
E3 ligase: Proc Natl Acad Sci U S A, v. 102, p. 7635-40.

Hirota, T., J. J. Lipp, B. H. Toh, and J. M. Peters, 2005, Histone H3 serine 10
    phosphorylation by Aurora B causes HP1 dissociation from heterochromatin:
    Nature, v. 438, p. 1176-80.

Hu, G., K. Cui, D. Northrup, C. Liu, C. Wang, Q. Tang, K. Ge, D. Levens, C. Crane-
    Robinson, and K. Zhao, 2013, H2A.Z facilitates access of active and repressive
    complexes to chromatin in embryonic stem cell self-renewal and
    differentiation: Cell Stem Cell, v. 12, p. 180-92.

Hua, G., T. H. Thin, R. Feldman, A. Haimovitz-Friedman, H. Clevers, Z. Fuks, and R.
    Kolesnick, 2012, Crypt base columnar stem cells in small intestines of mice
    are radioresistant: Gastroenterology, v. 143, p. 1266-76.

Huangfu, D., R. Maehr, W. Guo, A. Eijkelenboom, M. Snitow, A. E. Chen, and D. A.
    Melton, 2008, Induction of pluripotent stem cells by defined factors is greatly
    improved by small-molecule compounds: Nat Biotechnol, v. 26, p. 795-7.

Itzkovitz, S., A. Lyubimova, I. C. Blat, M. Maynard, J. van Es, J. Lees, T. Jacks, H.
    Clevers, and A. van Oudenaarden, 2011, Single-molecule transcript counting
    of stem-cell markers in the mouse intestine: Nat Cell Biol, v. 14, p. 106-14.

Jang, C. W., Y. Shibata, J. Starmer, D. Yee, and T. Magnuson, 2015, Histone H3.3
    maintains genome integrity during mammalian development: Genes Dev, v.
    29, p. 1377-92.

Jin, C., C. Zang, G. Wei, K. Cui, W. Peng, K. Zhao, and G. Felsenfeld, 2009, H3.3/H2A.Z
    double variant-containing nucleosomes mark 'nucleosome-free regions' of
    active promoters and other regulatory regions: Nat Genet, v. 41, p. 941-5.

Kapoor, A., M. S. Goldberg, L. K. Cumberland, K. Ratnakumar, M. F. Segura, P. O. Emanuel, S. Menendez, C. Vardabasso, G. Leroy, C. I. Vidal, D. Polsky, I. Osman, B. A. Garcia, E. Hernando, and E. Bernstein, 2010, The histone variant macroH2A suppresses melanoma progression through regulation of CDK8: Nature, v. 468, p. 1105-9.

Karras, G. I., G. Kustatscher, H. R. Buhecha, M. D. Allen, C. Pugieux, F. Sait, M. Bycroft, and A. G. Ladurner, 2005, The macro domain is an ADP-ribose binding module: EMBO J, v. 24, p. 1911-20.

Kazakevych, J., S. Sayols, B. Messner, C. Krienke, and N. Soshnikova, 2017, Dynamic changes in chromatin states during specification and differentiation of adult intestinal stem cells: Nucleic Acids Res.

Khurana, S., M. J. Kruhlak, J. Kim, A. D. Tran, J. Liu, K. Nyswaner, L. Shi, P. Jailwala, M. H. Sung, O. Hakim, and P. Oberdoerffer, 2014, A macrohistone variant links dynamic chromatin compaction to BRCA1-dependent genome maintenance: Cell Rep, v. 8, p. 1049-62.

Kim, J. M., K. Heo, J. Choi, K. Kim, and W. An, 2013, The histone variant MacroH2A regulates Ca(2+) influx through TRPC3 and TRPC6 channels: Oncogenesis, v. 2, p. e77.

Kim, M. Y., T. Zhang, and W. L. Kraus, 2005, Poly(ADP-ribosyl)ation by PARP-1: 'PAR-laying' NAD+ into a nuclear signal: Genes Dev, v. 19, p. 1951-67.

Kim, R., K. L. Sheaffer, I. Choi, K. J. Won, and K. H. Kaestner, 2016, Epigenetic regulation of intestinal stem cells by Tet1-mediated DNA hydroxymethylation: Genes Dev, v. 30, p. 2433-2442.

Kim, T. H., F. Li, I. Ferreiro-Neira, L. L. Ho, A. Luyten, K. Nalapareddy, H. Long, M. Verzi, and R. A. Shivdasani, 2014, Broadly permissive intestinal chromatin underlies lateral inhibition and cell plasticity: Nature, v. 506, p. 511-5.

Kim, W., G. Chakraborty, S. Kim, J. Shin, C. H. Park, M. W. Jeong, N. Bharatham, H. S. Yoon, and K. T. Kim, 2012, Macro histone H2A1.2 (macroH2A1) protein suppresses mitotic kinase VRK1 during interphase: J Biol Chem, v. 287, p. 5278-89.

Kreiling, J. A., M. Tamamori-Adachi, A. N. Sexton, J. C. Jeyapalan, U. Munoz-Najar, A. L. Peterson, J. Manivannan, E. S. Rogers, N. A. Pchelintsev, P. D. Adams, and J. M. Sedivy, 2011, Age-associated increase in heterochromatic marks in murine and primate tissues: Aging Cell, v. 10, p. 292-304.

Kustatscher, G., M. Hothorn, C. Pugieux, K. Scheffzek, and A. G. Ladurner, 2005, Splicing regulates NAD metabolite binding to histone macroH2A: Nat Struct Mol Biol, v. 12, p. 624-5.

Lavigne, M. D., G. Vatsellas, A. Polyzos, E. Mantouvalou, G. Sianidis, I. Maraziotis, M. Agelopoulos, and D. Thanos, 2015, Composite macroH2A/NRF-1 Nucleosomes Suppress Noise and Generate Robustness in Gene Expression: Cell Rep, v. 11, p. 1090-101.

Li, L., and H. Clevers, 2010, Coexistence of quiescent and active adult stem cells in mammals: Science, v. 327, p. 542-5.

Li, N., A. Nakauka-Ddamba, J. Tobias, S. T. Jensen, and C. J. Lengner, 2016, Mouse Label-Retaining Cells Are Molecularly and Functionally Distinct From Reserve Intestinal Stem Cells: Gastroenterology, v. 151, p. 298-310.e7.

Li, N., M. Yousefi, A. Nakauka-Ddamba, R. Jain, J. Tobias, J. A. Epstein, S. T. Jensen, and
C. J. Lengner, 2014, Single-cell analysis of proxy reporter allele-marked
epithelial cells establishes intestinal stem cell hierarchy: Stem Cell Reports, v.
3, p. 876-91.

Luger, K., A. W. Mäder, R. K. Richmond, D. F. Sargent, and T. J. Richmond, 1997,
Crystal structure of the nucleosome core particle at 2.8 A resolution: Nature,
v. 389, p. 251-60.

Maherali, N., R. Sridharan, W. Xie, J. Utikal, S. Eminli, K. Arnold, M. Stadtfeld, R.
Yachechko, J. Tchieu, R. Jaenisch, K. Plath, and K. Hochedlinger, 2007, Directly
reprogrammed fibroblasts show global epigenetic remodeling and
widespread tissue contribution: Cell Stem Cell, v. 1, p. 55-70.

Mahmoudi, T., S. F. Boj, P. Hatzis, V. S. Li, N. Taouatas, R. G. Vries, H. Teunissen, H.
Begthel, J. Korving, S. Mohammed, A. J. Heck, and H. Clevers, 2010, The
leukemia-associated Mllt10/Af10-Dot1l are Tcf4/β-catenin coactivators
essential for intestinal homeostasis: PLoS Biol, v. 8, p. e1000539.

Malanga, M., L. Atorino, F. Tramontano, B. Farina, and P. Quesada, 1998, Poly(ADP-
ribose) binding properties of histone H1 variants: Biochim Biophys Acta, v.
1399, p. 154-60.

Mansour, A. A., O. Gafni, L. Weinberger, A. Zviran, M. Ayyash, Y. Rais, V. Krupalnik, M.
Zerbib, D. Amann-Zalcenstein, I. Maza, S. Geula, S. Viukov, L. Holtzman, A.
Pribluda, E. Canaani, S. Horn-Saban, I. Amit, N. Novershtern, and J. H. Hanna,
2012, The H3K27 demethylase Utx regulates somatic and germ cell
epigenetic reprogramming: Nature, v. 488, p. 409-13.

Merlos-Suárez, A., F. M. Barriga, P. Jung, M. Iglesias, M. V. Céspedes, D. Rossell, M. Sevillano, X. Hernando-Momblona, V. da Silva-Diz, P. Muñoz, H. Clevers, E. Sancho, R. Mangues, and E. Batlle, 2011, The intestinal stem cell signature identifies colorectal cancer stem cells and predicts disease relapse: Cell Stem Cell, v. 8, p. 511-24.

Mermoud, J. E., C. Costanzi, J. R. Pehrson, and N. Brockdorff, 1999, Histone macroH2A1.2 relocates to the inactive X chromosome after initiation and propagation of X-inactivation: J Cell Biol, v. 147, p. 1399-408.

Mermoud, J. E., A. M. Tassin, J. R. Pehrson, and N. Brockdorff, 2001, Centrosomal association of histone macroH2A1.2 in embryonic stem cells and somatic cells: Exp Cell Res, v. 268, p. 245-51.

Metcalfe, C., N. M. Kljavin, R. Ybarra, and F. J. de Sauvage, 2014, Lgr5+ stem cells are indispensable for radiation-induced intestinal regeneration: Cell Stem Cell, v. 14, p. 149-59.

Mikkelsen, T. S., J. Hanna, X. Zhang, M. Ku, M. Wernig, P. Schorderet, B. E. Bernstein, R. Jaenisch, E. S. Lander, and A. Meissner, 2008, Dissecting direct reprogramming through integrative genomic analysis: Nature, v. 454, p. 49-55.

Mito, Y., J. G. Henikoff, and S. Henikoff, 2007, Histone replacement marks the boundaries of cis-regulatory domains: Science, v. 315, p. 1408-11.

Mitsui, K., Y. Tokuzawa, H. Itoh, K. Segawa, M. Murakami, K. Takahashi, M. Maruyama, M. Maeda, and S. Yamanaka, 2003, The homeoprotein Nanog is

required for maintenance of pluripotency in mouse epiblast and ES cells: Cell, v. 113, p. 631-42.

Montgomery, R. K., D. L. Carlone, C. A. Richmond, L. Farilla, M. E. Kranendonk, D. E. Henderson, N. Y. Baffour-Awuah, D. M. Ambruzs, L. K. Fogli, S. Algra, and D. T. Breault, 2011, Mouse telomerase reverse transcriptase (mTert) expression marks slowly cycling intestinal stem cells: Proc Natl Acad Sci U S A, v. 108, p. 179-84.

Mortusewicz, O., J. C. Amé, V. Schreiber, and H. Leonhardt, 2007, Feedback-regulated poly(ADP-ribosyl)ation by PARP-1 is required for rapid response to DNA damage in living cells: Nucleic Acids Res, v. 35, p. 7665-75.

Muñoz, J., D. E. Stange, A. G. Schepers, M. van de Wetering, B. K. Koo, S. Itzkovitz, R. Volckmann, K. S. Kung, J. Koster, S. Radulescu, K. Myant, R. Versteeg, O. J. Sansom, J. H. van Es, N. Barker, A. van Oudenaarden, S. Mohammed, A. J. Heck, and H. Clevers, 2012, The Lgr5 intestinal stem cell signature: robust expression of proposed quiescent '+4' cell markers: EMBO J, v. 31, p. 3079-91.

Nakagawa, M., M. Koyanagi, K. Tanabe, K. Takahashi, T. Ichisaka, T. Aoi, K. Okita, Y. Mochiduki, N. Takizawa, and S. Yamanaka, 2008, Generation of induced pluripotent stem cells without Myc from mouse and human fibroblasts: Nat Biotechnol, v. 26, p. 101-6.

Nashun, B., M. Yukawa, H. Liu, T. Akiyama, and F. Aoki, 2010, Changes in the nuclear deposition of histone H2A variants during pre-implantation development in mice: Development, v. 137, p. 3785-94.

Novikov, L., J. W. Park, H. Chen, H. Klerman, A. S. Jalloh, and M. J. Gamble, 2011, QKI-
mediated alternative splicing of the histone variant MacroH2A1 regulates
cancer cell proliferation: Mol Cell Biol, v. 31, p. 4244-55.

Nusinow, D. A., I. Hernández-Muñoz, T. G. Fazzio, G. M. Shah, W. L. Kraus, and B.
Panning, 2007, Poly(ADP-ribose) polymerase 1 is inhibited by a histone H2A
variant, MacroH2A, and contributes to silencing of the inactive X
chromosome: J Biol Chem, v. 282, p. 12851-9.

Onder, T. T., N. Kara, A. Cherry, A. U. Sinha, N. Zhu, K. M. Bernt, P. Cahan, B. O.
Marcarci, J. Unternaehrer, P. B. Gupta, E. S. Lander, S. A. Armstrong, and G. Q.
Daley, 2012, Chromatin-modifying enzymes as modulators of
reprogramming: Nature, v. 483, p. 598-602.

Ouararhni, K., R. Hadj-Slimane, S. Ait-Si-Ali, P. Robin, F. Mietton, A. Harel-Bellan, S.
Dimitrov, and A. Hamiche, 2006, The histone variant mH2A1.1 interferes
with transcription by down-regulating PARP-1 enzymatic activity: Genes
Dev, v. 20, p. 3324-36.

Pasque, V., A. Gillich, N. Garrett, and J. B. Gurdon, 2011, Histone variant macroH2A
confers resistance to nuclear reprogramming: EMBO J, v. 30, p. 2373-87.

Pasque, V., A. Radzisheuskaya, A. Gillich, R. P. Halley-Stott, M. Panamarova, M.
Zernicka-Goetz, M. A. Surani, and J. C. Silva, 2012, Histone variant macroH2A
marks embryonic differentiation in vivo and acts as an epigenetic barrier to
induced pluripotency: J Cell Sci, v. 125, p. 6094-104.

Pasque, V., J. Tchieu, R. Karnik, M. Uyeda, A. Sadhu Dimashkie, D. Case, B. Papp, G.
Bonora, S. Patel, R. Ho, R. Schmidt, R. McKee, T. Sado, T. Tada, A. Meissner,

and K. Plath, 2014, X chromosome reactivation dynamics reveal stages of reprogramming to pluripotency: Cell, v. 159, p. 1681-97.

Pazienza, V., M. Borghesan, T. Mazza, F. Sheedfar, C. Panebianco, R. Williams, G. Mazzoccoli, A. Andriulli, T. Nakanishi, and M. Vinciguerra, 2014, SIRT1-metabolite binding histone macroH2A1.1 protects hepatocytes against lipid accumulation: Aging (Albany NY), v. 6, p. 35-47.

Pehrson, J. R., L. N. Changolkar, C. Costanzi, and N. A. Leu, 2014, Mice without macroH2A histone variants: Mol Cell Biol, v. 34, p. 4523-33.

Pehrson, J. R., C. Costanzi, and C. Dharia, 1997, Developmental and tissue expression patterns of histone macroH2A1 subtypes: J Cell Biochem, v. 65, p. 107-13.

Pehrson, J. R., and V. A. Fried, 1992, MacroH2A, a core histone containing a large nonhistone region: Science, v. 257, p. 1398-400.

Pehrson, J. R., and R. N. Fuji, 1998, Evolutionary conservation of histone macroH2A subtypes and domains: Nucleic Acids Res, v. 26, p. 2837-42.

Pinto, D., A. Gregorieff, H. Begthel, and H. Clevers, 2003, Canonical Wnt signals are essential for homeostasis of the intestinal epithelium: Genes Dev, v. 17, p. 1709-13.

Poirier, G. G., G. de Murcia, J. Jongstra-Bilen, C. Niedergang, and P. Mandel, 1982, Poly(ADP-ribosyl)ation of polynucleosomes causes relaxation of chromatin structure: Proc Natl Acad Sci U S A, v. 79, p. 3423-7.

Potten, C. S., 1977, Extreme sensitivity of some intestinal crypt cells to X and gamma irradiation: Nature, v. 269, p. 518-21.

Potten, C. S., L. Kovacs, and E. Hamilton, 1974, Continuous labelling studies on
mouse skin and intestine: Cell Tissue Kinet, v. 7, p. 271-83.

Powell, A. E., Y. Wang, Y. Li, E. J. Poulin, A. L. Means, M. K. Washington, J. N.
Higginbotham, A. Juchheim, N. Prasad, S. E. Levy, Y. Guo, Y. Shyr, B. J. Aronow,
K. M. Haigis, J. L. Franklin, and R. J. Coffey, 2012, The pan-ErbB negative
regulator Lrig1 is an intestinal stem cell marker that functions as a tumor
suppressor: Cell, v. 149, p. 146-58.

Rasmussen, T. P., T. Huang, M. A. Mastrangelo, J. Loring, B. Panning, and R. Jaenisch,
1999, Messenger RNAs encoding mouse histone macroH2A1 isoforms are
expressed at similar levels in male and female cells and result from
alternative splicing: Nucleic Acids Res, v. 27, p. 3685-9.

Ratnakumar, K., L. F. Duarte, G. LeRoy, D. Hasson, D. Smeets, C. Vardabasso, C.
Bönisch, T. Zeng, B. Xiang, D. Y. Zhang, H. Li, X. Wang, S. B. Hake, L.
Schermelleh, B. A. Garcia, and E. Bernstein, 2012, ATRX-mediated chromatin
association of histone variant macroH2A1 regulates α-globin expression:
Genes Dev, v. 26, p. 433-8.

Ritsma, L., S. I. Ellenbroek, A. Zomer, H. J. Snippert, F. J. de Sauvage, B. D. Simons, H.
Clevers, and J. van Rheenen, 2014, Intestinal crypt homeostasis revealed at
single-stem-cell level by in vivo live imaging: Nature, v. 507, p. 362-5.

Rogakou, E. P., D. R. Pilch, A. H. Orr, V. S. Ivanova, and W. M. Bonner, 1998, DNA
double-stranded breaks induce histone H2AX phosphorylation on serine 139:
J Biol Chem, v. 273, p. 5858-68.

Sangiorgi, E., and M. R. Capecchi, 2008, Bmi1 is expressed in vivo in intestinal stem

   cells: Nat Genet, v. 40, p. 915-20.

Sato, T., J. H. van Es, H. J. Snippert, D. E. Stange, R. G. Vries, M. van den Born, N.

   Barker, N. F. Shroyer, M. van de Wetering, and H. Clevers, 2011, Paneth cells

   constitute the niche for Lgr5 stem cells in intestinal crypts: Nature, v. 469, p.

   415-8.

Sato, T., R. G. Vries, H. J. Snippert, M. van de Wetering, N. Barker, D. E. Stange, J. H.

   van Es, A. Abo, P. Kujala, P. J. Peters, and H. Clevers, 2009, Single Lgr5 stem

   cells build crypt-villus structures in vitro without a mesenchymal niche:

   Nature, v. 459, p. 262-5.

Sheedfar, F., M. Vermeer, V. Pazienza, J. Villarroya, F. Rappa, F. Cappello, G.

   Mazzoccoli, F. Villarroya, H. van der Molen, M. H. Hofker, D. P. Koonen, and M.

   Vinciguerra, 2015, Genetic ablation of macrohistone H2A1 leads to increased

   leanness, glucose tolerance and energy expenditure in mice fed a high-fat

   diet: Int J Obes (Lond), v. 39, p. 331-8.

Singhal, N., J. Graumann, G. Wu, M. J. Araúzo-Bravo, D. W. Han, B. Greber, L. Gentile,

   M. Mann, and H. R. Schöler, 2010, Chromatin-Remodeling Components of the

   BAF Complex Facilitate Reprogramming: Cell, v. 141, p. 943-55.

Sommer, C. A., M. Stadtfeld, G. J. Murphy, K. Hochedlinger, D. N. Kotton, and G.

   Mostoslavsky, 2009, Induced pluripotent stem cell generation using a single

   lentiviral stem cell cassette: Stem Cells, v. 27, p. 543-9.

Sporn, J. C., and B. Jung, 2012, Differential regulation and predictive potential of

   MacroH2A1 isoforms in colon cancer: Am J Pathol, v. 180, p. 2516-26.

Sporn, J. C., G. Kustatscher, T. Hothorn, M. Collado, M. Serrano, T. Muley, P. Schnabel, and A. G. Ladurner, 2009, Histone macroH2A isoforms predict the risk of lung cancer recurrence: Oncogene, v. 28, p. 3423-8.

Stadtfeld, M., N. Maherali, D. T. Breault, and K. Hochedlinger, 2008, Defining molecular cornerstones during fibroblast to iPS cell reprogramming in mouse: Cell Stem Cell, v. 2, p. 230-40.

Stamataki, D., M. Holder, C. Hodgetts, R. Jeffery, E. Nye, B. Spencer-Dene, D. J. Winton, and J. Lewis, 2011, Delta1 expression, cell cycle exit, and commitment to a specific secretory fate coincide within a few hours in the mouse intestinal stem cell system: PLoS One, v. 6, p. e24484.

Su, L. K., K. W. Kinzler, B. Vogelstein, A. C. Preisinger, A. R. Moser, C. Luongo, K. A. Gould, and W. F. Dove, 1992, Multiple intestinal neoplasia caused by a mutation in the murine homolog of the APC gene: Science, v. 256, p. 668-70.

Sullivan, K. F., M. Hechenberger, and K. Masri, 1994, Human CENP-A contains a histone H3 related histone fold domain that is required for targeting to the centromere: J Cell Biol, v. 127, p. 581-92.

Syed, K. M., S. Joseph, A. Mukherjee, A. Majumder, J. M. Teixeira, D. Dutta, and M. R. Pillai, 2016, Histone chaperone APLF regulates induction of pluripotency in murine fibroblasts: J Cell Sci, v. 129, p. 4576-4591.

Takahashi, K., and S. Yamanaka, 2006, Induction of pluripotent stem cells from mouse embryonic and adult fibroblast cultures by defined factors: Cell, v. 126, p. 663-76.

Takeda, N., R. Jain, M. R. LeBoeuf, Q. Wang, M. M. Lu, and J. A. Epstein, 2011,
Interconversion between intestinal stem cell populations in distinct niches:
Science, v. 334, p. 1420-4.

Tanasijevic, B., and T. P. Rasmussen, 2011, X chromosome inactivation and
differentiation occur readily in ES cells doubly-deficient for macroH2A1 and
macroH2A2: PLoS One, v. 6, p. e21512.

Tao, S., D. Tang, Y. Morita, T. Sperka, O. Omrani, A. Lechel, V. Sakk, J. Kraus, H. A.
Kestler, M. Kühl, and K. L. Rudolph, 2015, Wnt activity and basal niche
position sensitize intestinal stem and progenitor cells to DNA damage: EMBO
J, v. 34, p. 624-40.

Tetteh, P. W., O. Basak, H. F. Farin, K. Wiebrands, K. Kretzschmar, H. Begthel, M. van
den Born, J. Korving, F. de Sauvage, J. H. van Es, A. van Oudenaarden, and H.
Clevers, 2016, Replacement of Lost Lgr5-Positive Stem Cells through
Plasticity of Their Enterocyte-Lineage Daughters: Cell Stem Cell, v. 18, p. 203-
13.

Tian, H., B. Biehs, S. Warming, K. G. Leong, L. Rangell, O. D. Klein, and F. J. de Sauvage,
2011, A reserve stem cell population in small intestine renders Lgr5-positive
cells dispensable: Nature, v. 478, p. 255-9.

Timinszky, G., S. Till, P. O. Hassa, M. Hothorn, G. Kustatscher, B. Nijmeijer, J.
Colombelli, M. Altmeyer, E. H. Stelzer, K. Scheffzek, M. O. Hottiger, and A. G.
Ladurner, 2009, A macrodomain-containing histone rearranges chromatin
upon sensing PARP1 activation: Nat Struct Mol Biol, v. 16, p. 923-9.

van Es, J. H., T. Sato, M. van de Wetering, A. Lyubimova, A. N. Nee, A. Gregorieff, N. Sasaki, L. Zeinstra, M. van den Born, J. Korving, A. C. Martens, N. Barker, A. van Oudenaarden, and H. Clevers, 2012, Dll1+ secretory progenitor cells revert to stem cells upon crypt damage: Nat Cell Biol, v. 14, p. 1099-104.

Wernig, M., A. Meissner, J. P. Cassady, and R. Jaenisch, 2008, c-Myc is dispensable for direct reprogramming of mouse fibroblasts: Cell Stem Cell, v. 2, p. 10-2.

Wernig, M., A. Meissner, R. Foreman, T. Brambrink, M. Ku, K. Hochedlinger, B. E. Bernstein, and R. Jaenisch, 2007, In vitro reprogramming of fibroblasts into a pluripotent ES-cell-like state: Nature, v. 448, p. 318-24.

Xu, C., Y. Xu, O. Gursoy-Yuzugullu, and B. D. Price, 2012, The histone variant macroH2A1.1 is recruited to DSBs through a mechanism involving PARP1: FEBS Lett, v. 586, p. 3920-5.

Yan, K. S., L. A. Chia, X. Li, A. Ootani, J. Su, J. Y. Lee, N. Su, Y. Luo, S. C. Heilshorn, M. R. Amieva, E. Sangiorgi, M. R. Capecchi, and C. J. Kuo, 2012, The intestinal stem cell markers Bmi1 and Lgr5 identify two functionally distinct populations: Proc Natl Acad Sci U S A, v. 109, p. 466-71.

Yanai, H., N. Atsumi, T. Tanaka, N. Nakamura, Y. Komai, T. Omachi, K. Tanaka, K. Ishigaki, K. Saiga, H. Ohsugi, Y. Tokuyama, Y. Imahashi, S. Ohe, H. Hisha, N. Yoshida, K. Kumano, M. Kon, and H. Ueno, 2017, Intestinal cancer stem cells marked by Bmi1 or Lgr5 expression contribute to tumor propagation via clonal expansion: Sci Rep, v. 7, p. 41838.

Yildirim, O., J. H. Hung, R. J. Cedeno, Z. Weng, C. J. Lengner, and O. J. Rando, 2014, A system for genome-wide histone variant dynamics in ES cells reveals

dynamic MacroH2A2 replacement at promoters: PLoS Genet, v. 10, p. e1004515.

Yousefi, M., N. Li, A. Nakauka-Ddamba, S. Wang, K. Davidow, J. Schoenberger, Z. Yu, S. T. Jensen, M. G. Kharas, and C. J. Lengner, 2016, Msi RNA-binding proteins control reserve intestinal stem cell quiescence: J Cell Biol, v. 215, p. 401-413.

Zhang, R., M. V. Poustovoitov, X. Ye, H. A. Santos, W. Chen, S. M. Daganzo, J. P. Erzberger, I. G. Serebriiskii, A. A. Canutescu, R. L. Dunbrack, J. R. Pehrson, J. M. Berger, P. D. Kaufman, and P. D. Adams, 2005, Formation of MacroH2A-containing senescence-associated heterochromatin foci and senescence driven by ASF1a and HIRA: Dev Cell, v. 8, p. 19-30.

Zink, L. M., and S. B. Hake, 2016, Histone variants: nuclear function and disease: Curr Opin Genet Dev, v. 37, p. 82-9.